UNIVERSITY OF CALIFORNIA, SAN DIEGO

SYNOVIAL FLUID HOMEOSTASIS: BULK FLOW, LUBRICANT TRANSPORT, AND BIOPHYSICAL RESTORATION

A dissertation submitted in partial satisfaction of the

requirements for the degree Doctor of Philosophy

in

Bioengineering

by

William Joseph McCarty

Committee in charge:

Professor Robert L.Sah, Chair
Professor Shu Chien
Professor Gary S. Firestein
Professor Jeff M. Hasty
Professor Koichi Masuda

2012

The dissertation of William J. McCarty is approved, and it is acceptable in quality and form for publication on microfilm and electronically:

_____

_____

_____

_____

_____

Chair

University of California, San Diego

2012

TABLE OF CONTENTS

LIST OF FIGURES

LIST OF TABLES

ACKNOWLEDGMENTS

I would first like to gratefully acknowledge my graduate research advisor and dissertation committee chair, Robert Sah, and thank him for welcoming me into his lab, instructing me in all the tools necessary for an experimentalist, providing me the opportunity and time to learn a long list of experimental techniques, teaching me how to write papers and grants, countless hours of research planning and discussions of musculoskeletal physiology, and his example as a scientist and professor.

I would also like to thank the other members of my dissertation committee: Shu Chien, Gary Firestein, Jeff Hasty, and Koichi Masuda for their valuable input at various times throughout my time at UCSD, but especially during my thesis proposal.

I am very appreciative of the advice and support I've received from collaborating scientists and clinicians: Koichi Masuda, Anthony Ratcliffe, Mohammad Sotoudeh, William Bugbee, Anna Plaas, and John Sandy. In particular, I'd like to thank Koichi Masuda for teaching me how to run *in vivo* studies, perform surgery, and utilize the confocal microscope, in addition to generously donating his time and resources to my work, consistently providing strong advice, and encouraging me to always do (and work!) more.

I would like to thank the many undergraduate students whom I mentored over the years, especially Anna Luan and Justin Cheng for their time and commitment to the many projects we created together.

I would also like to thank all the current and former members of the CTE lab who have helped me in innumerable ways over the years.

Finally, I offer many thanks to my friends, siblings, and parents for their time, patience, curiosity, understanding, motivation, and encouragement.

Portions of Chapter 1 are reproduced from "Cartilage Tissue Engineering", In: Comprehensive Biomaterials, 1st Ed., eds: Ducheyne P, Healy KE, Hutmacher DE, Grainger DE, Kirkpatrick CJ. Elsevier, 2011, vol 5, p 199-212, with permission from Elsevier. The dissertation author was the primary author and thanks co-authors Quynhhoa T. Nguyen, Alexander Y. Hui, Albert C. Chen, and Robert L. Sah.

Chapter 2, in full, is reproduced from the *Journal of Biomechanics*, volume 44, number 16, p. 2761-7, 2011 with permission from Elsevier. The dissertation author was the primary author and thanks co-authors Koichi Masuda, and Robert L. Sah. The authors would like to thank Esther Cory Burak and Elise F. Morgan for their helpful discussions. This work was supported by grants from the National Institute of Arthritis, Musculoskeletal and Skin Diseases, a Ruth L. Kirschstein National Research Service Award predoctoral fellowship from the National Institute on Aging (for WJM), and an award to UCSD from the Howard Hughes Medical Institute through the HHMI Professors Program (for RLS).

Chapter 3, in full, is reproduced from the *Journal of Orthopaedic Research*, volume 29, number 2, p. 240-6, 2011 with permission from Wiley, Inc. The dissertation author was the primary author and thanks co-authors Anna Luan, Meena Siddiqui, Bradley C. Hansen, Koichi Masuda, and Robert L. Sah. This work was supported by grants from the National Institute of Arthritis, Musculoskeletal and Skin

Diseases and an award to UCSD from the Howard Hughes Medical Institute through the HHMI Professors Program (for RLS).

Chapter 4 will be submitted to *Arthritis & Rheumatism*. The dissertation author was the primary author and thanks co-authors Justin C. Cheng, Bradley C. Hansen, Tomonori Yamaguchi, Koichi Masuda, and Robert L. Sah. This work was supported by grants from the National Institute of Arthritis, Musculoskeletal and Skin Diseases and a Ruth L. Kirschstein National Research Service Award predoctoral fellowship from the National Institute on Aging (for WJM).

Chapter 5 will be submitted to the *Journal of Biological Chemistry*. The dissertation author was the primary author and thanks co-authors Justin C. Cheng, William D. Bugbee, and Robert L. Sah. This work was supported by grants from the National Institute of Arthritis, Musculoskeletal and Skin Diseases and a Ruth L. Kirschstein National Research Service Award predoctoral fellowship from the National Institute on Aging (for WJM).

Appendix A, in full, is reproduced from the *Annals of Biomedical Engineering*, volume 39, number 4, p. 1306-12, 2011 with permission of the authors, as authors retain copyright with Springer, Inc. The dissertation author was the primary author and thanks co-authors Anna Luan, Priya Sundaramurthy, Caryn Urbanczyk, Atal Patel, Jacob Hahr, Mohammad Sotoudeh, Anthony Ratcliffe, and Robert L. Sah. This work was supported by grants from the National Institutes of Health and an award to UCSD from the Howard Hughes Medical Institute through the HHMI Professors Program (for RLS). The authors would like to thank the UCSD Senior Design course BENG 187.

Appendix B, in full, is reproduced from *Tissue Engineering Part A*, volume 16, number 5, p. 1717-27, 2010 with permission from Mary Ann Liebert, Inc. The dissertation author was the primary author and thanks co-authors Andrea L. Pallante, Rebecca J. Rone, William D. Bugbee, and Robert L. Sah. This work was supported by grants from the National Institutes of Health and an award to UCSD from the Howard Hughes Medical Institute through the HHMI Professors Program (for RLS). The authors would like to thank Harold M. Aberman, DVM, MSE for his donation of goat tissue, Won C. Bae, Ph.D for his work on the image processing script, and EunHee Han, Ph.D for her donation of link protein.

VITA

2004	B.S., Biomedical Engineering Northwestern University, Evanston, Illinois
2006	M.S., Biomedical Engineering Northwestern University, Evanston, Illinois
2006-2012	Graduate Student Researcher Cartilage Tissue Engineering Laboratory University of California, San Diego, La Jolla, California
2011-2012	NRSA Fellow, NIH - National Institute on Aging F31AG039939, 04/05/2011 – 06/30/2012 *Joint Capsule Biomechanics and Transport in Rat Models of Aging and Disease*
2012	Ph.D., Bioengineering University of California, San Diego, La Jolla, California

Journal Articles

McCarty WJ, Cheng JC, Bugbee WD, Sah RL. Control of the biophysical properties of hyaluronan solutions and osteoarthritic synovial fluid with inter-α-trypsin inhibitor heavy chains.*Journal of Biological Chemistry* (in preparation).

McCarty WJ, Cheng JC, Hansen BC, Yamaguchi T, Masuda K, Sah RL. The biophysical mechanisms of altered hyaluronan concentration in synovial fluid after anterior cruciate ligament transection.*Arthritis & Rheumatism* (submitted).

McCarty WJ, Masuda K, Sah RL. Fluid Movement and Joint Capsule Strain due to Flexion in Rabbit Knees.*J Biomech*. 44(16):2761-7, 2011.

McCarty WJ, Luan A, Sundaramurthy P, Urbanczyk C, Patel A, Hahr J, Sotoudeh M, Ratcliffe A, Sah RL: An arthroscopic device to assess articular cartilage defects and treatment with a hydrogel. *Ann Biomed Eng*. 39(4):1306-12, 2011.

McCarty WJ, Luan A, Siddiqui M, Hansen BC, Masuda K, Sah RL: Biomechanical properties of mixtures of blood and synovial fluid. *J Orthop Res*. 29(2):240-6, 2011.

McCarty WJ, Pallante AL, Rone RJ, Bugbee WD, Sah RL: The proteoglycan metabolism of articular cartilage in joint-scale culture. *Tissue Eng Part A*. 16:1717-27, 2010.

Blewis ME, Lao BJ, Jadin KD, **McCarty WJ**, Bugbee WD, Firestein GS, Sah RL: Semi-permeable membrane retention of synovial fluid lubricants hyaluronan and proteoglycan 4 for a biomimetic bioreactor. *Biotechnol Bioeng.* 106:149-60, 2010.

McCarty WJ, Chimento MF, Curcio CA, Johnson M. Effects of particulates and lipids on the hydraulic conductivity of Matrigel. *J Appl Physiol*. 105(2):621-8, 2008.

McCarty WJ, Johnson M. The hydraulic conductivity of Matrigel. *Biorheology* 44(5-6):303-17, 2007.

Reviews

Hui AY, **McCarty WJ**, Masuda K, Firestein GS, Sah RL: A systems biology approach to synovial joint lubrication in health, injury, and disease. Wiley Interdiscip Rev SystBiol Med 4:15-37, 2012.

Book Chapters

McCarty WJ, Nguyen QT, Hui AY, Chen AC, Sah RL: Cartilage Tissue Engineering. In: Comprehensive Biomaterials, 1st Ed., ed by Ducheyne P, Healy KE, Hutmacher DE, Grainger DE, Kirkpatrick CJ. Elsevier, vol 5, p.199-212, 2011.

Theses

McCarty WJ. *A Matrigel Model of the Hydraulic Conductivity of Bruch's Membrane in Age-Related Maculopathy*. M.S. Thesis supervised by Professor Mark Johnson, Northwestern University, Evanston, IL, 2006.

Selected Abstracts

McCarty WJ, Cheng JC, Sah RL: Biomimetic restoration of the biophysical properties of osteoarthritic synovial fluid. *JSOE Res Expo,* 2012.

McCarty WJ, Cheng JC, Hansen BC, Yamaguchi T, Masuda K, Sah RL: Hyaluronan residence time in the joint is decreased at early times after ACLT. *Trans Orthop Res Soc* 37:791, 2012.

ABSTRACT OF THE DISSERTATION

SYNOVIAL FLUID HOMEOSTASIS:
BULK FLOW, LUBRICANT TRANSPORT,
AND BIOPHYSICAL RESTORATION

by

William Joseph McCarty

Doctor of Philosophy in Bioengineering
University of California, San Diego, 2012
Professor Robert L. Sah, Chair

Synovial fluid (SF) is an ultrafiltrate of blood plasma found in diathrodial joints that contributes to low-friction and low-wear joint articulation. SF normally contains high molecular mass (M_r) hyaluronan (HA), secreted in response to mechanical and biological cues from local cell populations, and a major contributor to the fluid's biophysical properties. During joint pathology, the composition of SF, including HA M_r, is decreased, resulting in decreased viscosity and altered biophysics. *The overall motivation of this dissertation work was to contribute to the understanding of synovial fluid physiology, including fluid movement during flexion, post-injury rheology, lubricant homeostasis, and biophysical properties.*

The objectives were to determine 1) SF movement and joint capsule strain due to flexion, 2) the rheological and biomechanical properties of mixtures of SF and blood, 3) the mechanisms of lubricant homeostasis in normal and injured joints, and 4) the molecular determinants of the biophysical properties of SF and to utilize them to control those properties in solutions of HA and in OA SF. 1) *Ev vivo* and *in vivo* imaging of rabbit joints were used to determine that flexion of the knee shifts SF from anterior to posterior, and the joint capsule undergoes proximal-distal tension and circumferential shortening relative to the femur axis. 2) Dilution with SF altered the coagulation torque profile of blood over time, resulting in a decreased maximum torque generation and clot mechanical stiffness. 3) *In vivo* in the adult rabbit, endogenous secretion of high-M_r HA after washout replenished in SF over time, secretion rates were diminished after ACLT, and HA loss from the SF occurred in a M_r-dependent manner leading to decreased residence times of HA at day 7 after ACLT, likely due to subsynovial cell infiltration. 4) The importance of HA binding proteins to OA SF viscosity was demonstrated, with protein removal resulting in significant viscosity decreases. Modification of HA with inter-α-inhibitor heavy chains increased the viscosity of HA solutions and OA SF.

Major contributions of this work include to understanding the structural physiology of the joint, molecular homeostasis in SF, the effects of injury on joints, and clinical implications for joint disease.

CHAPTER 1:

INTRODUCTION

1.1 Synovial Joint Physiology

Synovial, or diathrodial, joints contain synovial fluid (SF) bounded by the joint capsule, or articular capsule, a thin, but strong and flexible fibrous membrane. This membrane is strengthened by fibrous bands connected to it derived from the fascia lata and tendons surrounding the joint [17]. The joint capsule contains intimal and sub-intimal membranous lining layers called synovium and subsynovium, respectively. SF baths the synovium lining and the cartilaginous ends of long bones, as well as the other tissues within the joint cavity including the meniscus and anterior and posterior cruciate ligaments (**Fig. 1.1**). These tissues together allow for the low-friction and low-wear articulation of long bones that normally enables a lifetime of ambulatory movement.

1.1.1 Synovial Fluid

Synovial fluid (SF) is normally a clear, viscous liquid found inside synovial joints that functions as a biomechanical lubricant and as a medium for metabolites and soluble signaling factors. In the normal human knee joint, the volume of SF is on the order of 1mL [65]. In their typical proportions and concentrations, the molecular constituents comprising normal SF give rise to its unique properties and functions in maintaining joint homeostasis. SF is composed of a blood plasma dialysate and

molecules secreted by cells lining the synovial joint, including hyaluronan (HA) and proteoglycan 4 (PRG4, also known as lubricin and superficial zone protein). One main function of SF is to lubricate articulating joints, facilitating the low-friction and low-wear properties of cartilage. Additionally, it serves metabolic functions, facilitating the transport of nutrients, waste products, and other metabolites to and from synovial tissues. Finally, it mediates molecular communication by soluble factors between disparate cell populations in the joint.

Formation

SF is an ultrafiltrate of blood plasma with additional molecules secreted by cells lining synovial joints. The synovium functions as a semi-permeable membrane that selectively retains and permits specific molecules based on size. The biosynthetic sources of SF lubricant molecules are the cell populations lining the synovial cavity, with synoviocytes mainly secreting HA and superficial zone chondrocytes [73], synoviocytes [24, 26, 74], and meniscal cells [75] secreting PRG4. High molecular weight species, such as the lubricant molecules HA and PRG4, are selectively retained within the synovial joint, while low molecular weight species, such as most metabolic substrates and byproducts, cytokines, and growth factors, are not. Molecular sieving by the synovial membrane matrix is size dependent [66]. An active filtration process, together with secretory contributions from the cell populations lining the synovial joint, result in fluid with typical steady-state concentrations of 1-4mg/ml HA [51] and 0.05-0.35mg/ml PRG4.

Plasma Proteins

The composition of SF reflects its origin as a plasma ultrafiltrate. The protein composition of SF is similar to that of plasma [69, 70], though synovium selectively retains most large plasma proteins in the vasculature and limits their entry into the synovial joint space. In normal human SF, the total protein concentration is 25-28 mg/ml, which is approximately one-third of the total protein concentration in plasma [65]. Large molecular weight plasma proteins, such as β_2 macroglobulin (1,000kDa), fibrinogen (340kDa), β_1 lipoprotein (3,200kDa), α_2 macroglobulin (820kDa), and α_2 glycoprotein (1,000kDa) are low or undetectable in normal SF, while small molecular weight plasma proteins, such as albumin (69kDa), α_1 glycoproteins, transferrin (90kDa), and γ globulin (160kDa) are found in high quantities in plasma and SF [9, 76]. The most abundant macromolecule in SF is albumin (~10mg/mL), which is found in SF at 40-45% of its plasma concentration, and is a major contributor to SF colloidal osmotic pressure and a minor contributor to SF viscosity [47].

Lubricant Macromolecules

The main lubricating macromolecules present in SF are HA [60] and PRG4 [89, 90]. HA is a glycosaminoglycan consisting of repeating disaccharide units of D-glucuronic acid and D-N-acetylglucosamine. It exists in SF as a polydisperse population with 60-70% of the HA having a molecular weight greater than 4MDa and a weight average molecular weight of 4-6MDa [39]. The concentration of HA plays a major role in determining the viscosity of SF. In addition, HA provides outflow

buffering, a phenomenon which decreases trans-SF loss under raised intra-articular pressures [54]. PRG4 is a mucinous glycoprotein with multiple O-linked β(1-3)Gal-GalNAc oligosaccharides, which mediate the molecule's function as a boundary lubricant [25], and has a molecular weight of ~300kDa [73]. The PRG4 gene encodes a lubricating glycoprotein known as SZP, lubricin, or PRG4 that is found in synovial fluid, articular cartilage, synovium, and other synovial tissues [2, 40].

Synovial Fluid Rheology

The rheological properties of SF have been characterized using measurements of viscosity and viscoelasticity. The viscosity of SF strongly correlates with the concentration of HA present [11]. SF exhibits non-Newtonian viscous behavior, acting as a shear-thinning fluid over a wide range of shear rates, with higher viscosities reported at higher HA concentrations [77]. Viscoelastic models of SF have demonstrated an elastic-like response from 'normal' SF at high frequencies of oscillation, with dynamic storage and loss moduli on the order of ~10Pa, depending on shear rate [68].

1.1.2 Synovium and Subsynovium

Synovium is a thin membrane that lines the intraarticular (IA) surface of the joint capsule and performs important secretory and regulatory functions. Synovium is distinguished by a highly fibrillar interstitial matrix that is ~20-50μm thick [4, 83, 87], which is composed of collagen types I, III, V, and VI, HA, chondroitin 4 and 6 sulphates, heparan sulfate, and laminin [45, 63], and has an effective pore size of ~20-

90nm [16, 66]. The matrix is densely populated with synoviocytes 1-3 layers deep, though the cells are not laminar, do not share tight junctions, and lack a basement membrane [52, 83]. Two main types of synoviocytes predominate in synovium: macrophage-like synoviocytes (MLS, ~33% of cells) and fibroblast-like synoviocytes (FLS, ~67% of cells). FLS secrete hyaluronan (HA) [86] as well as connective tissue matrix components including types IV and VI collagens, laminin, and chondrotin proteoglycans [23]. The secretion of HA by FLS is an important contributor to SF lubrication ability. Synovium also functions as a semi-permeable barrier that restricts fluid and molecular flux between SF and blood plasma in the microvasculature, thus regulating the composition of SF.

Subsynovium is a sub-intimal, supportive, loose connective tissue layer below synovium that contains microvasculature. Subsynovium is composed of adipose, areolar, and fibrous connective tissues in variable distributions. Fibrous connective tissue is hypocellular and covers less of the joint capsule area than areolar and adipose connective tissues [4]. The superficial region of subsynovium contains a high density of microvasculature, including arterioles, capillary networks, venuoles, lymphatic vessels, and nerves [6, 7]. Capillaries are present in both fenestrated and unfenestrated varieties, with the fenestrations, when present, occurring on the intra-articular capillary wall [88]. Trans-synovial fluid turnover has been suggested as occurring via fluid movement through the capillary fenestrae, across synovium into the intra-articular space, and back through synovium into the lymphatic vessels [45]. Molecules that diffuse or convect through synovium and broken down waste products from the MLS are also removed by the lymphatic vessels [28].

1.1.3 Cartilage

Articular cartilage is a connective tissue that covers the ends of long bones and functions as a load-bearing, low friction, and wear resistant surface to facilitate joint movement. Articular cartilage is composed of chondrocytes embedded in a hydrated and specialized extracellular matrix (ECM) that consists mostly of collagen type II (COL) and proteoglycan (PG) [50]. PG provides cartilage with compressive stiffness due to the fixed charge density of these molecules that create an osmotic swelling pressure. The COL network resists the swelling tendency of PG molecules and provides cartilage functional integrity, tensile and shear stiffness and strength. Cell and matrix contents, as well as mechanical properties of cartilage, vary with depth from the superficial surface.

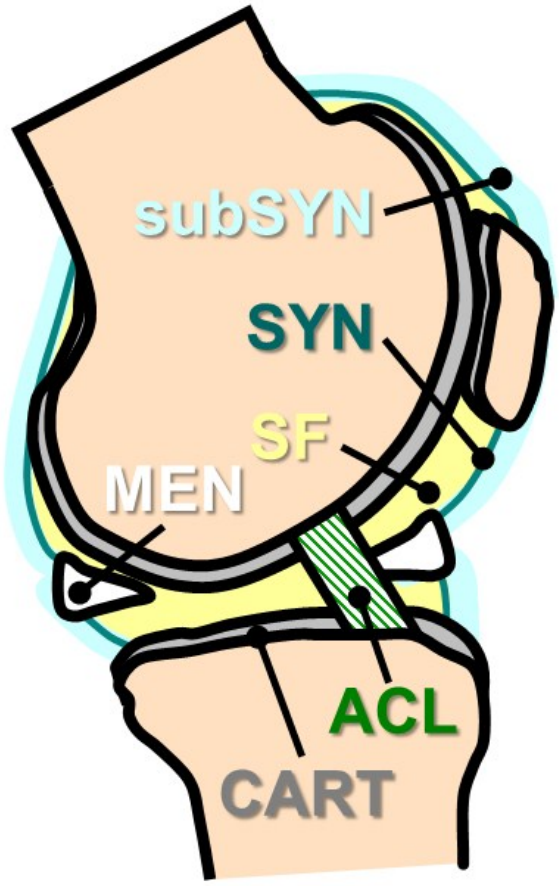

Figure 1.1: Schematic view of an example synovial joint, the knee, with subsynovium (subSYN), synovium (SYN), synovial fluid (SF), meniscus (MEN), anterior cruciate ligament (ACL), and cartilage (CART) indicated.

1.2 Joint Capsule Biomechanics and Lubricant Mechanobiology

During normal joint articulation, the bulk of the SF shifts within the joint cavity and joint capsule tissues deform, though little is known about the magnitude of these deformations and their effect on molecular transport. Joint capsule strain patterns are likely inhomogeneous due to the anatomy of the joint, specifically the presence of the patellar ligament restricting anterior, compared to medial and lateral, expansions. Although the strains have not been investigated, synoviocytes and superficial zone chondrocytes are sensitive to mechanical stimuli and alter their metabolism in response to the appropriate stimuli (**Fig. 1.2**).

1.2.1 Joint Capsule Strain and Synovial Fluid Pressurization

Despite the mechanosensitive nature of synovium, the physiological tissue strains in the joint capsule of the knee have not been reported. Potential methodologies appropriate for determining strain in joint capsule and synovium, including biaxial and volumetric strain techniques, have been developed: the mechanical properties of rabbit skin [37, 38] and dog lung [93], among many others, have been investigated using imposed biaxial strain. Generalized constitutive models for soft tissue biaxial strain [81] and detailed analyses of experimental setup [10] and data manipulation [92] for this type of mechanical test are available.

The intra-articular pressure in SF of the knee changes with SF volume, joint flexion, and loading. Intra-articular pressure in the knee is typically slightly negative in extension (-2cm·H_2O) and increases with flexion, with higher increases in pressure at larger SF volumes [41], peaking during the loading phase of the gait cycle [27]. Pressure-volume curves have been measured in rabbit knees, by injecting minimally absorbable oil and monitoring pressure, to determine synovium elastance and

hysteresis during inflation/deflation cycles [32], and connections between synovial bursae [31].

1.2.2 Synovium and Cartilage Lubricant Mechanobiology

The secretion rates of the main lubricant molecules HA and PRG4 into SF by synoviocytes and superficial zone chondrocytes, respectively, are mechanosensitive. At the cellular level, HA secretion by isolated synoviocytes grown to confluence increased by 57% over 3hrs when stretched by 10% for as little as 10min [56]. At the joint scale, passive flexion of anesthetized rabbit knees resulted in a 100% increase in HA secretion over 5hrs, decreasing the HA turnover time estimates from 17-30hrs to 8-15hrs [22]. Dynamic mechanical shear of calf cartilage explants increased PRG4 expression to 300-400% of free-swelling and static compression controls [59]. In an experiment applying continuous passive motion to *en bloc* calf knee joints, increased local cartilage superficial zone secretion rates of PRG4 correlated with areas in continuous or intermittent sliding contact with apposing surfaces [58].

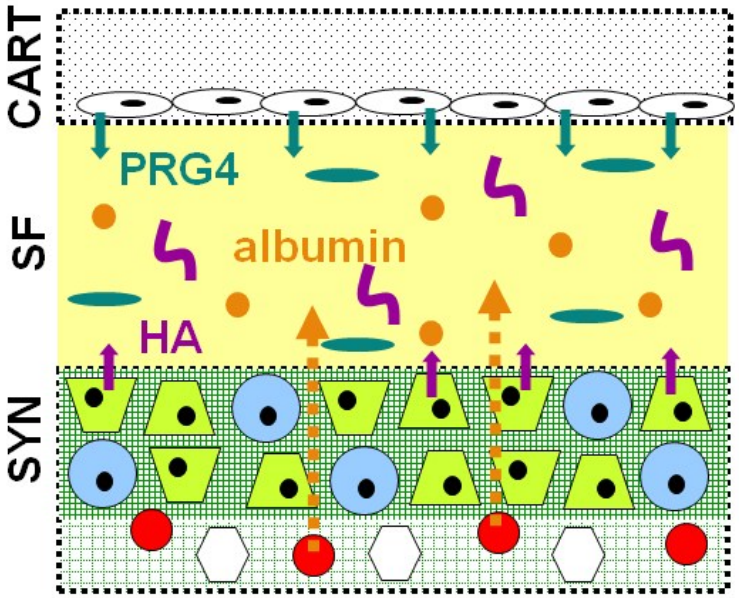

Figure 1.2: HA is mainly secreted by fibroblast-like synoviocytes in synovium and PRG4 is mainly secreted by superficial zone chondrocytes in cartilage, whereas plasma proteins convect into SF from capillaries in the subsynovium. Stretch of synovium and shear of cartilage increase lubricant secretion rates.

1.3 Synovial Fluid Flux: Transport Across Synovium

Synovium is the main barrier to the flow of fluid and transport of molecules, such as lubricants, into and out of SF (**Fig. 1.3**). The hydraulic conductivity of extracellular matrices depends on the matrix constituent molecule concentration and fiber diameters [44]. Fluid flow between the SF and microvasculature can be described by Starling's law:

$$J_v = k\left(\left[\Delta P_{SF}^{capillary}\right] - \sigma\left[\Delta\Pi_{SF}^{capillary}\right]\right) \qquad \text{(Eq. 1.3.1)}$$

with fluid flow rate per area J_v (cm/s), hydraulic conductivity k (cm/(s·cmH_2O)), hydrostatic pressure difference between capillaries and SF $\Delta P_{SF}^{capillary}$ (cmH_2O), reflection coefficient σ, and oncontic pressure difference between capillaries and SF $\Delta\Pi_{SF}^{capillary}$ (cmH_2O) [30]. In normal knees, the time and space averaged $\Delta P_{SF}^{capillary}$ is greater than $\Delta\Pi_{SF}^{capillary}$, implying there is an average influx of fluid from the capillaries to SF. This influx has been measured as ~2μL/(cm^2·hr) of synovium [33], suggesting the volume of synovial fluid is replaced on the order of hours [43].

1.3.1 Hydraulic Conductivity of Synovium

The synovium matrix hydraulic conductivity, a measure of ease of fluid flow that depends on matrix content, is generally low, but increases with inflammation and increased pressure. Fluid flow through synovium occurs through the ~2μm [46] wide intercellular spaces of ECM, which has a hydraulic conductivity of ~10^{-11}cm^4/(s·dyne) in rabbits [47]. The resistance to fluid flow is mainly determined by synovium, though subsynovium also plays a role [79]. At elevated intra-articular pressures, the matrix stretches, increasing surface area and reducing fluid path-length [46]. The concentration of matrix constituents, including collagens and GAGs, are altered due to the joint capsule stretch at elevated intra-articular pressures, effectively diluting their

concentration, explaining some of the increased conductivity of synovium [62, 63]. Direct manipulation of the matrix content by digesting synovium GAGs [78] or injecting exogenous HA [5] confirms the importance of matrix molecules in determining synovium hydraulic conductivity.

1.3.2 Macromolecular Flux

Synovium interstitium determines the rates of molecular flux per area of synovium into SF, and those rates are increased due to synovitis. Diffusive and convective passive transport of molecules occurs through pores in the ECM (~20-90nm) [16, 66] at these intercellular openings, making synovium permeability inversely related to molecule size. High MW lubricant molecules are retained in the joint, as the reflection coefficient of synovium to high MW HA has been reported as ~57-75% [67]. Protein flux between the microvasculature and SF has been measured using a variety of techniques, including the SF to serum ratio [36], injection of radioactive tracers and sampling [57, 85], and tracer injection with clearance measurements [82, 84, 94]. Data from these methods consistently show an increase in protein molecular flux with synovitis and joint inflammation.

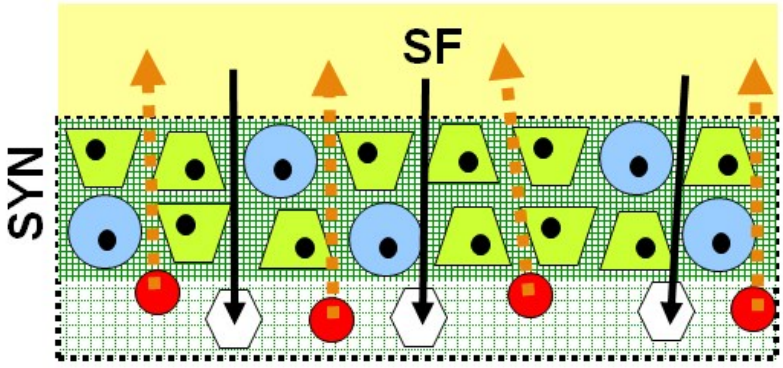

Figure 1.3: Net fluid flow from the capillaries convects plasma proteins and nutrients into SF, while diffusive diffusion through the interstitial spaces between synoviocytes to the lymphatics in subsynovium and cellular uptake remove molecules from SF.

1.4 Lubrication of Joint Articulation by Synovial Fluid

One important function of SF is to contribute to the lubrication of joint articulation. The composition, and specifically the concentration, of molecules in SF is important in determining the rheological properties of the fluid itself, as well as maintaining specific lubricant molecules in the proper amounts on the surfaces of cartilage and ligament. Due to the complex geometry and loading in joints, different regions of the joint undergo varied types of lubrication at any given time, requiring different forms of lubrication to maintain low-friction and low-wear articulation.

1.4.1 Lubrication Regimes

Lubrication of cartilage-on-cartilage articulation in joints occurs by various mechanisms or 'regimes'. The dominant regime in a particular location of a joint depends on many factors, including the articulation frequency, the distance between opposing surfaces, the magnitude of normal load being supported, and time. As joint surfaces begin to approach each other while supporting a load, the SF between them is pressurized. This pressure is dissipated by fluid flow away from the surfaces, decreasing the separation distance, which is known as "hydrodynamic lubrication". As the separation distance approaches zero, molecules on the two surfaces begin to interact. The load at this point is supported by direct molecular contact between the surfaces, as well as pockets of pressurized SF and interstitial fluid in the cartilage, which is known as "mixed-mode lubrication". SF viscosity is an important determinant of the amount of pressure that can be supported by SF during "hydrodynamic mode" and "mixed mode" lubrication [14]. As the amount of time the surfaces have been in contact increases, the pressurized interstitial fluid flows away

from the loaded stress points, and eventually the full load is supported via direct molecular interaction between surfaces, known as “boundary mode lubrication” [1].

1.4.2 Contributions of Synovial Fluid Constituents

Studies using a cartilage-on-cartilage friction test have identified HA and PRG4 as primary boundary mode lubricants in SF [8, 13], lowering friction in a dose-dependent manner, both alone and in combination [71, 72]. Normal bovine SF values of boundary-mode kinetic friction coefficient in this setup were ~0.025.Cartilage on glass friction testing has shown that recombinant human lubricin lubricates cartilage in a dose-dependent manner and involves lubricin bound to the surface and lubricin in solution [15].

In addition to friction, the wear-reducing properties of SF have been measured at the tissue and joint scales. Using a cartilage-on-cartilage system, the contributions of various SF lubricants to reducing wear have been determined [91]. Other counter surfaces have also been used to investigate cartilage wear, including stainless steel [3, 49] and polymers [29, 34]. At the joint-scale, synovial fluid lubrication has been assessed using pendulum instruments on intact joints [48].

1.5 Osteoarthritis and Inflammatory Joint Pathology

Osteoarthritis (OA) refers to a group of chronic, disabling joint diseases that exhibit degenerative and inflammatory effects on the joint. OA is characterized by degeneration of cartilage and is the most common form of arthritis. Over 27 million people in the United States alone are affected by osteoarthritis, which is also the leading cause of disability and costs the healthcare system $180 billion per year in out of pocket and insurer payments [35]. OA is often described as "non-inflammatory" arthritis to distinguish it from rheumatoid arthritis, but the role of inflammation in disease symptoms and progression is increasingly being recognized, including the presence of chronic and acute synovitis, effusion, increased fibroblast proliferation, and angiogenesis (**Fig. 1.4**) [80].

1.5.1 Synovitis and Synovial Fluid Effusion

Subclinical chronic synovitis and effusion are often present in OA joints. Evidence of synovitis, including cellular infiltration by macrophages and T cells, increased cellular turnover, angiogenesis, and tissue thickening have been observed histologically in OA synovium [12, 18, 19, 95]. Synovial thickening has been correlated with knee effusion observed by magnetic resonance imaging, likely indicating increased fluid volume, cell-infiltration, and mass of subsynovium [61]. Moderate and large knee effusions and synovial thickening, all of which were commonly seen in older persons by magnetic resonance imaging, were associated with knee pain in one cohort of weight-bearing patients [20].

1.5.2 Changes to Synovial Fluid Formation, Composition, and Rheology

Pathological synovium displays altered transport characteristics, directly affecting the composition of SF. The permeability of synovium from joints with rheumatoid arthritis to proteins is increased [42, 82], with proportionately larger increases in permeability for larger proteins [36]. Increased Starling pressure, either due to the reduced oncotic gradient as protein accumulates in SF [53] and increased permeability of capillaries during inflammation, or to increased SF pressure with effusion, contribute to the buildup of fluid and protein in SF.

The concentration and quality of lubricant molecules are altered in different ways in OA, RA, and injury. Changes in SF HA in OA and RA have been reviewed elsewhere [11]. Briefly, the concentration of HA in SF is decreased in RA samples and, to a lesser extent, in OA samples. The molecular weight of HA in OA is much lower than is found in normal SF, while the molecular weight of HA from RA is only slightly smaller than that found in normal SF. In patients undergoing total knee arthroplasty, those requiring revision surgery for prosthetic failure have lower concentrations of HA [51].

Pathological SF displays altered rheological properties. Lower viscosity and lower molecular weight of HA have been reported in SF from OA joints compared to normal controls. In inflammatory diseases, such as RA, very low viscosities and concentrations of HA are typically reported.

1.5.3 Joint Injury and Hemarthrosis

During acute trauma, advanced stage OA, and bone marrow stimulation cartilage repair procedures, blood is introduced into the joint and mixes with variable amounts of SF, creating the conditions in the joint when repair is initiated. Hemarthosis, or bleeding into the joint, can occur during traumatic events, such as

intra-articular fracture and anterior cruciate ligament rupture, as well as in advanced stage OA. Although there is evidence that hemarthrosis may lead to cartilage erosion [21] and decreased matrix synthesis [64], certain cartilage repair procedures used to treat focal defects, such as microfracture [55], encourage hemarthrosis through subchondral penetrations as a source of hematopoietic stem cells for repair. Whole blood entering the intra-articular space mixes with SF, or is diluted with saline during surgeries, and these mixtures can form the initial structural material for cartilage repair. However, the effects of SF on the coagulation properties of blood have not yet been described.

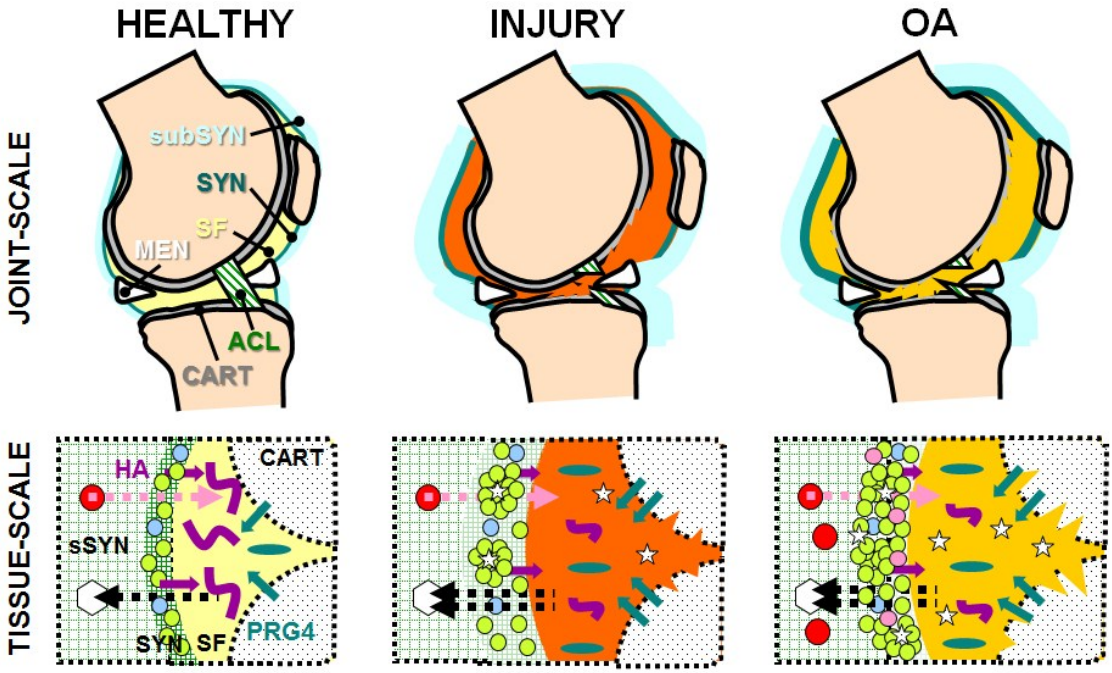

Figure 1.4: Acute injury to the joint, such as ACL transection, can lead to hemarthrosis, effusion, decreased HA concentration and molecular weight, cartilage erosion, and synovitis. Many similar pathologies are observed in OA, with increasing cartilage degeneration and inflammatory response in the joint capsule over time.

1.6 Thesis Objectives and Overview

The overall motivation of this dissertation work was to contribute to the understanding of synovial fluid physiology, including fluid movement, rheology, lubricant homeostasis, and biophysical properties. The objectives were to determine 1) SF movement and joint capsule strain due to flexion, 2) the rheological and biomechanical properties of mixtures of SF and blood, 3) the mechanisms of lubricant homeostasis in normal and injured joints, and 4) the molecular determinants of the biophysical properties of SF and to utilize them to control those properties in solutions of HA and in OA SF.

In Chapter 2, published in the *Journal of Biomechanics*, the movement of synovial fluid and the strain that occurs in joint capsule during flexion are described. *Ex vivo* and *in vivo* measurements of fluid movement were made using the rabbit knees after injecting 3 volumes of radiopaque contrast agent and imaging the joint at several flexion angles using a digital X-ray or micro-computed tomography (μCT) scanner. Fiducial markers were created at different locations in the joint capsule and were tracked during flexion using μCT imaging. Joint capsule strains were calculated for different flexion ranges based on the relative displacements of the markers.

In Chapter 3, published in the *Journal of Orthopedic Research*, the rheological and biomechanical properties of mixtures of blood and SF are described. A thromboelastograph-like test was created to measure the mechanical strength of mixtures of blood and SF as they clotted, and compared to blood alone or mixtures of blood and saline. In addition, the mechanical properties of the clots formed from different mixtures, including stiffness and permeability, were assessed using confined compression testing. Finally, the HA content and of the clots was assessed after protein digestion.

In Chapter 4, which will be submitted to *Arthritis & Rheumatism*, the biophysical mechanisms that determine HA molecular homeostasis in SF are described. *In vivo* experiments in the knees of adult rabbits were undertaken to show the effects of ACL transection on 1) pseudo steady-state HA concentration and molecular weight, 2) secretion of HA into SF, 3) loss of HA from SF over time to calculate the residence time of HA by molecular weight, and 4) the inflammatory state of the joint via synovium and subsynovium cellularity and serum HA concentration.

In Chapter 5, which will be submitted to the *Journal of Biological Chemistry*, control of the biophysical properties of solutions of HA and of OA SF using inter-α-inhibitor heavy chains is described. The contributions of different constituents, proteins and the concentration and molecular weight of HA, of OA SF to its viscosity were determined. The well-characterized transesterification reaction that modifies HA with heavy chains from inter-α-inhibitor, which occurs naturally during joint inflammation, was utilized to alter the viscosity, pressurization capability, and membrane permeability of solutions of HA and OA SF in a dose-dependent manner.

In Chapter 6, the major conclusions from this work are summarized and future directions for these projects are discussed.

The appendices contain additional published projects undertaken in the field of musculoskeletal tissue engineering. In Appendix A, published in the *Annals of Biomedical Engineering*, a novel arthroscopic device for the analysis of cartilage focal defects and treatment with hydrogels is described. In Appendix B, published in *Tissue Engineering Part A*, the proteoglycan metabolism of cartilage cultured as an intact hemi-joint is described.

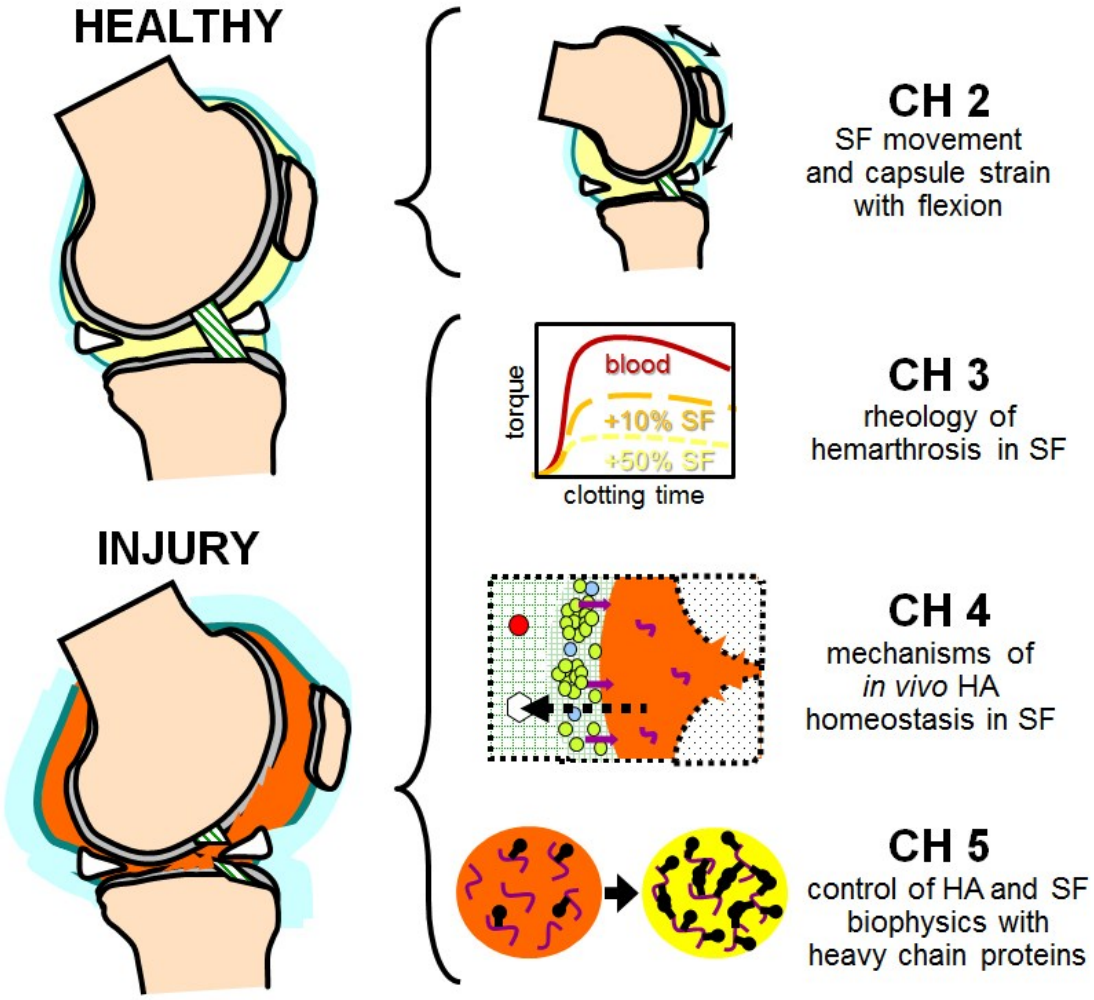

Figure 1.5: Summary of the aims of the dissertation by chapter, including SF movement during flexion, altered rheology after hemarthrosis, mechanisms of HA homeostasis after injury, and control of the biophysical properties of HA solutions and SF.

1.7 Acknowledgements

Portions of Chapter 1 are reproduced from “Cartilage Tissue Engineering”, In: Comprehensive Biomaterials, 1st Ed., eds: Ducheyne P, Healy KE, Hutmacher DE, Grainger DE, Kirkpatrick CJ. Elsevier, 2011, vol 5, p 199-212, with permission from Elsevier. The dissertation author was the primary author and thanks co-authors Quynhhoa T. Nguyen, Alexander Y. Hui, Albert C. Chen, and Robert L. Sah.

1.8 References

1. Ateshian GA: The role of interstitial fluid pressurization in articular cartilage lubrication. *Journal of biomechanics* 42:1163-76, 2009.

2. Bao JP, Chen WP, Wu LD: Lubricin: a novel potential biotherapeutic approaches for the treatment of osteoarthritis. *Mol Biol Rep*, 2010.

3. Berrien LS, Furey MJ, Veit HP: Tribological study of joint pathology. *Crit Rev Biomed Eng* 28:103-8, 2000.

4. Castor CW: The microscopic structure of normal human synovial tissue. *Arthritis Rheum* 3:140-51, 1960.

5. Coleman PJ, Scott D, Mason RM, Levick JR: Characterization of the effect of high molecular weight hyaluronan on trans-synovial flow in rabbit knees. *J Physiol* 514 (Pt 1):265-82, 1999.

6. Davies DV: The lymphatics of the synovial membrane. *J Anat* 80:21-3, 1946.

7. Davies DV: Synovial membrane and synovial fluid of joints. *Lancet* 248:815-22, 1946.

8. Davis WH, Lee SL, Sokoloff L: Proposed Model of Boundary Lubrication by Synovial-Fluid - Structuring of Boundary Water. *Journal of Biomechanical Engineering-Transactions of the Asme* 101:185-92, 1979.

9. Decker B, Mc KB, Mc GW, Slocumb CH: Comparative distribution of proteins and glycoproteins of serum and synovial fluid. *Arthritis Rheum* 2:162-77, 1959.

10. Eilaghi A, Flanagan JG, Brodland GW, Ethier CR: Strain uniformity in biaxial specimens is highly sensitive to attachment details. *J Biomech Eng* 131:091003, 2009.

11. Fam H, Bryant JT, Kontopoulou M: Rheological properties of synovial fluids. *Biorheology* 44:59-74, 2007.

12. Fernandez-Madrid F, Karvonen RL, Teitge RA, Miller PR, An T, Negendank WG: Synovial thickening detected by MR imaging in osteoarthritis of the knee confirmed by biopsy as synovitis. *Magn Reson Imaging* 13:177-83, 1995.

13. Forster H, Fisher J: The influence of loading time and lubricant on the friction of articular cartilage. *Proc Inst Mech Eng H* 210:109-19, 1996.

14. Gleghorn JP, Bonassar LJ: Lubrication mode analysis of articular cartilage using Stribeck surfaces. *J Biomech* 41:1910-8, 2008.

15. Gleghorn JP, Jones AR, Flannery CR, Bonassar LJ: Boundary mode lubrication of articular cartilage by recombinant human lubricin. *J Orthop Res* 27:771-7, 2009.

16. Granger HJ, Taylor AE: Permeability of connective tissue linings isolated from implanted capsules; implications for interstitial pressure measurements. *Circ Res* 36:222-8, 1975.

17. Gray H. Anatomy of the human body. 30th ed. Philadelphia: Lea & Febiger; 1985.

18. Haynes MK, Hume EL, Smith JB: Phenotypic characterization of inflammatory cells from osteoarthritic synovium and synovial fluids. *Clin Immunol* 105:315-25, 2002.

19. Haywood L, McWilliams DF, Pearson CI, Gill SE, Ganesan A, Wilson D, Walsh DA: Inflammation and angiogenesis in osteoarthritis. *Arthritis Rheum* 48:2173-7, 2003.

20. Hill CL, Gale DG, Chaisson CE, Skinner K, Kazis L, Gale ME, Felson DT: Knee effusions, popliteal cysts, and synovial thickening: association with knee pain in osteoarthritis. *J Rheumatol* 28:1330-7, 2001.

21. Hoaglund FT: Experimental hemarthrosis. The response of canine knees to injections of autologous blood. *J Bone Joint Surg Am* 49:285-98, 1967.

22. Ingram KR, Wann AK, Angel CK, Coleman PJ, Levick JR: Cyclic movement stimulates hyaluronan secretion into the synovial cavity of rabbit joints. *J Physiol* 586:1715-29, 2008.

23. Iwanaga T, Shikichi M, Kitamura H, Yanase H, Nozawa-Inoue K: Morphology and functional roles of synoviocytes in the joint. *Arch Histol Cytol* 63:17-31, 2000.

24. Jay GD, Britt DE, Cha CJ: Lubricin is a product of megakaryocyte stimulating factor gene expression by human synovial fibroblasts. *J Rheumatol* 27:594-600, 2000.

25. Jay GD, Harris DA, Cha CJ: Boundary lubrication by lubricin is mediated by O-linked beta(1-3)Gal-GalNAc oligosaccharides. *Glycoconj J* 18:807-15, 2001.

26. Jay GD, Tantravahi U, Britt DE, Barrach HJ, Cha CJ: Homology of lubricin and superficial zone protein (SZP): products of megakaryocyte stimulating factor (MSF) gene expression by human synovial fibroblasts and articular chondrocytes localized to chromosome 1q25. *J Orthop Res* 19:677-87, 2001.

27. Jayson MI, Dixon AS: Intra-articular pressure in rheumatoid arthritis of the knee. 3. Pressure changes during joint use. *Ann Rheum Dis* 29:401-8, 1970.

28. Jensen LT, Henriksen JH, Olesen HP, Risteli J, Lorenzen I: Lymphatic clearance of synovial fluid in conscious pigs: the aminoterminal propeptide of type III procollagen. *Eur J Clin Invest* 23:778-84, 1993.

29. Katta JK, Marcolongo M, Lowman A, Mansmann KA: Friction and wear behavior of poly(vinyl alcohol)/poly(vinyl pyrrolidone) hydrogels for articular cartilage replacement. *J Biomed Mater Res A* 83:471-9, 2007.

30. Kedem O, Katchalsky A: Thermodynamic analysis of the permeability of biological membranes to non-electrolytes. *Biochim Biophys Acta* 27:229-46, 1958.

31. Knight AD, Levick JR: Physiological compartmentation of fluid within the synovial cavity of the rabbit knee. *J Physiol* 331:1-15, 1982.

32. Knight AD, Levick JR: Time-dependence of the pressure-volume relationship in the synovial cavity of the rabbit knee. *J Physiol* 335:139-52, 1983.

33. Knight AD, Levick JR: The influence of blood pressure on trans-synovial flow in the rabbit. *J Physiol* 349:27-42, 1984.

34. Kobayashi M, Oka M: Characterization of a polyvinyl alcohol-hydrogel artificial articular cartilage prepared by injection molding. *J Biomater Sci Polym Ed* 15:741-51, 2004.

35. Kotlarz H, Gunnarsson CL, Fang H, Rizzo JA: Insurer and out-of-pocket costs of osteoarthritis in the US: evidence from national survey data. *Arthritis Rheum* 60:3546-53, 2009.

36. Kushner I, Somerville JA: Permeability of human synovial membrane to plasma proteins. Relationship to molecular size and inflammation. *Arthritis Rheum* 14:560-70, 1971.

37. Lanir Y, Fung YC: Two-dimensional mechanical properties of rabbit skin. I. Experimental system. *J Biomech* 7:29-34, 1974.

38. Lanir Y, Fung YC: Two-dimensional mechanical properties of rabbit skin. II. Experimental results. *J Biomech* 7:171-82, 1974.

39. Lee HG, Cowman MK: An agarose gel electrophoretic method for analysis of hyaluronan molecular weight distribution. *Anal Biochem* 219:278-87, 1994.

40. Lee SY, Niikura T, Reddi AH: Superficial zone protein (lubricin) in the different tissue compartments of the knee joint: modulation by transforming growth factor beta 1 and interleukin-1 beta. *Tissue Eng Part A* 14:1799-808, 2008.

41. Levick JR: An investigation into the validity of subatmospheric pressure recordings from synovial fluid and their dependence on joint angle. *J Physiol* 289:55-67, 1979.

42. Levick JR: Permeability of rheumatoid and normal human synovium to specific plasma proteins. *Arthritis Rheum* 24:1550-60, 1981.

43. Levick JR: Blood flow and mass transport in synovial joints. In: *Handbook of Physiology Section 2, The Cardiovascular System, Microcirculation,* ed. by EM Renkin, MIchel CC, American Physiological Society, Bethesda, MD, 1984.

44. Levick JR: Flow through interstitium and other fibrous matrices. *Q J Exp Physiol* 72:409-37, 1987.

45. Levick JR: Microvascular architecture and exchange in synovial joints. *Microcirculation* 2:217-33, 1995.

46. Levick JR, McDonald JN: Ultrastructure of transport pathways in stressed synovium of the knee in anaesthetized rabbits. *J Physiol* 419:493-508, 1989.

47. Levick JR, McDonald JN: Fluid movement across synovium in healthy joints: role of synovial fluid macromolecules. *Ann Rheum Dis* 54:417-23, 1995.

48. Linn FC: Lubrication of animal joints. I. the arthrotripsometer. *J Bone Joint Surg Am* 49-A:1079-98, 1967.

49. Lipshitz H, Glimcher MJ: In vitro studies of the wear of articular cartilage. II. characteristics of the wear of articular cartilage when worn against stainless steel plates having characterized surfaces. *Wear* 52:297-339, 1979.

50. Maroudas A: Physicochemical Properties of Articular Cartilage. In: *Adult Articular Cartilage,* ed. by MAR Freeman, Pitman Medical, Tunbridge Wells, England, 1979, 215-90.

51. Mazzucco D, Scott R, Spector M: Composition of joint fluid in patients undergoing total knee replacement and revision arthroplasty: correlation with flow properties. *Biomaterials* 25:4433-45, 2004.

52. McDonald JN, Levick JR: Morphology of surface synoviocytes in situ at normal and raised joint pressure, studied by scanning electron microscopy. *Ann Rheum Dis* 47:232-40, 1988.

53. McDonald JN, Levick JR: Effect of extravascular plasma protein on pressure-flow relations across synovium in anaesthetized rabbits. *J Physiol* 465:539-59, 1993.

54. McDonald JN, Levick JR: Effect of intra-articular hyaluronan on pressure-flow relation across synovium in anaesthetized rabbits. *J Physiol* 485 (Pt 1):179-93, 1995.

55. Mithoefer K, Williams RJ, 3rd, Warren RF, Potter HG, Spock CR, Jones EC, Wickiewicz TL, Marx RG: Chondral resurfacing of articular cartilage defects in the knee with the microfracture technique. Surgical technique. *J Bone Joint Surg Am* 88 Suppl 1 Pt 2:294-304, 2006.

56. Momberger TS, Levick JR, Mason RM: Hyaluronan secretion by synoviocytes is mechanosensitive. *Matrix Biol* 24:510-9, 2005.

57. Myers SL, Brandt KD, Eilam O: Even low-grade synovitis significantly accelerates the clearance of protein from the canine knee. Implications for measurement of synovial fluid "markers" of osteoarthritis. *Arthritis Rheum* 38:1085-91, 1995.

58. Nugent-Derfus GE, Takara T, O'Neill JK, Cahill SB, Gortz S, Pong T, Inoue H, Aneloski NM, Wang WW, Vega KI, Klein TJ, Hsieh-Bonassera ND, Bae WC, Burke JD, Bugbee WD, Sah RL: Continuous passive motion applied to whole joints stimulates chondrocyte biosynthesis of PRG4. *Osteoarthritis Cartilage* 15:566-74, 2007.

59. Nugent GE, Aneloski NM, Schmidt TA, Schumacher BL, Voegtline MS, Sah RL: Dynamic shear stimulation of bovine cartilage biosynthesis of proteoglycan 4 (PRG4). *Arthritis Rheum* 54:1888-96, 2006.

60. Ogston AG, Stanier JE: The physiological function of hyaluronic acid in synovial fluid; viscous, elastic and lubricant properties. *J Physiol* 119:244-52, 1953.

61. Ostergaard M, Stoltenberg M, Lovgreen-Nielsen P, Volck B, Jensen CH, Lorenzen I: Magnetic resonance imaging-determined synovial membrane and joint effusion volumes in rheumatoid arthritis and osteoarthritis: comparison with the macroscopic and microscopic appearance of the synovium. *Arthritis Rheum* 40:1856-67, 1997.

62. Price FM, Levick JR, Mason RM: Changes in glycosaminoglycan concentration and synovial permeability at raised intra-articular pressure in rabbit knees. *J Physiol* 495 (Pt 3):821-33, 1996.

63. Price FM, Levick JR, Mason RM: Glycosaminoglycan concentration in synovium and other tissues of rabbit knee in relation to synovial hydraulic resistance. *J Physiol (Lond)* 495:803-20, 1996.

64. Roosendaal G, Vianen ME, Marx JJ, van den Berg HM, Lafeber FP, Bijlsma JW: Blood-induced joint damage: a human in vitro study. *Arthritis Rheum* 42:1025-32, 1999.

65. Ropes MW, Rossmeisl EC, Bauer W: The origin and nature of normal human synovial fluid. *J Clin Invest* 19:795-9, 1940.

66. Sabaratnam S, Arunan V, Coleman PJ, Mason RM, Levick JR: Size selectivity of hyaluronan molecular sieving by extracellular matrix in rabbit synovial joints. *J Physiol* 567:569-81, 2005.

67. Sabaratnam S, Coleman PJ, Mason RM, Levick JR: Interstitial matrix proteins determine hyaluronan reflection and fluid retention in rabbit joints: effect of protease. *J Physiol* 578:291-9, 2007.

68. Safari M, Bjelle A, Gudmundsson M, Hogfors C, Granhed H: Clinical assessment of rheumatic diseases using viscoelastic parameters for synovial fluid. *Biorheology* 27:659-74, 1990.

69. Schmid K, Macnair MB: Characterization of the proteins of human synovial fluid in certain disease states. *J Clin Invest* 35:814-24, 1956.

70. Schmid K, Macnair MB: Characterization of the proteins of certain postmortem human synovial fluids. *J Clin Invest* 37:708-18, 1958.

71. Schmidt TA, Gastelum NS, Nguyen QT, Schumacher BL, Sah RL: Boundary lubrication of articular cartilage: role of synovial fluid constituents. *Arthritis Rheum* 56:882-91, 2007.

72. Schmidt TA, Sah RL: Effect of synovial fluid on boundary lubrication of articular cartilage. *Osteoarthritis Cartilage* 15:35-47, 2007.

73. Schumacher BL, Block JA, Schmid TM, Aydelotte MB, Kuettner KE: A novel proteoglycan synthesized and secreted by chondrocytes of the superficial zone of articular cartilage. *Arch Biochem Biophys* 311:144-52, 1994.

74. Schumacher BL, Hughes CE, Kuettner KE, Caterson B, Aydelotte MB: Immunodetection and partial cDNA sequence of the proteoglycan, superficial zone protein, synthesized by cells lining synovial joints. *J Orthop Res* 17:110-20, 1999.

75. Schumacher BL, Schmidt TA, Voegtline MS, Chen AC, Sah RL: Proteoglycan 4 (PRG4) synthesis and immunolocalization in bovine meniscus. *J Orthop Res* 23:562-8, 2005.

76. Schur PH, Sandson J: Immunologic studies of the proteins of human synovial fluid. *Arthritis Rheum* 6:115-29, 1963.

77. Schurz J, Ribitsch V: Rheology of synovial fluid. *Biorheology* 24:385-99, 1987.

78. Scott D, Coleman PJ, Mason RM, Levick JR: Glycosaminoglycan depletion greatly raises the hydraulic permeability of rabbit joint synovial lining. *Exp Physiol* 82:603-6, 1997.

79. Scott D, Levick JR, Miserocchi G: Non-linear dependence of interstitial fluid pressure on joint cavity pressure and implications for interstitial resistance in rabbit knee. *Acta Physiol Scand* 179:93-101, 2003.

80. Sellam J, Berenbaum F: The role of synovitis in pathophysiology and clinical symptoms of osteoarthritis. *Nat Rev Rheumatol* 6:625-35, 2010.

81. Shoemaker PA, Schneider D, Lee MC, Fung YC: A constitutive model for two-dimensional soft tissues and its application to experimental data. *J Biomech* 19:695-702, 1986.

82. Simkin PA: Synovial permeability in rheumatoid arthritis. *Arthritis Rheum* 22:689-96, 1979.

83. Simkin PA: Physiology of normal and abnormal synovium. *Semin Arthritis Rheum* 21:179-83, 1991.

84. Simkin PA: Synovial perfusion and synovial fluid solutes. *Ann Rheum Dis* 54:424-8, 1995.

85. Sliwinski AJ, Zvaifler NJ: The removal of aggregated and nonaggregated autologous gamma globulin from rheumatoid joints. *Arthritis Rheum* 12:504-14, 1969.

86. Smith MM, Ghosh P: The synthesis of hyaluronic acid by human synovial fibroblasts is influenced by the nature of the hyaluronate in the extracellular environment. *Rheumatol Int* 7:113-22, 1987.

87. Stevens CR, Blake DR, Merry P, Revell PA, Levick JR: A comparative study by morphometry of the microvasculature in normal and rheumatoid synovium. *Arthritis Rheum* 34:1508-13, 1991.

88. Suter ER, Majno G: Ultrastructure of the Joint Capsule in the Rat: Presence of Two Kinds of Capillaries. *Nature* 202:920-1, 1964.

89. Swann DA, Slayter HS, Silver FH: The molecular structure of lubricating glycoprotein-I, the boundary lubricant for articular cartilage. *J Biol Chem* 256:5921-5, 1981.

90. Swann DA, Sotman S, Dixon M, Brooks C: The isolation and partial characterization of the major glycoprotein (LGP-I) from the articular lubricating fraction from bovine synovial fluid. *Biochem J* 161:473-85, 1977.

91. Temple MM, Nguyen Q, Moy TM, Cardenas CO, Nguyen TD, Bugbee WD, Wong VW, Sah RL: Synovial fluid and cartilage degeneration modulate in vitro wear of articulating cartilage. *Trans Orthop Res Soc,* 32:611, 2007.

92. Upton ML, Gilchrist CL, Guilak F, Setton LA: Transfer of macroscale tissue strain to microscale cell regions in the deformed meniscus. *Biophys J* 95:2116-24, 2008.

93. Vawter DL, Fung YC, West JB: Elasticity of excised dog lung parenchyma. *J Appl Physiol* 45:261-9, 1978.

94. Wallis WJ, Simkin PA, Nelp WB: Protein traffic in human synovial effusions. *Arthritis Rheum* 30:57-63, 1987.

95. Walsh DA, Wade M, Mapp PI, Blake DR: Focally regulated endothelial proliferation and cell death in human synovium. *Am J Pathol* 152:691-702, 1998.

CHAPTER 2:

FLUID MOVEMENT AND JOINT CAPSULE STRAIN DUE TO FLEXION IN RABBIT KNEES

2.1 Abstract

Diarthrodial joints are freely moveable joints containing synovial fluid (SF) within a connective tissue joint capsule that allows for low-friction and low-wear articulation of the cartilaginous ends of long bones. Biomechanical cues from joint articulation regulate synoviocyte and cartilage biology via joint capsule strain, in turn altering the composition of SF. Joint flexion is clinically associated with pain in knees with arthritis and effusion, with the nociception possibly originating from joint capsule strain. The hypothesis of this study was that knee fluid volume distribution and joint capsule strain are altered with passive flexion in the rabbit model. The aims were to: a) determine the volume distribution of fluid in the joint at different total volumes and with flexion of rabbit knees *ex vivo*, b) correlate the volume distribution for the *ex vivo* model to *in vivo* data, and c) determine the strains at different locations in the joint capsule with flexion. During knee flexion, ~20% of anteriorly located joint fluid moved posteriorly, correlating well with the fluid motion observed in *in vivo* joints. Planar joint capsule principal strains were ~100% (tension) in the proximal-distal direction and ~-40% (shortening) in the circumferential direction, relative to the femur

axis and 30° strain state. The joint capsule strains with flexion are consistent with the mechanics of the tendons and ligaments from which the capsule tissue is derived. The movement and mixing of SF volume with flexion determine the mechanical and biological fluid environment within the knee joint. Joint fluid movement and capsular strains affect synovial cell biology and likely modulate trans-synovial transport.

2.2 Introduction

Diarthrodial joints are freely moveable and contain synovial fluid (SF) within a connective tissue capsule that allows for low-friction and low-wear articulation. In the knee, the joint capsule (a.k.a. articular capsule or capsular ligament) is a thin, but strong and flexible fibrous membrane derived from the fascia lata, quadriceps tendon, and surrounding ligaments [10]. The intra-articular face of the joint capsule is covered by the synovial membrane, which contains a highly fibrillar intimal matrix layer, synovium, that is densely populated with synoviocytes [22, 30].

Biomechanical cues from joint articulation regulate synoviocyte biology, in turn altering the composition of SF. SF contains several lubricant molecules, including high molecular weight hyaluronan (HA) [1, 6, 21] mainly secreted by synoviocytes [31]. The secretion rate of HA by synoviocytes is mechanosensitive at the cellular [24] and joint scale [12]. Despite the mechanosensitive nature of these tissues, the biomechanics of knee joint capsule *in situ* are largely unexplored.

The overall and local SF volumes are important physiological quantities, as the biological and biomechanical effects of SF are concentration-dependent, and joint effusions may alter such concentrations. SF exhibits a number of volume-dependent mechanobiological features, including modulation of tissue biology by providing cytokines and alteration of joint friction and wear biomechanics based on lubricant concentration [29]. SF volume can be increased with therapeutic injections, in diseases such as osteoarthritis (OA), and after traumatic injury.

In addition to the basic science motivations for understanding synovial fluid movement and capsule strain during articulation, joint flexion is clinically associated with pain in knees with effusion, and the nociception possibly originates from joint capsule strain. Patients typically maintain knees with effusion at 30-60° flexion, with pain and intra-articular fluid pressure increasing during further flexion [8, 13]. The nociception of such joint pain may originate in the capsule, as joint capsule strain has been correlated with afferent nerve impulses in an animal model [17]. Elucidation of the patterns of fluid movement and capsule strain with flexion may help explain the origin of this pain.

Micro-computed tomography (μCT) enhanced with contrast agents can provide high resolution 3D structural information of soft tissues and cavities, but has not previously been applied to quantify and localize joint fluid volume or capsule strains. Barium sulfate is a nearly insoluble contrast agent with high X-ray attenuation used clinically with CT to image the gastrointestinal tract [14, 25]. Intra-articular injection of a contrast agent suspension allows for visualization of the bursae that compose the joint space.

The rabbit model has frequently been used for studies in biomechanics and orthopedics. The structural mechanics of the knee joint have been investigated using the rabbit model, both *ex vivo* [33] and *in vivo* [11]. In addition, rabbit models of osteoarthritis, such as the anterior cruciate ligament transection model, have been well-characterized [3, 28, 34]. In this study, *in vivo* and *ex vivo* fluid motions with flexion were determined and correlated; capsule strains were determined *ex vivo*, as

the imaging and marker methods could not be used *in vivo* due to the size of live rabbits and the capacity of the μCT scanner.

Thus, the hypothesis of this study was that knee fluid volume distribution and joint capsule strain are altered with flexion. The aims were to: 1) determine the volume distribution of fluid in the joint at different total volumes and with flexion in *ex vivo* rabbit knees, 2) compare and correlate the volume distribution for the *ex vivo* model with the more physiological *in vivo* data, and 3) determine the strains at different locations in the joint capsule with flexion *ex vivo*.

2.3 Materials and Methods

2.3.1 Study Design

Fluid movement and joint capsule strains during flexion were investigated using *ex vivo* and *in vivo* rabbit knees. The joint space was divided into 4 quadrants – medial and lateral anterior and posterior (**Fig. 2.1A-C**) – following knee anatomy, which includes distinct, but connected, medial and lateral posterior bursae, and the anterior bursa being conveniently divided along the proxial-distal axis by the patellofemoral groove. Fluid volume was localized to these quadrants in (n=6) *ex vivo* rabbit knees (3 right, 3 left) using contrast-enhanced μCT. SF volume in rabbit knees has been estimated as 50-400μL in normal knees, increasing to 600-2200 μL with induced arthritis or arthroplasty [4, 5, 7, 20]. Rabbit knees were injected sequentially with volumes in these ranges, totaling (i) 0.05mL, (ii) 0.25mL, and (iii) 0.95mL and imaged by μCT at 60° flexion, and also subsequently imaged (with 0.95mL) at (iv) 30° and (v) 90° flexion, to mimic flexion during hopping (~30-60°) and sitting (~90°) [19].

As a more physiological comparison to the *ex vivo* data, fluid was also localized in *in vivo* rabbit knees using plain X-rays. Six rabbits were anesthetized and one knee (3 right, 3 left) received a 0.95mL injection of contrast agent. Frontal and anteroposterior (AP) plain X-rays were taken at 30, 60, and 90° flexion and the % fluid area in the medial vs lateral and anterior vs posterior joint spaces was assessed and compared to the μCT data.

Plane strains in the joint capsule during flexion were determined from marker locations in *ex vivo* rabbit knees. Principal strains for 30 to 60°, 60 to 90°, and 30 to 90° flexions were determined in (n=6) rabbit knees (3 right, 3 left) by creating triads of radio-opaque fiducial markers using stainless steel suture and tracking their relative motion after scanning the joints with contrast-enhanced μCT at 30, 60, and 90° flexion. Principal strains were calculated from the relative changes in the triad coordinates in the proximal-distal and circumferential directions as defined by the long axis of the femur.

2.3.2 Animal Use, Tissue Harvest, and Storage

All animal protocols for these studies were approved by the local IACUC committee. For the *in vivo* experiments, New Zealand white rabbits (~4.5kg) were anesthetized, contrast agent was injected into one knee, X-rays were taken at 3 different flexion angles, and then the rabbit was euthanized. For the *ex vivo* experiments, the hind limbs of similar rabbits being euthanized for other purposes were obtained immediately after euthanasia by removing the skin, transecting the muscle and soft tissue near the greater trochanter of the femur, dislocating the hip, and storing at -80°C until use.

2.3.3 μCT and X-ray Imaging

Contrast-enhanced μCT and X-ray imaging were performed to determine fluid volumes and areas. Phosphate-buffered saline with 60% barium sulfate (Sigma-Aldrich Co., Saint Louis, MO) was used as the contrast agent, analogous to that used

clinically. Volumes of contrast agent were injected into the joint space via 22ga hypodermic needle through the patellar ligament. After injection, joints were gently flexed to distribute the contrast agent throughout the joint space.

Ex vivo rabbit hind limbs were thawed, trimmed, and imaged on a μCT scanner. Thawed limbs were trimmed by transecting mid-femur and mid-tibia without opening the joint capsule and keeping the musculature surrounding the capsule intact. Joints were scanned in air in a Skyscan 1076 μCT scanner (Skyscan, Kontich, Belgium) at 70kV and $(35\mu m)^3$ voxel resolution. Full data sets were reconstructed with NRecon software (Skyscan) and thresholded above 80 grayscale to select only the contrast media, as its attenuation was much larger than bone. Data sets were divided into volumes of interest corresponding to the compartment quadrants, as above. The volume of contrast agent in each quadrant was determined using CTAn (Skyscan), and volumes were also normalized to the total volume in each knee to determine relative volume (%).

The hind limbs of anesthetized rabbits were imaged *in vivo* using plain X-rays and analyzed for fluid movement with flexion in 2D. AP and frontal views of the knee were taken using direct digital radiography CCD imaging at 52kV, 10mA·s, and 356dpi (NAOMI-DR, RF Co., Nagano, Japan). X-ray images were locally thresholded using CTAn software, with the threshold level set as the minimum grayscale value between the contrast agent and bone peaks in a grayscale histogram made from the region of interest surrounding the knee. The fluid areas in the anterior and posterior (on the AP views, divided as in **Fig. 2.1C**) and medial and lateral (on the frontal views, divided through the patellofemoral groove as in **Fig. 2.1A, B**) regions were

determined and normalized as % of the total fluid area detected for each view. Virtual X-ray images in the AP and frontal views, directly analogous to the X-ray data, were constructed from the μCT data sets by collapsing all the 3D set slices to a single 2D plane using a custom Matlab program. Virtual X-ray images were analyzed as described above for X-ray images.

2.3.4 Strain Analysis

Fiducial markers were created on the joint capsule of *ex vivo* rabbit knees before scanning at different flexion angles. The joint space was injected with 0.95mL of contrast agent, and nine lengths of stainless steel 5-0 suture (Med-Vet International, Mettawa, IL) were stitched through the joint capsule: 3 proximal to the patella, 3 in the central patellar region, and 3 distal to the patella. The 9 sutures entered on one side of the capsule and exited on the far side, creating 18 radio-opaque fiducial markers on the joint capsule where the sutures intersected the contrast agent, grouped as triads in 6 locations around the patella. Joint were then scanned, as before, at 30, 60, and 90° flexion and reconstructed in NRecon. The coordinates of each fiducial marker were recorded for all scans in DataViewer (Skyscan). In addition, a vector pointing proximal to distal along the centroid of the femur axis deep to each triad was defined from two points along the femur axis.

Principal strains in the joint capsule for 30 to 60° and 60 to 90° flexions were calculated from the relative change in fiducial marker coordinates. A change of basis was performed to map the triad locations from the arbitrary scanner coordinates to a coordinate system for each triad within the plane of the tissue, as defined by the

normal vector to the triad plane, the orthogonal projection of the proximal-distal vector on the triad plane, and their cross-product, pointing in the circumferential direction towards the patella. The two-dimensional components of Green's strain E_{ij} were calculated from

$$ds^2 - ds_0^2 = 2E_{ij}dX_i dX_j\,,\ i,j = 1,\ 2 \qquad \text{(Eq. 2.1)}$$

where $ds_0^2 = dX_i dX_j$ is a squared segment length of the triad in the reference configuration, and ds^2 is the squared length in the deformed configuration [9]. Principal strains and the angle of the principal axes were calculated from the Green's strain components.

2.3.5 µCT and X-ray Measurement Precision

The precision of the µCT data and X-ray measurement methods were determined by 3 repeated scans and analysis of rabbit knees with contrast agents. For the µCT data, the average measured standard deviation (SD) in fluid area from virtual X-ray reconstructions was 1.2%. The average SD in volume determined from the reconstruction data was <1µL (0.4%) for repeated scans of 0.25mL volumes. Fluid volume loss due to leakage from the joint space was not detectable at 0.05 or 0.25mL, and a loss rate of approximately 1µL/min was determined for the 0.95mL volume, leading to an estimated loss of ~45µL (~4.7%) over the course of the 3 experimental µCT scans at that volume. The average SD in fiducial marker location between repeated scans was 73µm (~3.4%), indicating relative stability of the sutures, since the

average measured distance between markers to determine strain was 2160μm. For the X-ray data, the average SD in fluid area was 3.6%.

2.3.6 Statistical Analysis

Data are expressed as mean±SEM, values of $P<0.05$ were considered significant. Measured volume was compared to injected volume and over flexion angles by linear regression. Repeated measures ANOVAs were used to assess the effects of injected volume and flexion angle on quadrant volumes with Bonferroni-corrected post-hoc tests. 2-way ANOVAs were used to assess the effect of side with injection volume and flexion angle. 1-way ANOVAs were used to assess the effect of flexion angle on % anterior and medial fluid detection with Tukey post-hoc tests. 3-way ANOVAs were used to assess the effects of axis, side, and triad location on strain values. Percentile data were arcsine transformed for normality. Statistical analyses were performed using Systat 10.2 (Systat Software Inc, Chicago, IL).

2.4 Results

2.4.1 Fluid Distribution

Fluid volume was found mostly in the anterior compartment at all injection volumes. The attenuation of the contrast agent was higher than bone, allowing for clear distinction between the fluid space and bone, as seen in typical transverse and longitudinal μCT slices of joints scanned at 60° flexion (**Fig. 2.1B-G**). Qualitatively, fluid volume increased with injection volume at 60° flexion, and the majority of fluid volume was in the anterior compartment, though the relative amount in the posterior compartment increased at higher volumes (**Fig. 2.1D-G**).

Detected fluid volume scaled linearly with injection volume and volume was not detectably lost during scans at multiple flexion angles. The fluid volume detected was a high proportion (85%) of the total injected volume ($P<0.001$), and the injected and detected volumes were highly correlated ($R^2=0.99$, **Fig. 2.2A**). The fluid volume detected for the 0.95mL injection volume remained constant after successive scans at different flexion angles ($P=0.27$, **Fig. 2.2B**).

Quantification of absolute and relative volumes in each compartment mirrored the trends observed qualitatively. The precision of the measured fluid volumes was 0.4% (<1μL of 250 injected), adequate for the range of recovered volumes, which accounted for 2-40%, 6-37%, and 11-39% of that injected (50, 250, and 950μL, respectively). With increasing injection volume, side (medial vs lateral, $P<0.0001$), injection volume ($P<0.0001$), and the interaction side*injection volume ($P<0.0001$) affected detected volume in the anterior compartment, and injection volume

(P<0.0001) affected detected volume in the lateral compartment (**Fig. 2.3A**). All in-quadrant measured volumes (0.05 vs 0.25 vs 0.95mL) were significantly different from each other (P<0.001). The fluid volume % decreased in the anterior medial and increased in the posterior medial quadrants between 0.05mL and 0.95mL injections (P<0.05, **Fig. 2.3B**).

Fluid shifted from the anterior lateral to the posterior compartments at higher flexion angles. With increasing flexion, side (P<0.0001), flexion angle (P<0.0001), and side*flexion (P<0.0001) affected detected volume in the anterior compartment, and flexion (P<0.0001) affected detected volume in the posterior compartment (**Fig. 2.3A**). At 30° and 60° flexion, fluid volume was localized primarily in the anterior lateral quadrant; with flexion to 90°, fluid shifted to the posterior lateral and medial quadrants (P<0.05, **Fig. 2.3A, B**). The posterior shift of fluid volume with flexion angle was also observed in 3D volume renderings, which show the geometry of the joint space (**Fig. 2.4**).

2.4.2 Ex Vivo and In Vivo Fluid Localization

The effects of flexion angle on % fluid area detected by virtual X-rays from *ex vivo* μCT data correlated well with that detected on digital X-rays of *in vivo* rabbit knees. The precision of measured % fluid areas was 1.2% by μCT and 3.6% by X-ray, substantially less than the range of measured areas (48-83%). Flexion angle significantly affected the % fluid detected in the anterior region assessed by X-ray (P<0.001) and μCT (P<0.001, **Fig 2.5A**). Flexion angle did not affect the % fluid detected in the medial region assessed by μCT (P=0.34) or X-ray (P=0.67, **Fig 2.5B**).

The slopes of the regression lines through the individual X-ray and μCT data sets in the anterior compartment were significant ($P<0.001$ and $P<0.0001$, respectively), and not different than each other ($P=0.99$, **Fig. 2.5C**). In the medial compartment, the slopes were not significant ($P=0.86$ and $P=0.30$, respectively), and not different than each other ($P=0.38$, **Fig. 2.5D**).

2.4.3 Joint Capsule Strain with Flexion

The joint capsule, relative to the 30° strain state, stretched in the proximal-distal direction and shortened in the circumferential direction with flexion. The precision of strain determination was 3.4%, substantially less than the range of experimental strains (15-178%). Strain was evaluated at 6 locations around the patella (**Figs. 2.6, 2.7A-C**) and primarily occurred along the proximal-distal axis. For flexion from 30 to 60°, axis (P1 vs P2, $P<0.0001$) and location (proximal vs central vs distal, $P<0.05$) significantly affected strain values, with P1 positive and larger in magnitude than P2, which were negative (**Fig. 2.7B, D**). Strain magnitudes tended to be larger in the distal than proximal regions ($P<0.05$), and there was a trend for an effect of side (medial vs lateral, $P=0.08$). For flexion from 60 to 90°, axis ($P<0.0001$) significantly affected the strain values, (**Fig. 2.7C, E**) though side was not significant ($P=0.35$). Similarly, for flexion from 30 to 90°, axis ($P<0.0001$) significantly affected the strain values (**Fig. 2.7F**), and side was not significant ($P=0.99$).

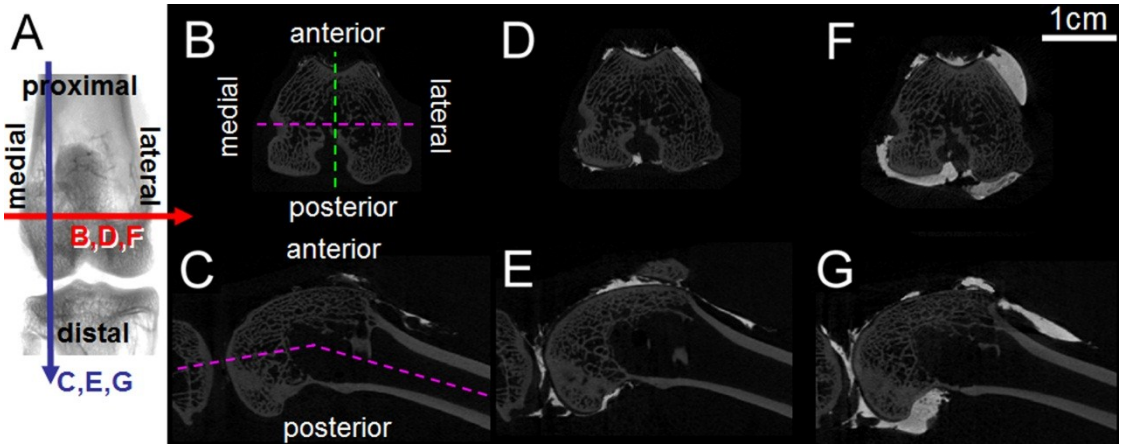

Figure 2.1: Typical μCT slices (**A**) of *ex vivo* rabbit knees (right knee shown) with 0.05 (**B,C**), 0.25 (**D,E**), or 0.95mL (**F,G**) injected fluid volume in transverse (**B,D,F**) or longitudinal (**C,E,G**) sections at 60° flexion.

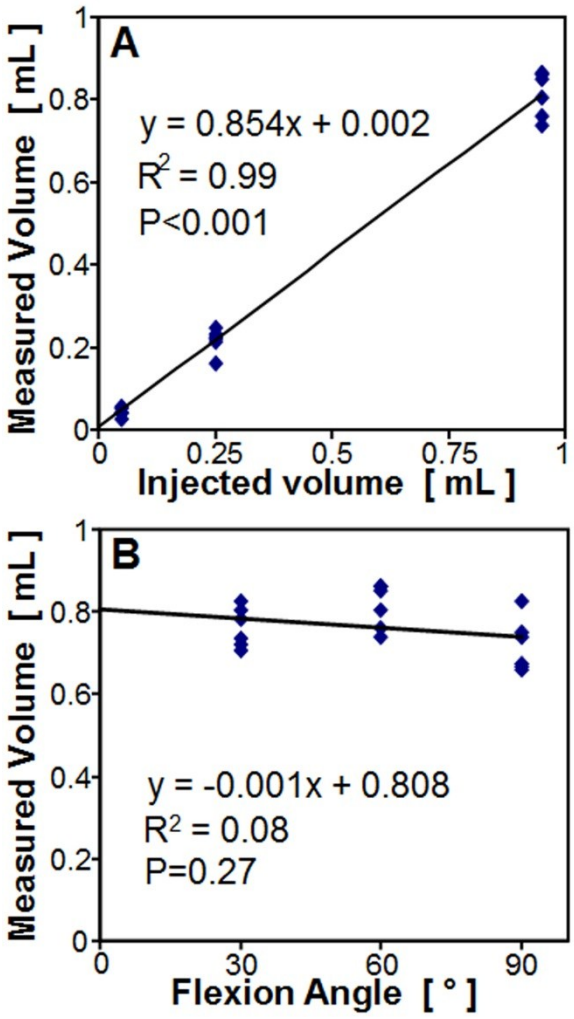

Figure 2.2: Relationship between joint space volume, injected volume, and knee flexion angle. Measured volume vs (**A**) injected volume and (**B**) flexion angle. Mean±SEM, n=18.

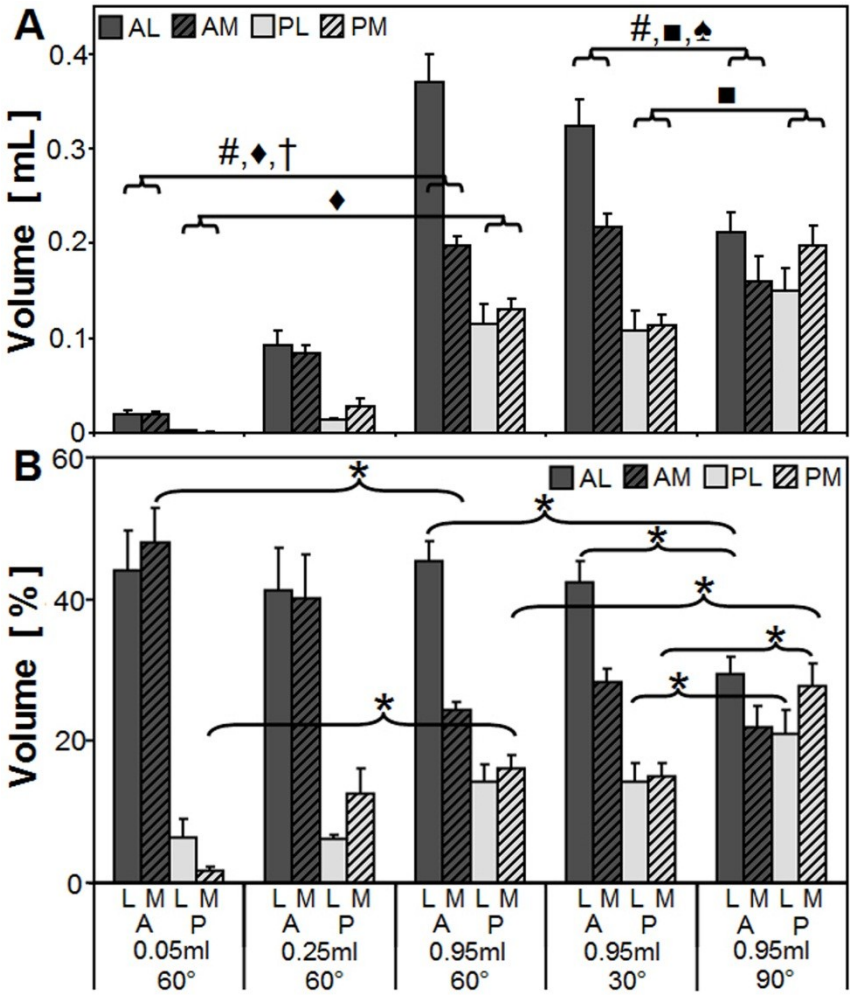

Figure 2.3: Measured volume (**A**) and % volume (**B**) by compartment for 3 injection volumes (0.05, 0.25, and 0.95mL) and 3 flexion angles (60°, 30°, 90°) A: anterior, P: posterior, M: medial, L: lateral. * P<0.05. #,♦,†, ■, ♠: P<0.0001 effect for side (#), injection volume (♦), side*injection volume (†), flexion (■), and side*flexion (♠). All in-quadrant measured volume comparisons (0.05 vs 0.25 vs 0.95mL) were significantly different from each other (not shown in symbols, P<0.001).

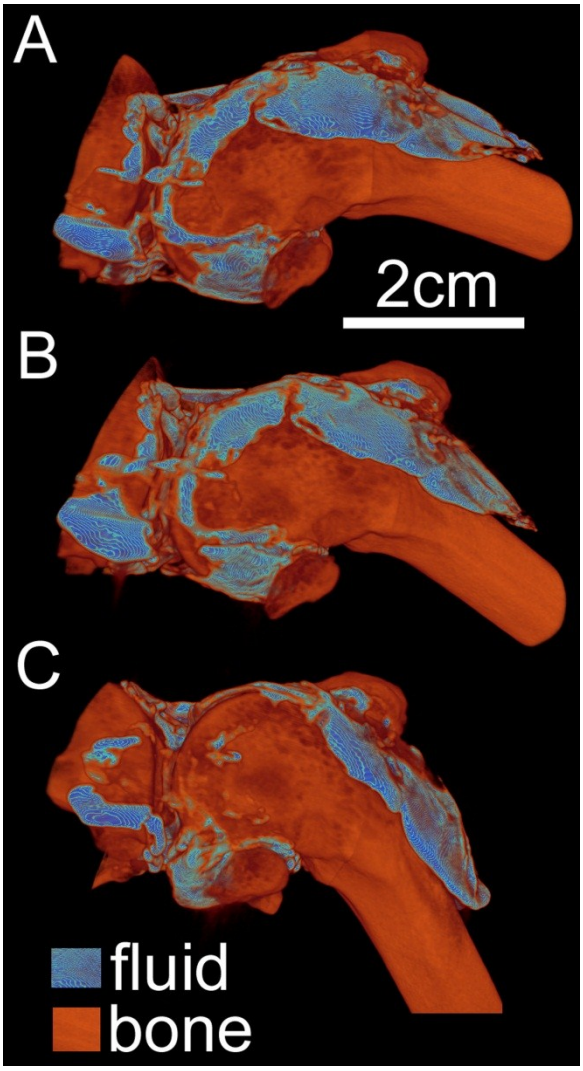

Figure 2.4: Typical volume rendering of fluid and bone at 3 joint flexion angles (**A**) 30°, (**B**) 60°, (**C**) 90° after 0.95mL fluid injection.

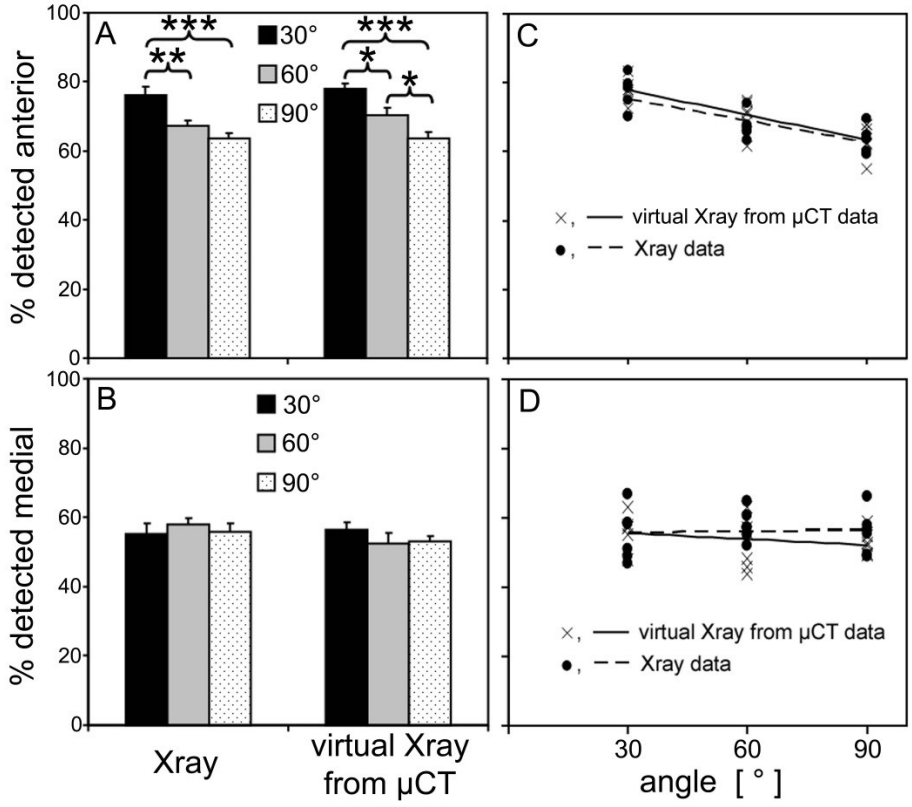

Figure 2.5: Fluid detected in the (**A**) anterior and (**B**) medial compartments as a % of the total detected, assessed by virtual X-rays from µCT data for *ex vivo* joints and with lateral and AP X-rays of *in vivo* rabbit knees, and correlations showing similar flexion effects from both methods in the anterior compartment (**C**) and no effects in the medial compartment (**D**). The slopes of the regression lines through the X-ray and µCT data were each individually significant ($P<0.001$, $P<0.0001$) and not different than each other ($P=0.99$) in the anterior compartment, and not significant ($P=0.86$, $P=0.30$) in the medial compartment. *: $P<0.05$, **: $P<0.01$, ***: $P<0.001$.

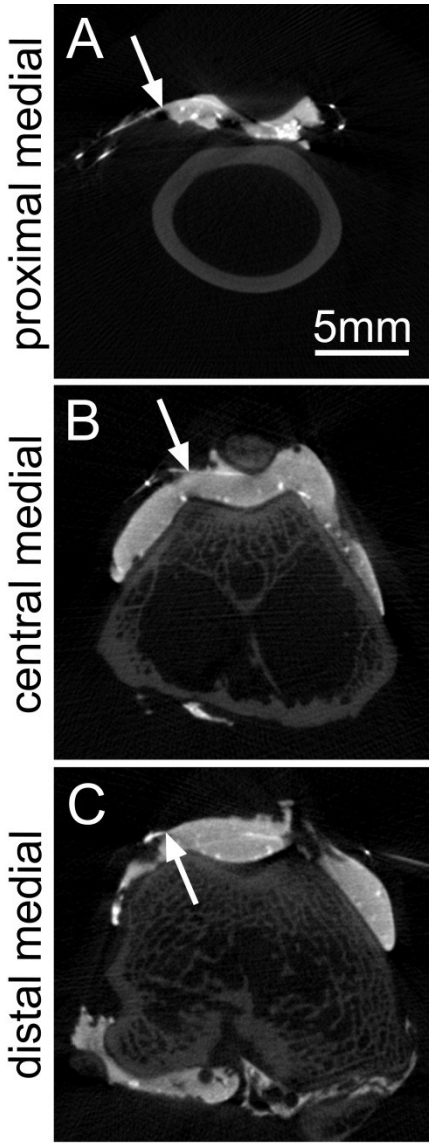

Figure 2.6: Example transverse slices showing the radio-opaque fiducial marker locations on the joint capsule as the intersections of the steel suture and contrast agent in the 3 medial regions analyzed.

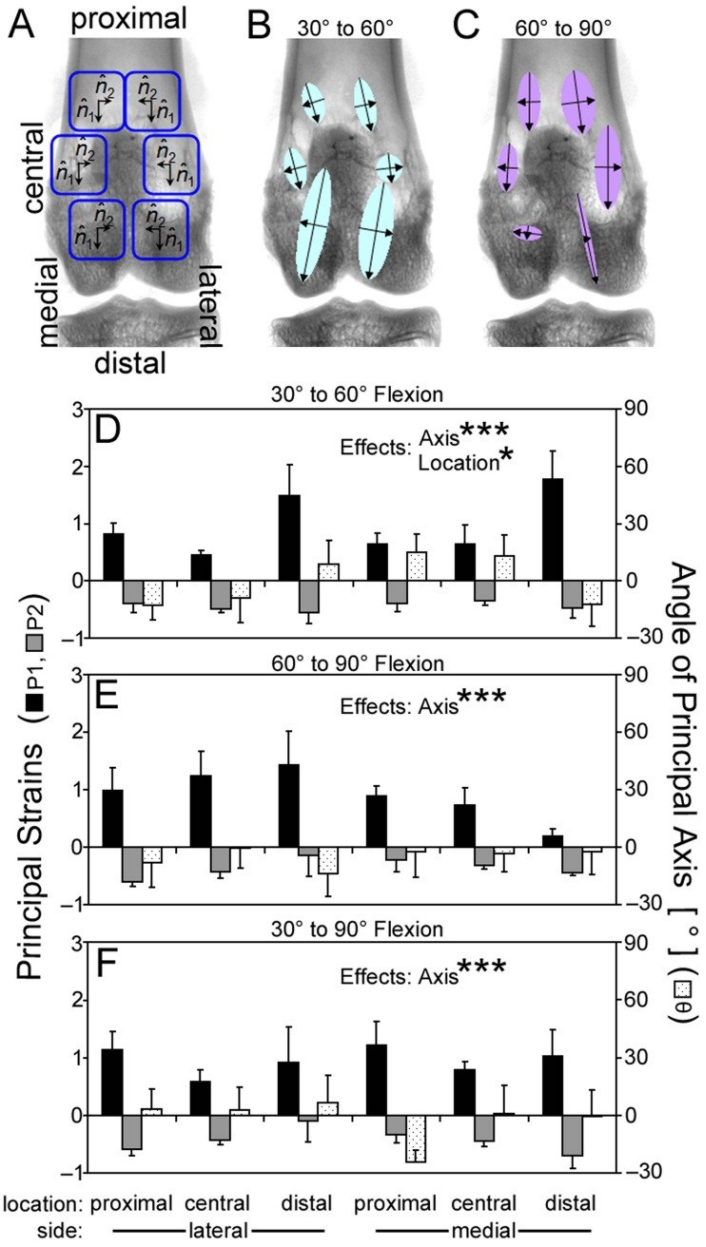

Figure 2.7: Joint capsule strain in *ex vivo* rabbit knees at (**A**) 6 locations, with principal strains and directions depicted as vectors at those locations (**B** and **C**). Detailed principal strains (P1 and P2) and principal axis angle (θ) for (**D**) 30° to 60°, (**E**) 60° to 90°, and (**F**) 30° to 90° flexions. There were significant effects of principal axis (P1 vs P2) and location (proximal vs central vs distal patellar) on strain values. *: P<0.05, ***:P<0.0001.

2.5 Discussion

These results demonstrate that during knee flexion, joint fluid moves posteriorly and the joint capsule is variably strained based on location. Fluid volume in the knee, as observed by contrast enhanced μCT (**Figs. 2.1 and 2.2**), pools mainly in the anterior (supra- and latero-patellar) bursae, increasing more in the anterior lateral compared to medial sides with increasing volume (**Fig. 2.3**). With increasing joint flexion, fluid volume moves from the anterior to the posterior bursae (**Figs. 2.3** and **2.4**), which was also found in the *in vivo* joints (**Fig. 2.5**). Planar joint capsule strains indicated stretch in the proximal-distal direction and shortening in the circumferential direction with flexion from the 30° strain state (**Fig. 2.7**), which may be responsible for the movement of fluid.

Volume shifts and capsule strains reported here were determined *ex vivo*, which may differ from an *in vivo* joint. For *ex vivo* joints, the contrast enhanced imaging methods resulted in detection of <100% (85%, **Fig. 2.2**) of the injected volume, likely due to minor fluid loss through the synovial lining. The inactive musculature surrounding the joint and loss of tension in the quadriceps tendon in *ex vivo* samples may have affected the measurements made. In addition, the capsule strains were determined after injection of fluid, mimicking an inflamed joint, likely resulting in the strain estimates being larger than would be present for a normal joint. However, the trends in the *ex vivo* % fluid data correlate well with analogous *in vivo* imaging data. With only one small difference between the μCT and X-ray data (**Fig. 2.5A**), suggesting that the μCT data may be more sensitive than the X-ray data, the *ex*

vivo samples appear to be reasonable approximations of the *in vivo* situation. The use of different groups of animals for the two methods illustrates the trends are not animal-specific, and points to their robustness despite inter-animal variability.

The movement and mixing of SF volume with flexion are likely important determinants of the mechanical and biological fluid environment within the knee joint. Increasing flexion angle from 30 to 90° shifts ~20% of the anterior volume to the posterior compartments. This shift in fluid towards the posterior bursae with flexion is consistent with a qualitative description of joint fluid motion in human knees seen via X-ray after injection of 3-4mL of contrast agent [23]. Such SF mixing is important for nutrient transport from synovium to cartilage [15], lubricant distribution, and movement of cytokines and cellular signaling molecules throughout the joint. Joint capsule strain and posterior fluid motion may also contribute to pain via intra-articular pressure and capsule strain during flexion.

The anisotropy and Poisson's ratio of joint capsule strains are consistent with the mechanical properties of tendon, the tissue from which the capsule is derived. Tendons are highly anisotropic, with a larger modulus in the fiber-aligned compared to transverse direction, and an average Poisson's ratio of ~0.5 in the transverse direction [18]. Similarly, the principal strains in the joint capsule were also larger overall in the proximal-distal direction, which is the fiber-aligned direction for the quadriceps tendon, than in the transverse direction. Further, the strains were negative in the transverse direction, indicating circumferential shortening, corresponding to a Poisson's ratio of ~0.4 for the joint capsule.

The strains reported here are for the relative change in capsule tissue between flexion angles, which may be different than the absolute strain state as defined by changes from a completely unloaded condition. The capsule tissue deforms during both flexion and extension, making defining an unloaded, laxity-free state difficult. The strains are reported for increasing flexion angles since joint fluid appears to move from anterior to posterior with flexion, suggesting a reduction in anterior bursae volume, which is consistent with anterior capsule lengthening and circumferential shortening.

Joint capsule strains and fluid movement likely alter synovial cell biology, as well as the fluid and macromolecular transport across synovium. Since HA secretion by synoviocytes is mechanosensitive [12, 24], the fluid volume shifts and capsule strains during flexion may contribute to the regulation of lubricant secretion. The synovium layer is a thin ~20-50μm [2, 30, 32], disorganized extracellular matrix [16, 26, 27] probably with compliant mechanical properties. The thicker and more fibrous joint capsule, to which synovium is attached, likely determines its mechanical state. However, the translation of strain from capsule to synovium is complicated as the synovium layer is not completely flat, it contains villi and fringe-like folds. Under strain, the synovium layer probably undergoes a complex mixture of unfolding and strain based on local microstructure (**Fig. 2.8**). Thus, although the capsule strains are important determinants of the local strains felt by synoviocytes, analysis of local microstructural deformations would facilitate understanding how the macroscopic capsule strain translates to local cellular deformations. In addition to cellular responses, fluid and macromolecular transport across synovium from the vasculature

and to the lymphatics are likely altered by joint capsule and synovium strain due to changes in the synovium layer thickness and extracellular matrix fiber density.

The approach of assessing fluid volume movement and tissue strain with radio-opaque contrast and μCT may be useful for a variety of experimental studies. Examination of fluid movement and capsular strains in other joints than the knee, such as the hip and shoulder, use of various contrast agents, and in various models of arthritis may be of clinical interest. In addition, following and quantifying the movement of meniscus, muscle, tendon, and ligaments during joint articulation may be possible.

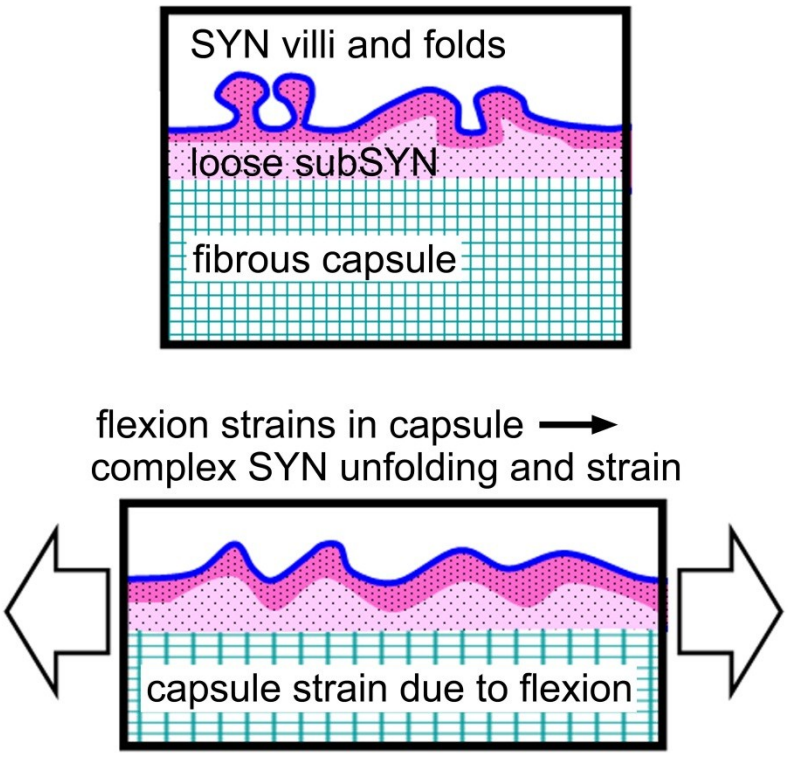

Figure 2.8: Schematic depicting structural deformation due to strain in the joint capsule tissue translating through the loose connective layer, subsynovium (subSYN), to a complex mixture of synovium (SYN) unfolding and strain, leading to synoviocyte deformation determined by local microstructure.

2.6 Acknowledgments

Chapter 2, in full, is reproduced from the *Journal of Biomechanics*, volume 44, number 16, p. 2761-7, 2011 with permission from Elsevier. The dissertation author was the primary author and thanks co-authors Koichi Masuda, and Robert L. Sah. The authors would like to thank Esther Cory Burak and Elise F. Morgan for their helpful discussions. This work was supported by grants from the National Institute of Arthritis, Musculoskeletal and Skin Diseases, a Ruth L. Kirschstein National Research Service Award predoctoral fellowship from the National Institute on Aging (for WJM), and an award to UCSD from the Howard Hughes Medical Institute through the HHMI Professors Program (for RLS).

2.7 References

1. Balazs EA: The physical properties of synovial fluid and the special role of hyaluronic acid. In: *Disorders of the Knee,* ed. by AJ Helfet, Lippincott Co., Philadelphia, 1974, 63-75.

2. Castor CW: The microscopic structure of normal human synovial tissue. *Arthritis Rheum* 3:140-51, 1960.

3. Chang DG, Iverson EP, Schinagl RM, Sonoda M, Amiel D, Coutts RD, Sah RL: Quantitation and localization of cartilage degeneration following the induction of osteoarthritis in the rabbit knee. *Osteoarthritis Cartilage* 5:357-72, 1997.

4. Choi SI, Heo TR, Min BH, Cui JH, Choi BH, Park SR: Alleviation of osteoarthritis by calycosin-7-O-beta-D-glucopyranoside (CG) isolated from Astragali radix (AR) in rabbit osteoarthritis (OA) model. *Osteoarthritis Cartilage* 15:1086-92, 2007.

5. Coleman PJ, Scott D, Ray J, Mason RM, Levick JR: Hyaluronan secretion into the synovial cavity of rabbit knees and comparison with albumin turnover. *J Physiol* 503 (Pt 3):645-56, 1997.

6. Dahl LB, Dahl IM, Engstrom-Laurent A, Granath K: Concentration and molecular weight of sodium hyaluronate in synovial fluid from patients with rheumatoid arthritis and other arthropathies. *Ann Rheum Dis* 44:817-22, 1985.

7. Delecrin J, Oka M, Takahashi S, Yamamuro T, Nakamura T: Changes in joint fluid after total arthroplasty. A quantitative study on the rabbit knee joint. *Clin Orthop Relat Res*:240-9, 1994.

8. Eyring EJ, Murray WR: The Effect of Joint Position on the Pressure of Intra-Articular Effusion. *J Bone Joint Surg Am* 46:1235-41, 1964.

9. Fung YC, Tong P. Classical and Computational Solid Mechanics. Singapore: World Scientific Publishing Company; 2001.

10. Gray H. Anatomy of the human body. In: WH Lewis, ed. 20 ed. Philadelphia: Lea & Febiger; 1918.

11. Gushue DL, Houck J, Lerner AL: Rabbit knee joint biomechanics: motion analysis and modeling of forces during hopping. *J Orthop Res* 23:735-42, 2005.

12. Ingram KR, Wann AK, Angel CK, Coleman PJ, Levick JR: Cyclic movement stimulates hyaluronan secretion into the synovial cavity of rabbit joints. *J Physiol* 586:1715-29, 2008.

13. Jayson MI, Dixon AS: Intra-articular pressure in rheumatoid arthritis of the knee. 3. Pressure changes during joint use. *Ann Rheum Dis* 29:401-8, 1970.

14. Johnson CD, Chen MH, Toledano AY, Heiken JP, Dachman A, Kuo MD, Menias CO, Siewert B, Cheema JI, Obregon RG, Fidler JL, Zimmerman P, Horton KM, Coakley K, Iyer RB, Hara AK, Halvorsen RA, Jr., Casola G, Yee J, Herman BA, Burgart LJ, Limburg PJ: Accuracy of CT colonography for detection of large adenomas and cancers. *N Engl J Med* 359:1207-17, 2008.

15. Levick JR: Blood flow and mass transport in synovial joints. In: *Handbook of Physiology, Section 2, The Cardiovascular System, Volume IV, The Microcirculation,* ed. by M Renkin, Michel C, The American Physiological Society, 1984, 917-47.

16. Levick JR: Microvascular architecture and exchange in synovial joints. *Microcirculation* 2:217-33, 1995.

17. Lu Y, Chen C, Kallakuri S, Patwardhan A, Cavanaugh JM: Neurophysiological and biomechanical characterization of goat cervical facet joint capsules. *J Orthop Res* 23:779-87, 2005.

18. Lynch HA, Johannessen W, Wu JP, Jawa A, Elliott DM: Effect of fiber orientation and strain rate on the nonlinear uniaxial tensile material properties of tendon. *J Biomech Eng* 125:726-31, 2003.

19. Mansour JM, Wentorf FA, Degoede KM: In vivo kinematics of the rabbit knee in unstable models of osteoarthrosis. *Ann Biomed Eng* 26:353-60, 1998.

20. Matsuzaka S, Sato S, Miyauchi S: Estimation of joint fluid volume in the knee joint of rabbits by measuring the endogenous calcium concentration. *Clin Exp Rheumatol* 20:531-4, 2002.

21. Mazzucco D, Scott R, Spector M: Composition of joint fluid in patients undergoing total knee replacement and revision arthroplasty: correlation with flow properties. *Biomaterials* 25:4433-45, 2004.

22. McDonald JN, Levick JR: Morphology of surface synoviocytes in situ at normal and raised joint pressure, studied by scanning electron microscopy. *Ann Rheum Dis* 47:232-40, 1988.

23. Menschik A: Die Synoviapumpe des Kniegelenkes. *Z Orthop Ihre Grenzgeb* 114:89-94, 1976.

24. Momberger TS, Levick JR, Mason RM: Hyaluronan secretion by synoviocytes is mechanosensitive. *Matrix Biol* 24:510-9, 2005.

25. Ott DJ, Gelfand DW: Gastrointestinal contrast agents. Indications, uses, and risks. *JAMA* 249:2380-4, 1983.

26. Price FM, Levick JR, Mason RM: Glycosaminoglycan concentration in synovium and other tissues of rabbit knee in relation to synovial hydraulic resistance. *J Physiol (Lond)* 495:803-20, 1996.

27. Revell PA, al-Saffar N, Fish S, Osei D: Extracellular matrix of the synovial intimal cell layer. *Ann Rheum Dis* 54:404-7, 1995.

28. Sah RL, Yang AS, Chen AC, Hant JJ, Halili RB, Yoshioka M, Amiel D, Coutts RD: Physical properties of rabbit articular cartilage after transection of the anterior cruciate ligament. *J Orthop Res* 15:197-203, 1997.

29. Schmidt TA, Gastelum NS, Nguyen QT, Schumacher BL, Sah RL: Boundary lubrication of articular cartilage: role of synovial fluid constituents. *Arthritis Rheum* 56:882-91, 2007.

30. Simkin PA: Physiology of normal and abnormal synovium. *Semin Arthritis Rheum* 21:179-83, 1991.

31. Smith MM, Ghosh P: The synthesis of hyaluronic acid by human synovial fibroblasts is influenced by the nature of the hyaluronate in the extracellular environment. *Rheumatol Int* 7:113-22, 1987.

32. Stevens CR, Blake DR, Merry P, Revell PA, Levick JR: A comparative study by morphometry of the microvasculature in normal and rheumatoid synovium. *Arthritis Rheum* 34:1508-13, 1991.

33. Woo SL, Hollis JM, Roux RD, Gomez MA, Inoue M, Kleiner JB, Akeson WH: Effects of knee flexion on the structural properties of the rabbit femur-anterior cruciate ligament-tibia complex (FATC). *J Biomech* 20:557-63, 1987.

34. Yoshioka M, Coutts RD, Amiel D, Hacker SA: Characterization of a model of osteoarthritis in the rabbit knee. *Osteoarthritis Cartilage* 4:87-98, 1996.

CHAPTER 3:

BIOMECHANICAL PROPERTIES OF MIXTURES OF BLOOD AND SYNOVIAL FLUID

3.1 Abstract

Synovial fluid (SF) is a viscous ultrafiltrate of plasma that lubricates articulating joint motion. During acute trauma and certain cartilage repair procedures, blood is introduced into the joint and mixes with variable amounts of SF. The hypothesis of this study was that the dilution of blood with SF alters the rheological properties of the blood and the mechanical properties of the clot formed. The objectives were to determine the composition (solid fraction, protein content), coagulation (fibrin polymerization time, torsional strength), and mechanical (stiffness, permeability) properties of mixtures of blood with 10 or 50% SF. While the initial stages of coagulation of blood were not markedly affected by the presence of the SF, dilution with SF altered the coagulation torque profile over time, decreased the final clot structure mechanical stiffness (42 to 90% decrease), and increased the fluid permeability of the clots (41 to 468-fold). Compared to diluting blood with PBS, SF had a smaller effect on the mechanical properties of the clot, possibly due to the presence of high molecular weight hyaluronan. These properties of blood/SF mixtures

may facilitate an understanding of the repair environment in the joint and of mechanisms of cartilage repair.

3.2 Introduction

Synovial fluid (SF) is a viscous ultrafiltrate of plasma that lubricates articulating joint motion. SF contains several lubricant molecules, including high molecular weight hyaluronan (HA, ~2-10MDa, ~1-4mg/mL) [1, 4, 13] and proteoglycan 4 (PRG4, also called lubricin or SZP, ~0.05-0.5mg/mL) [20]. Articular cartilage, lubricated by SF, normally provides a low-friction, low-wear, load-bearing surface on the ends of bones, in part through the ability of cartilage to facilitate fluid pressurization during load bearing [24]. Focal defects in cartilage due to trauma, as well as less localized degradation common in osteoarthritis (OA), increase the local strain in cartilage near the defects [5], while deficiencies in lubricating molecules increase the friction generated between cartilage surfaces during boundary lubrication [21, 22].

During acute trauma, advanced stage OA, and bone marrow stimulation cartilage repair procedures, blood is introduced into the joint and mixes with variable amounts of SF, creating the conditions in the joint when repair is initiated. Hemarthosis, or bleeding into the joint, can occur during traumatic events, such as intra-articular fracture and anterior cruciate ligament rupture, as well as in advanced stage OA. Although there is evidence that hemarthrosis may lead to cartilage erosion [8] and decreased matrix synthesis [18], certain cartilage repair procedures used to treat focal defects, such as microfracture [14], encourage hemarthrosis through subchondral penetrations as a source of hematopoietic stem cells for repair. Whole blood entering the intra-articular space mixes with synovial fluid, or is diluted with

saline during surgeries, and these mixtures can form the initial structural material for cartilage repair.

The rheological properties and coagulation cascade of blood have each been well-characterized and are analyzed by clinical tests, including activated thromboplastin time (aPTT) and thromboelastography (TEG). An aPTT test indicates the time to fibrin fiber formation and lateral aggregation of fibers, typically by measuring solution turbidity using a sample of blood plasma combined with phospholipid and an activator, such as kaolin or silica [17]. TEG testing is typically used during orthotopic liver transplantation and cardiopulmonary bypass to monitor the clotting time and tensile strength of a patient's blood during coagulation [19]. A sample of whole blood is placed in a cup that rotates ±4.75° over ~11s, with a torsion-sensing pin suspended in the sample [7]. As the sample coagulates, increasing torque is sensed by the pin, describing the torsional strength of the clot over time. A TEG system has recently been used to evaluate solidification of a chitosan-glycerol phosphate/blood implant [12]. However, comparisons of the coagulation properties of mixtures of blood with synovial fluid have not yet been described.

Thus, the hypothesis of this study was that the dilution of blood with SF alters the rheological properties of the blood and the mechanical properties of the clot formed. The objectives were to determine the compositional (solid fraction, protein content), coagulation (fibrin polymerization time, torsional strength), and mechanical (stiffness, permeability) properties of mixtures of blood and SF.

3.3 Materials and Methods

3.3.1 Study Design

Bovine SF (bSF) and whole blood were obtained from adult bovine animals via an abattoir and stored at 4°C for up to 2 weeks until use. Whole blood was obtained in 4 lots, anticoagulated by addition of sodium citrate to 3.8% (Animal Technologies Inc., Tyler, TX), each from a single animal. Fresh arterial blood was also obtained from 5 anesthetized rabbits, under a protocol approved by the UCSD IACUC. Bovine SF lots were pooled from ~10 animal donors (Animal Technologies Inc.). Mixtures of blood diluted with SF or phosphate buffered saline (PBS) at 10% or 50% by volume were prepared and analyzed as follows.

3.3.2 Clot Composition

Uniform discs of clotted blood and PBS or SF mixtures were created and weighed. Clotting was initiated in citrated blood mixtures by addition of $CaCl_2$ to 28mM (enough $CaCl_2$ to saturate the citrate anticoagulant and result in even clotting based on theoretical calculations and pilot experiments) in a custom 2x3.6x0.16cm silastic mold between two glass plates, followed by incubation at 37°C and 5% CO_2 for 1 hr. Cylindrical disks initially of 1.6mm thickness and 10mm diameter were removed from the clotted material using a dermal biopsy punch. Clots were allowed to equilibrate with PBS for at least 1hr before being weighed wet, lyophilized overnight, and reweighed.

The protein content of the clotted mixtures was evaluated. Lyophilized clots were digested in 1mL of PBS with 0.2mg/ml trypsin (Sigma-Aldrich, St. Louis, MO) for 18hr at 37°C. Portions of the digests were assayed for protein content using the Pierce BCA Protein Assay kit (Thermo Scientific, Rockford, IL) according to the manufacturer's instructions.

Additional clots were prepared for histology. Clots were fixed in 1mL of 4% paraformaldehyde (USB Corp., Cleveland, OH) in PBS overnight, snap frozen in embedding medium (Tissue-Tek, Andwin Scientific, Addison, IL), and cut to 10µm sections. Sections were stained with hematoxylin and eosin Y (H&E, Sigma-Aldrich) and imaged on a microscope (Eclipse TE300, Nikon, Melville, NY) at 20x magnification.

3.3.3 Coagulation Properties

An aPTT-like test was performed to determine the time to clot formation based on solution turbidity. Plasma was substituted for whole blood in the mixture for this test to mimic clinical aPTT assays [17]. Bovine plasma was obtained by spinning down whole blood at 800g for 30min and decanting the supernatant. 0.3mL of each mixture (plasma with 10 or 50% PBS or SF) were prepared in duplicate, combined with 0.3mL of 0.1% kaolin in PBS (Sigma-Aldrich), and incubated for 1hr at 37°C. 0.3mL of PBS was added to one replicate of each group and used to blank the spectrophotometer (Beckman DU640, Beckman Instruments, Inc., Fullerton, CA), and 0.3 mL of $CaCl_2$ was added to the other sample to 8.3mM to initiate clotting immediately before measuring absorbance. Absorbance was recorded at 460nm every

10s for up to 12min. Absorbance versus time data were fit to a generalized logistic function using a least square error nonlinear regression (MATLAB R2008b, The MathWorks, Inc., Natick, MA). The clotting time was determined as the time at half-maximum absorbance.

A TEG-like test was performed to determine the coagulation torque over time and reaction time (r) and maximum amplitude (MA) parameters. Sample mixtures (472 μL) were stimulated to clot by addition of 28μL $CaCl_2$ to 10mM (following the protocol for citrated samples by the manufacturer of a clinical TEG apparatus; TEG Model 5000 Analyzer; Haemoscope Inc., Niles, IL), and were placed in a custom cup base that was rotated between 0 and 4.75° at 1.357°/s, with 2s delays at 0 and 4.75°, around a pin suspended in the mixture and connected to a torque cell (ElectroForce ELF-3220, Bose-Enduratec, Eden Prairie, MN). The gap width between the pin and cup was 1.0mm, and a small volume of mineral oil was layered above the sample to prevent evaporation. The torque generated on the suspended pin due to the coagulating mixture during rotation was recorded at 5Hz over a period of 3.5hr. The absolute difference in torque between the min and max values per cycle was plotted and used to determine r and MA. The r parameter was determined as the time that the torque increased at least two standard deviations above the baseline average, and MA as the maximum torque amplitude achieved during the test.

3.3.4 Mechanical and Structural Properties

Clots of citrated bovine or fresh rabbit blood mixed with PBS and SF were tested in confined compression in PBS to determine a confined compression aggregate

modulus (H_A) and strain-dependent hydraulic permeability (k_p). The thickness of each clot was measured in 3 locations using a non-contacting laser micrometer and then averaged for use in the compression test. The clots were placed in a confining ring between two porous platens in a mechanical testing machine (Dynastat, Northern Industrial, Albany, NY), and tested by sequential static compression to 15%, 30%, and 45% compressive strain based on thickness and low-amplitude oscillations at 0.01-1 Hz superimposed on static offsets [3]. The data were fit to theoretical models to determine H_A, and k_p at 30% compressive strain [10].

The molecular weight of hyaluronan in bSF and clotted mixtures was analyzed using gel electrophoresis. Clots of each sample mixture were prepared as above, and digested with 0.5mg/mL proteinase K (Roche Applied Science, Indianapolis, IN) in PBE at 60°C overnight. Portions of digests, a hyaluronan ladder, and bSF were run on a 1% agarose gel at 10V/cm for 100min in tris-acetate-EDTA buffer. The gel was fixed in 25% isopropanol, stained with Stains-all (Sigma-Aldrich) in formamide according to the manufacturer's instructions, destained in water, and imaged with a digital camera (D80, Nikon).

3.3.5 Statistical Analysis

The data are presented as mean±SEM for n=4 lots of bovine blood or n=5 rabbits. The effects of dilution (10 or 50%) and diluent (PBS or SF) on dry weight, protein, clotting time, r, MA, H_A, and k_p for mixture groups (+10%PBS, +10%SF, +50%PBS, +50%SF) normalized to the whole blood values were assessed using 2-way ANOVAs, with Tukey post-hoc tests to determine differences between groups where

significant effects were found. To compare the mixture groups to whole blood, the effect of experimental group on all outcome measures was assessed with 1-way ANOVAs, with differences between mixture groups and whole blood assessed with Dunnett tests where significant effects were found. The hydraulic permeability data were $\log_{10}$ transformed to improve homoscedasticity [23]. Significance was set as $P<0.05$ and statistical analyses were performed using Systat 10.2 (Systat Software Inc., Chicago, IL).

3.4 Results

3.4.1 Composition

Differences in clot size after equilibration in PBS were apparent in the digital images of the clots. The clots contracted with increasing dilution of PBS, and expanded with increasing dilution of SF (**Fig. 3.1, left column**). The H&E stained sections showed the red blood cell density in each clot was reasonably uniform, though there were lower cell densities in the 50%SF dilution and, to a lesser extent, the 50%PBS dilution compared to either 10% dilution or blood alone (**Fig. 3.1, right column**).

The clot dry weights per volume and protein content per volume varied with sample mixture, decreasing with increased dilution. Dry weights varied with dilution ($P<0.0001$), though not with diluent ($P=0.12$), and with a significant interaction effect ($P<0.05$) of dilution (10 vs 50%) and diluent (PBS vs SF, **Fig. 3.2A**). The dry weight of the 50%PBS and 50%SF clots were 47% and 36% lower, respectively, than that of the 10%PBS ($P<0.001$) and 10%SF ($P<0.001$) clots. In addition, the dry weight per volume of 10%SF ($P<0.05$), 50%PBS ($P<0.001$), and 50%SF ($P<0.001$) mixtures were significantly lower than blood alone. Protein content varied with dilution ($P<0.0001$), though not with diluent ($P=0.13$) and without an interaction effect ($P=0.70$, **Fig. 3.2B**). The protein content of the 50%PBS and 50%SF clots were 41% and 34% lower, respectively, than that of the 10%PBS ($P<0.001$) and 10%SF ($P<0.001$) clots. In addition, the protein content of 50%PBS ($P<0.001$), and 50%SF ($P<0.01$) mixtures were significantly lower than blood alone.

3.4.2 Coagulation Properties

The time to clot as measured by the aPTT-like assay did not vary with sample mixture. aPTT time did not vary with dilution (P=0.25) or diluent (P=0.21), and without an interaction effect (P=0.09, **Fig. 3.3**). However, the clotting time of the 50%PBS mixture was 46% higher than blood alone (P<0.01).

The torque trace over time indicated differences between the mixtures' coagulation parameters and clot strength. While the blood line (**Fig. 3.4A, solid line**) displayed the typical shape for a TEG-trace of normal blood, including little torque during the clotting time, a steep increase towards the maximum, and eventual decline, the other mixtures displayed altered characteristics. At the 10% dilution level, the shape of the curves was similar to blood alone at a decreased magnitude, though the PBS dilution did not peak and decline (**Fig. 3.4A, dotted line and large dashed line**). At the 50% dilution level, the shape of the curves changed to a more gradual increase without maximum or decline (**Fig. 3.4A, dot-dash line and small dashed line**), with a smaller magnitude of torque for the mixtures diluted with SF compared to PBS.

The time to clot as measured by the r parameter in the TEG-like assay did not vary with sample mixture. r time did not vary with dilution (P=0.71) or diluent (P=0.32), and without an interaction effect (P=0.65, **Fig. 3.4B**). The MA parameter did not vary with dilution (P=0.82), but tended to vary with diluent (P=0.05), and a trend for an interaction effect (P=0.08, **Fig. 3.4C**). The MA of the 10%PBS (P<0.05), 10%SF (P<0.05), and 50%SF (P<0.01) mixtures were significantly lower than blood alone.

3.4.3 Mechanical and Structural Properties

The clot aggregate compressive moduli from citrated bovine blood varied with sample mixture, decreasing with dilution level. Aggregate moduli varied with dilution ($P<0.001$), though not with diluent ($P=0.09$), while the interaction effect was significant ($P<0.05$, **Fig. 3.5A**). The modulus of the 10%PBS and 50%SF clots were 54% ($P<0.05$) and 82% ($P<0.01$) lower, respectively, than that of the 10%SF clots. In addition, the aggregate moduli of all groups (10%PBS, $P<0.01$; 10%SF, $P<0.01$; 50%PBS, $P<0.001$; 50%SF, $P<0.001$) were significantly less than blood alone. The clotted mixtures were more permeable than blood alone, but the hydraulic permeability did not vary between mixture groups. Hydraulic permeability did not vary with dilution ($P=0.30$) or diluent ($P=0.13$), nor was there an interaction effect ($P=0.26$, **Fig. 3.5B**). However, the hydraulic permeability of all groups (10%PBS, $P<0.001$; 10%SF, $P<0.05$; 50%PBS, $P<0.001$; 50%SF, $P<0.001$) were greater than blood alone.

The trends in aggregate compressive modulus and hydraulic permeability from fresh rabbit blood were similar to those from citrated bovine blood, though the modulus was higher in magnitude. Aggregate modulus varied with dilution ($P<0.001$), though not with diluent ($P=0.35$) and without an interaction effect ($P=0.58$, **Fig. 3.5C**). The moduli of the 10%PBS ($P<0.05$), 50%PBS ($P<0.001$), and 50%SF ($P<0.001$) mixtures were significantly less than that of blood alone. There was more variation between animals in the fresh rabbit blood than the citrated bovine blood, and though

the average hydraulic permeabilities tended to decrease with dilution, the differences were not significant (**Fig. 3.5D**).

Gel electrophoretic analysis of portions of clot digests demonstrated that the molecular weight of hyaluronan in the digests was unaffected by exposure to blood or by the clotting process. The electrophoretic mobility of the main band in the bSF was slightly slower than the 4000Da HA standard, indicating relatively high molecular weight HA (~4000Da) in the bSF (**Fig. 3.6, lanes 1 and 2**). Bands of similar staining and mobility were found in both mixtures with SF, and were more pronounced in 50%SF vs 10%SF (**Fig. 3.6, lanes 5 and 7**). The staining in lanes containing samples without SF was similar to blood alone (**Fig. 3.6, lanes 3, 4, and 6**).

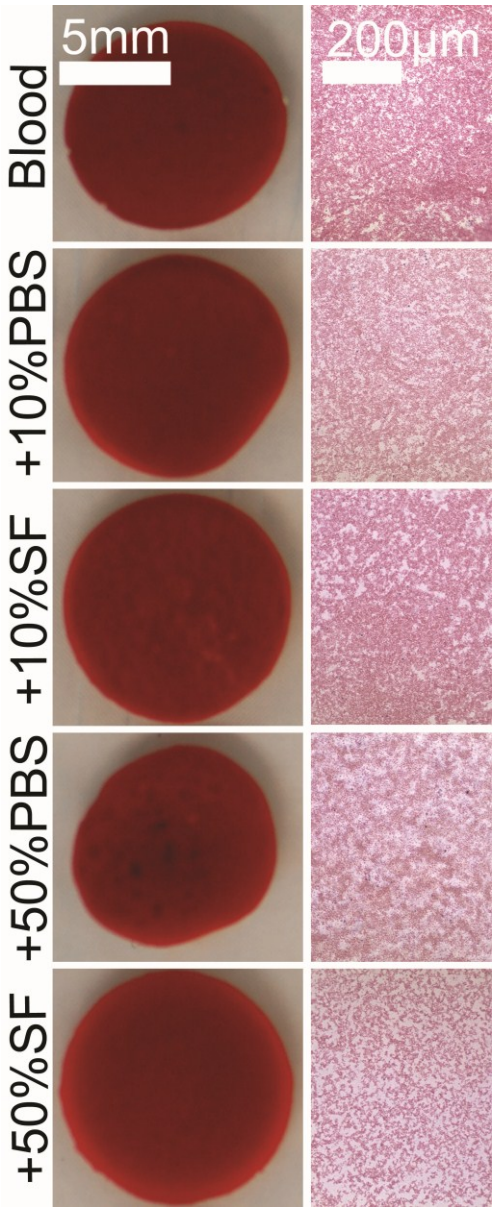

Figure 3.1: Digital images of clots from each group (left column). Clots were fixed, sectioned, stained with H&E, and imaged under a microscope at 20x magnification (right column).

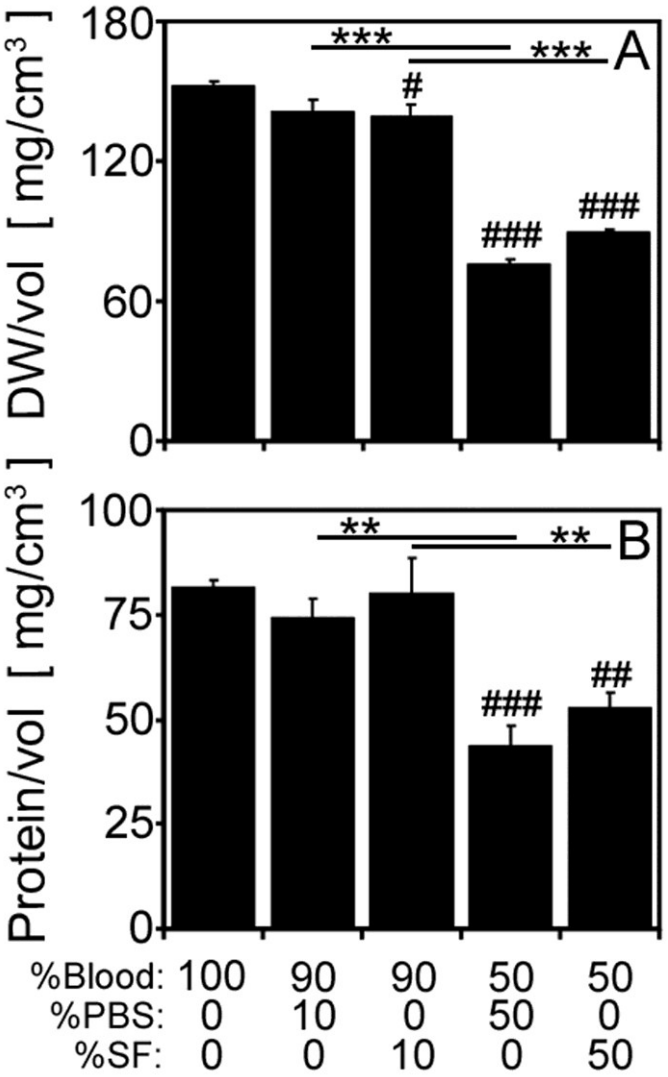

Figure 3.2: The dry weights (A) and protein content (B) of the clots normalized to volume. **: P<0.01, ***:P<0.001, #:P<0.05 vs blood, ###:P<0.001 vs blood.

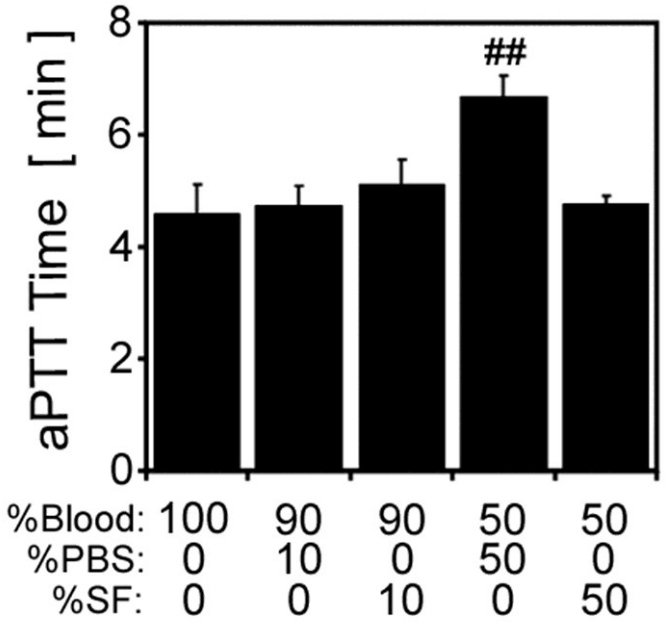

Figure 3.3: Clotting time for each group as measured by the aPTT-like test. ##:P<0.01 vs blood.

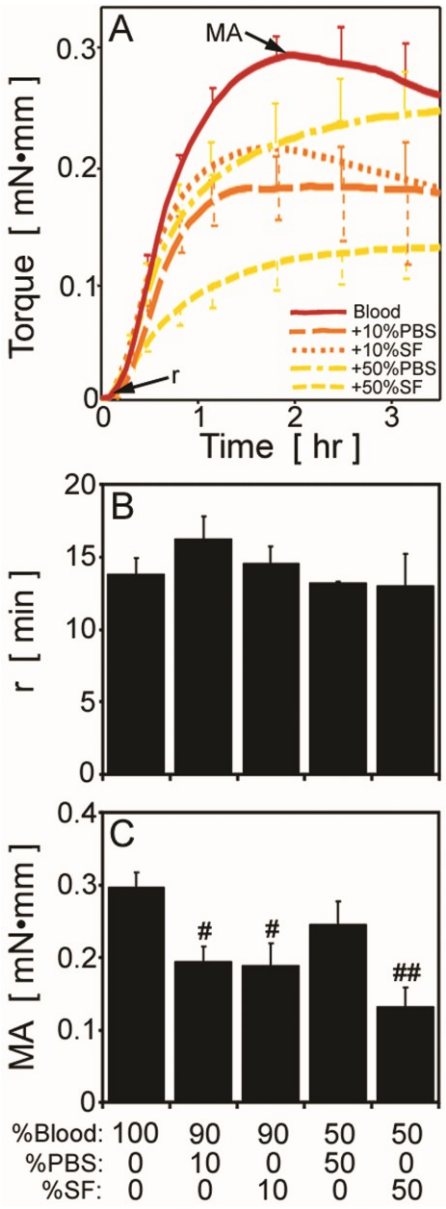

Figure 3.4: Average torque trace for each group during TEG-like testing (A), clotting time as determined by the r parameter (B), maximum torque amplitude (MA) reached during TEG-like testing (C). #:P<0.05 vs blood, ##:P<0.01 vs blood.

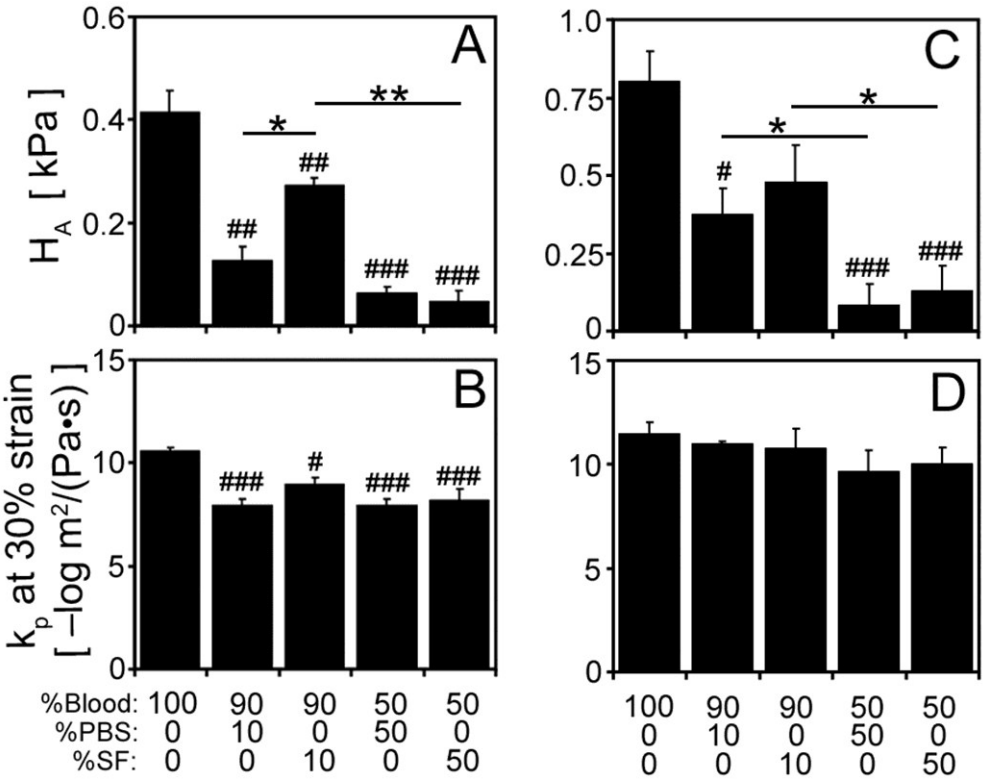

Figure 3.5: Aggregate compression modulus H_A and hydraulic permeability k_p at 30% compression for each blood/SF mixture from citrated bovine blood (A, B) or fresh rabbit blood (C, D). *: P<0.05, **: P<0.01, #:P<0.05 vs blood, ##:P<0.01 vs blood, ###:P<0.001 vs blood.

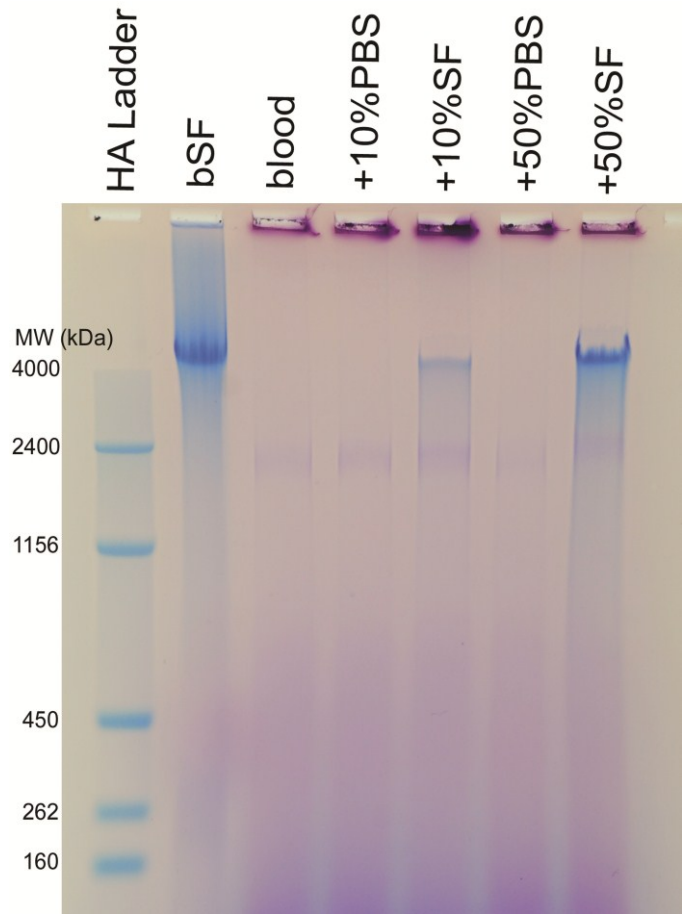

Figure 3.6: An HA ladder (lane 1), bSF (lane 2), and portions of blood/SF clots digested with proteinase K (lanes 3-7) were electrophoresed on a 1% agarose gel and stained with Stains-all.

3.5 Discussion

These results demonstrate the effects of SF on blood clot formation and help to characterize the initial repair environment in the synovial joint post-trauma or during bone marrow stimulation cartilage repair procedures. The properties of blood with little or no (0 or 10%) dilution with PBS or SF are likely applicable to the types of blood clotting that occur during the controlled bleeding in marrow stimulation cartilage repair techniques. In contrast, the properties of blood with higher (50%) dilutions with SF are likely applicable to traumatic bleeding, where clotted blood/SF mixtures are found post-hemarthrosis. In these experiments, the initial stages of coagulation of blood were not markedly affected by the presence of the SF, (**Figs. 3.3 and 3.4B**), the SF altered the coagulation torque profile over time (**Fig. 3.4A**), decreased the final clot structure mechanical stiffness (**Figs. 3.4C, 3.5A, and 3.5C**), and increased the fluid permeability (**Fig. 3.5B and 3.5D**) of the clots. Compared to diluting blood with PBS, diluting with SF had a smaller effect on the mechanical properties of the clot, possibly due to the protein content and presence of high molecular weight hyaluronan (**Fig. 3.6**) as a structural component.

These *in vitro* experiments present a detailed view of the rheology of mixtures of blood and SF in a controlled setting using standard and clinical-like assays, with results that relate to the joint environment post-trauma or surgery. Although these experiments were conducted *in vitro* for more control over the level of dilution and mixing for each sample, additional translational work to verify the applicability of these findings *in vivo* could be undertaken using an intra-articular fracture animal

model to create physiological hemarthrosis and blood/SF mixtures or using a defect/microfracture animal model to replicate the initial repair environment. Such experimental models could also be used to determine clotting times, homogeneity of clotted material, and diluent effects, which may be different *in vivo* compared to these *in vitro* data.

Similar trends in aggregate modulus and hydraulic permeability were found with anticoagulated and fresh blood, though there were differences in magnitude, which may be due to the anticoagulant or the difference in species. The effects of the anticoagulant on the coagulation properties of blood were not investigated here, but the anticoagulant, even after addition of Ca^{2+} to saturate the citrate, likely slowed the clotting time as measured by aPTT and TEG. The TEG and aPTT clinical tests are typically performed on proprietary systems where the exact nature of the measured variable is unclear; for TEG, the torque is translated into a 'deflection length' for historical reasons [7], while the criteria for coagulation by aPTT varies by test system company. Thus, these experimental tests were replicated in our lab to allow more control over how the measurements were made.

The initial fibrin polymerization time was apparently unaffected by dilution or diluent, though later stages of coagulation were abnormal as assessed by TEG-like testing. Changes in the turbidity of plasma correspond to changes in fibrin diameter [15], indicating fibrin polymerization. Neither this polymerization time, nor the time for significant torque to be generated by the clot in the TEG test were substantially altered, though dilution with 50%PBS tended to increase this time compared to blood alone. However, the TEG trace (**Fig. 3.4A**) displayed an abnormal clotting profile. The

dilution effect appeared to decrease the magnitude of the normal profile at 10% for both SF and PBS, while dilution to 50% altered the profile shape. At 50% dilution, SF as the diluent resulted in a further decrease in magnitude compared to PBS. Such results on a classical TEG test are indicative of dilutional coagulopathy [11], which is appropriate here as the blood samples were diluted. During surgery, lower than normal MA values are treated with additional platelets, while slowly increasing torque traces such as the 50% dilution profiles, would be treated with cryoprecipitate [16], which includes factor VIII, fibrinogen, von Willibrand factor, and factor XIII, which are likely at low concentrations in these diluted samples.

Dilution of blood with 10%PBS resulted in lower clot stiffness than dilution with 10%SF, suggesting additional structural organization in clots with SF, possibly due to the content of high molecular weight hyaluronan. Although there was swelling of clots diluted with SF and contraction of clots diluted with PBS due to variations in osmolality between whole blood (~300mOsm/kg) [2], SF (~400mOsm/kg) [2], and PBS (150mOsm/kg), those differences did not result in increased clot stiffness with more compaction. The largest (50%SF) and smallest (50%PBS) clots were of similar stiffness (**Fig. 3.5A**) and the marginally expanded 10%SF clot was significantly stiffer than the marginally contracted 10%PBS clot, suggesting a component of SF is increasing the clot stiffness. High molecular weight hyaluronan (~4MDa) in SF and within the clotted mixtures (**Fig. 3.6**) could be responsible for the increased stiffness, possibly through the ‘swelling pressure’ generated by its charged molecule segments.

The hydraulic permeability of clotted blood and SF in cartilage defects may facilitate the short-time distribution of load around a defect site via fluid

pressurization, as well as restrict molecular transport. The small effective size of interstitial pores in articular cartilage results in a normally low hydraulic permeability (~$1x10^{-15}$ to ~$1x10^{-16}$ $m^2/[Pa \cdot s]$) [3] and also restricted transport of macromolecules. Fluid pressurization of cartilage supports most of the imposed loads [24] and minimizes strain magnitudes. The presence of a full thickness cartilage defect exposes the permeable underlying subchondral bone [9], diminishing fluid pressurization and increasing the strain magnitudes in the surrounding tissue. Although the clot modulus is much lower than that of cartilage, clots, like other biphasic poroelastic materials, support fluid pressurization at short times (before stress relaxation occurs). For blood clots or clots with 10%SF (**Fig. 3.5**), the stress relaxation time constant, calculated from H_A and k_p for a 1mm thick sample [3], are on the order of ~10s, compared to ~10,000s for cartilage. Such clots may also hinder molecular convection of large molecules out of SF [6].

The properties of clotted mixtures of blood with PBS and SF may be important not only in trauma and cartilage repair procedures, but also other procedures in which blood becomes clotted in repair constructs, including tendon, ligament, and meniscus repair. In such procedures, understanding the rheological and mechanical properties of the construct or repair tissue may facilitate an understanding of the mechanisms and time-course of repair.

3.6 Acknowledgments

Chapter 3, in full, is reproduced from the *Journal of Orthopaedic Research*, volume 29, number 2, p. 240-6, 2011 with permission from Wiley, Inc. The dissertation author was the primary author and thanks co-authors Anna Luan, Meena Siddiqui, Bradley C. Hansen, Koichi Masuda, and Robert L. Sah. This work was supported by grants from the National Institute of Arthritis, Musculoskeletal and Skin Diseases and an award to UCSD from the Howard Hughes Medical Institute through the HHMI Professors Program (for RLS).

3.7 References

1. Balazs EA: The physical properties of synovial fluid and the special role of hyaluronic acid. In: *Disorders of the Knee,* ed. by AJ Helfet, Lippincott Co., Philadelphia, 1974, 63-75.

2. Baumgarten M, Bloebaum RD, Ross SD, Campbell P, Sarmiento A: Normal human synovial fluid: osmolality and exercise-induced changes. *J Bone Joint Surg Am* 67:1336-9, 1985.

3. Chen AC, Bae WC, Schinagl RM, Sah RL: Depth- and strain-dependent mechanical and electromechanical properties of full-thickness bovine articular cartilage in confined compression. *J Biomech* 34:1-12, 2001.

4. Dahl LB, Dahl IM, Engstrom-Laurent A, Granath K: Concentration and molecular weight of sodium hyaluronate in synovial fluid from patients with rheumatoid arthritis and other arthropathies. *Ann Rheum Dis* 44:817-22, 1985.

5. Gratz KR, Wong BL, Bae WC, Sah RL: The effects of focal articular defects on intra-tissue strains in the surrounding and opposing cartilage. *Biorheology* 45:193-207, 2008.

6. Happel J, Brenner H. Low Reynolds Number Hydrodynamics: With Special Applications to Particulate Media. Hingham: Martinus Nihjoff; 1973.

7. Hartert H: Blutgerninnungstudien mit der thromboelastographic, einen neven untersuchingsver fahren. *Klin Wochenschr* 26:577-83, 1948.

8. Hoaglund FT: Experimental hemarthrosis. The response of canine knees to injections of autologous blood. *J Bone Joint Surg Am* 49:285-98, 1967.

9. Hwang J, Bae WC, Shieu W, Lewis CW, Bugbee WD, Sah RL: Increased hydraulic conductance of human articular cartilage and subchondral bone plate with progression of osteoarthritis. *Arthritis Rheum* 58:3831-42, 2008.

10. Kwan MK, Hacker SA, Woo SL-Y, Wayne JS: The effect of storage on the biomechanical behavior of articular cartilage-a large strain study. *J Biomech Eng* 114:149-53, 1992.

11. Mallett SV, Cox DJ: Thrombelastography. *Br J Anaesth* 69:307-13, 1992.

12. Marchand C, Rivard GE, Sun J, Hoemann CD: Solidification mechanisms of chitosan-glycerol phosphate/blood implant for articular cartilage repair. *Osteoarthritis Cartilage* 17:953-60, 2009.

13. Mazzucco D, Scott R, Spector M: Composition of joint fluid in patients undergoing total knee replacement and revision arthroplasty: correlation with flow properties. *Biomaterials* 25:4433-45, 2004.

14. Mithoefer K, Williams RJ, 3rd, Warren RF, Potter HG, Spock CR, Jones EC, Wickiewicz TL, Marx RG: Chondral resurfacing of articular cartilage defects in the knee with the microfracture technique. Surgical technique. *J Bone Joint Surg Am* 88 Suppl 1 Pt 2:294-304, 2006.

15. Muzaffar TZ, Youngson GG, Bryce WA, Dhall DP: Studies on fibrin formation and effects of dextran. *Thromb Diath Haemorrh* 28:244-56, 1972.

16. Pool JG, Gershgold EJ, Pappenhagen AR: High-Potency Antihaemophilic Factor Concentrate Prepared From Cryoglobulin Precipitate. *Nature* 203:312, 1964.

17. Proven D, Singer C, Baglin T, Dokal I. Oxford Handbook of Clinical Haematology. 3rd ed: Oxford University Press; 2009.

18. Roosendaal G, Vianen ME, Marx JJ, van den Berg HM, Lafeber FP, Bijlsma JW: Blood-induced joint damage: a human in vitro study. *Arthritis Rheum* 42:1025-32, 1999.

19. Salooja N, Perry DJ: Thrombelastography. *Blood Coagul Fibrinolysis* 12:327-37, 2001.

20. Schmid T, Lindley K, Su J, Soloveychik V, Block J, Kuettner K, Schumacher B: Superficial zone protein (SZP) is an abundant glycoprotein in human synovial fluid and serum. *Trans Orthop Res Soc,* 26:82, 2001.

21. Schmidt TA, Gastelum NS, Nguyen QT, Schumacher BL, Sah RL: Boundary lubrication of articular cartilage: role of synovial fluid constituents. *Arthritis Rheum* 56:882-91, 2007.

22. Schmidt TA, Sah RL: Effect of synovial fluid on boundary lubrication of articular cartilage. *Osteoarthritis Cartilage* 15:35-47, 2007.

23. Sokal RR, Rohlf FJ. Biometry. 3rd ed. New York: WH Freeman and Co.; 1995.

24. Soltz MA, Ateshian GA: Experimental verification and theoretical prediction of cartilage interstitial fluid pressurization at an impermeable contact interface in confined compression. *J Biomech* 31:927-34, 1998.

CHAPTER 4:

BIOPHYSICAL MECHANICSMS OF ALTERD HYALURONAN CONCENTRATION IN SYNOVIAL FLUID AFTER ANTERIOR CRUCIATE LIGAMENT TRANSECTION

4.1 Abstract

Objectives: The residence time of hyaluronan (HA) in the synovial fluid (SF) of knee joints was investigated using the rabbit anterior cruciate ligament transection (ACLT) model. The aims were to assess at 7 and 28 days after surgery for non-operated (NonOp), ACLT, and SHAM groups: 1) HA molecular mass (M_r) distribution in SF, 2) endogenous replenishment of HA after saline washout, 3) HA residence times in SF, and 4) synovium and subsynovium cellularity.

Methods: Adult NZW rabbits underwent ACLT or SHAM surgeries on one hind limb, while each contralateral limb was a NonOp control. At 7 or 28d after surgery, joints were aspirated for SF, lavaged with saline, injected with saline or polydisperse HA, and sampled over 8hrs. Fluid samples were analyzed for HA concentration and M_r distribution to calculate HA residence times.

Results: HA M_r-distributions showed 1) loss of high-M_r HA at day 7, and a shift towards a lower-M_r HA distribution at day 28, 2) endogenous replenishment of high-M_r HA after washout, and 3) M_r-dependent HA loss, particularly at day 7 after ACLT. HA residence times decreased with M_r (~27hrs for high-M_r to ~7hrs for low-M_r) and at day 7 after ACLT (~70% decrease). The subsynovium of ACLT joints contained 4) increased cellularity and neovascularization at 7 and 28 days.

Conclusions: The residence time of HA in SF is transiently decreased after ACLT, suggesting a biophysical transport mechanism for the altered SF composition post-injury or during inflammation.

.

4.2 Introduction

Synovial fluid (SF) is an ultrafiltrate of plasma with additional molecules secreted by local cell populations. Hyaluronan (HA) is a major component of SF that is secreted in high molecular mass (M_r) form (~4-6MDa, ~2-4mg/mL) [3, 10, 22, 26] mostly by synoviocytes [44] in synovium, the inner lining of the joint. HA is also found on the surface of synovium, providing substantial resistance to fluid and macromolecular outflow [9], and helping to maintain the concentration of HA in SF. The protein composition of SF reflects its origins as plasma, though the distribution of those proteins [16, 32, 34, 35] differs from plasma due to the size-selective nature of synovium [6, 33], which allows higher flux of smaller molecules.

The composition of SF is normally in dynamic equilibrium through the processes of convection from plasma, secretion of molecules by local cells, diffusion out of SF to the lymphatics, accumulation at surfaces, and degradation within the joint cavity. Plasma, including small proteins and metabolites, is filtered into SF from capillaries. Larger molecules are secreted locally, such as HA, and are mainly removed from SF by diffusion through synovium to the lymphatics [4, 21], but also by accumulating at tissue surfaces [2, 8] and by degradation in SF [21]. A balance normally exists between secretion and loss processes that maintain a steady-state concentration of high-M_r HA in SF.

Injury and pathological conditions alter the protein and HA composition of SF due to shifts in the diffusion and transport rates of molecules out of SF. The permeability of synovium to proteins in joints with arthritis is increased [23, 40], with

proportionately larger increases in permeability for larger proteins [20]. Protein flux between the microvasculature and SF, measured by a variety of techniques including the SF to serum ratio [20], injection of radioactive tracers and sampling [29, 43], and tracer injection with clearance measurements [40, 42, 46], consistently show increased protein flux with synovitis or other indices of joint inflammation. For HA, the steady-state concentration is typically decreased and the M_r-distribution shifts towards lower M_r species after joint injury [5] and in rheumatoid arthritis [11, 14]. HA residence time in the joint might be expected to also be decreased, analogous to protein transport, though results from tracer studies involving injection of radiolabeled high-M_r HA and analysis of serum and SF are mixed. A type II collagen injection model in sheep showed SF half-life decreasing to 55% of normal (from ~21 to ~12hrs) after 2wks [13], while in a partial meniscectomy model of osteoarthritis (OA) in rabbits, high-M_r HA half-life tended to increase to 135% of normal at 4wks before returning to baseline by 12wks [25]. HA residence times for the rabbit anterior cruciate ligament transection (ACLT) model of joint injury and OA [7, 45, 49] have not been reported.

The diffusion rate of molecules out of SF is determined by the cellularity and extracellular matrix of synovium. Synovium is distinguished by densely populated synoviocytes 1-3 layers deep, though the cells are not laminar, do not share tight junctions, and lack a basement membrane [28, 41]. Transport occurs between cells in the highly fibrillar interstitial matrix [24, 31] that has an effective pore size of ~20-90nm [15, 33]. Direct manipulation of the matrix content by digesting synovium GAGs [38] and stretching the matrix through increased intra-articular pressure [30] delineated the importance of matrix molecules in determining synovium resistance to

fluid flow and molecular diffusion. Pathological changes to synovial matrix, due to cell infiltration or synovitis, may be responsible for the increased protein, and possibly HA, permeability observed.

Thus the hypothesis of this study was that HA loss from SF is M_r-dependent and is increased after ACLT compared to sham operated (SHAM) and non-operated (NonOp) joints. The aims were to assess at 7 and 28 days after surgery for non-operated (NonOp), ACLT, and SHAM groups: 1) HA concentration and M_r distribution in synovial fluid (SF), 2) endogenous replenishment of HA after saline washout, 3) HA retention over 8hrs in SF via HA residence times, and 4) synovium and subsynovium cellularity.

4.3 Materials and Methods

4.3.1 Study Design

The residence time of HA in the SF of knee joints was investigated using the rabbit ACLT model. All animal procedures were approved by the local IACUC committee. Young adult (11-13mo) New Zealand white rabbits (N=26 rabbits, n=52 knees) underwent ACLT (N=20) or SHAM (N=6) surgeries on their right hind limb, while each left limb was a NonOp control. At 7 (N=12 ACLT, N=6 SHAM) or 28days (N=8 ACLT) after surgery, joints were aspirated for SF, lavaged with saline, injected with saline or polydisperse HA, and flexed. Directly after flexing ($t=0^+$) or at 1, 3, or 8hrs after injection, 50μL of joint fluid was withdrawn (**Table 4.1**). Rabbits were euthanized after the 8hr time point and fluid samples and intact joints were stored at -80°C. Samples at 0^+, 1, 3, and 8hrs were analyzed for HA concentration (c^{HA}) and the HA M_r distribution to calculate HA residence time for various bins of M_r. SF and serum samples were also analyzed HA concentration. Synovium samples were analyzed for cell density.

4.3.2 Surgeries and Transport Study

ACLT or SHAM surgeries were performed. Rabbits were anesthetized, intubated, and the right hind limb was shaved and cleaned. The patella was displaced laterally and a ~3cm long incision medial to the patellar ligament was made through the skin and joint capsule. The infrapatellar fat pad was displaced and the ACL exposed. For ACLT surgeries, the ACL was then cut using curved, fine-tip scissors

and the transection verified by Lachman test. ACLT and SHAM groups were then rinsed with saline, the patella was realigned, the capsule was closed with 2-0 suture, and then the skin was closed with 4-0 suture.

Bolus injection and longitudinal sampling of knee fluid were performed on operated and NonOp hind limbs at 7 or 28d after surgery. Rabbits were anesthetized and neat SF was withdrawn using a 22g needle. Joints were lavaged 3x with 0.5mL saline, injected with 0.5mL of saline or 2.5mg/mL polydisperse HA (2500-50kDa, Lifecore Biomedical LLC, Chaska, MN), and flexed 10x. Additionally, 3 NonOp joints were injected with a FITC-labeled HA preparation [18] that included HA in the 4000kDa range (Healon®) to track high-M_r HA as well. Samples of the joint fluid (50μL) were taken with a 25g needle at $t=0^+$ or at 1, 3, and 8hrs after injection. Blood was drawn for serum after the 8hr time point and the animals were euthanized. The hind limbs were removed and the SF, joint fluid, serum, and limbs were stored at -80°C until processing.

4.3.3 HA Concentration, M_r Distribution, and Transport Analysis

Joint fluids were analyzed for c^{HA} and M_r. Portions of SF and joint fluid were digested overnight at 37°C with Proteinase K, loaded by volume in a 1% agarose gel, and electrophoresed at 150V in tris-acetate EDTA buffer. Gels were fixed in 25% isopropanol, stained overnight in Stainsall (Sigma-Aldrich, Saint Louis, MO), destained in water, and imaged on a lightbox. Gels with samples of FITC-HA were scanned on a fluorescent scanner (Storm, GE Healthcare, Piscataway, NJ). A custom MATLAB (Mathworks Inc, Natick, MA) program was used to quantify the % HA

intensity in M_r bins of 7000-2500, 2500-1000, 1000-500, 500-250, and 250-50kDa. The c^{HA} in each joint fluid and serum sample was determined by digesting portions with Proteinase K, inhibition of enzyme activity by boiling for 10min, and then using an ELISA-like assay (Corgenix, Broomfield, CO or R&D Systems, Minneapolis, MN). Total c^{HA} was multiplied by % intensity to give the c^{HA} in each M_r bin.

The residence time constants for HA by M_r were calculated. The endogenous secretion of HA was approximated by the average c^{HA} measured after saline injection, the majority of which was localized in the 7000-2500 bin. This endogenous secretion was subtracted from the total c^{HA} after polydisperse HA injection at each time point. A 2-parameter exponential decay was fit through the remaining c^{HA} at 0^+, 1, 3, and 8hrs for all bins except the 7000-2500 bin (due to the high secretion rate compared to injected c^{HA}, to calculate the best-fit residence time constant (τ) for each group.

4.3.4 Histology

The synovium and subsynovium matrix structure and cell density for each group were determined. Limbs were thawed at 4°C and samples of synovium were harvested from the medial and lateral distal patellar regions. Samples were fixed overnight in 4% paraformaldehyde in PBS, dehydrated, embedded in paraffin, and sectioned at 10 or 100μm thickness. Thin sections were stained with H&E or alcian blue, or were incubated with HABP-HRP (Corgenix), anti-CD4 (ab25804, Abcam, Cambridge, MA), or anti-CD11b (ab8878, Abcam) and imaged on an inverted microscope (Nikon Instruments, Melville, NY). Thick sections were incubated with 2μg/mL propidium iodide in saline and imaged with 20x objective, 0.75μm square

voxel size, and 1024x1024 pixels on a confocal microscope (Leica Microsystems, Wetzlar, Germany).

4.3.5 Statistical Analysis

The data are presented as mean±SEM. The fixed effects of SURGERY (NonOp, ACLT, or SHAM) and DAY (7 or 28d post-op) and repeated effects of TIME (1, 3, or 8hrs) and M_r (by bin) on c^{HA} after injection were assessed by 4-way ANOVA. The fixed effect of GROUP (NonOp, ACLT d7, SHAM d7, or ACLT d28) and repeated effect of M_r on steady-state neat SF c^{HA} were assessed by 2-way ANOVA with Dunnett post-hoc tests to determine differences from the NonOp group within each M_r bin. The fixed effect of GROUP on time constant and serum c^{HA} was assessed by 1-way ANOVA with Dunnett post-hoc tests to determine differences from the NonOp group. Significance was set as $P<0.05$ and statistical analyses were performed using Systat 10.2 (Systat Software Inc., Chicago, IL).

Table 4.1: Sample numbers per group (surgery, injection, time, and post-op day). Total: N=26 rabbits (n=52 knees).

surgery	**injection**	**time [hr]**		**n [# knees]**	
		0^+	**1, 3, 8**	**7d**	**28d**
NonOp	saline		✓	6	3
	HA	✓		4	-
			✓	5	5
	FITC-HA		✓	3	-
ACLT	saline		✓	3	3
	HA	✓		4	-
			✓	5	5
SHAM	saline		✓	3	-
	HA		✓	3	-

4.4 Results

4.4.1 HA Concentration and M_r-distribution in SF After Surgery

The M_r-distribution of HA in SF shifted towards lower M_r HA after surgery. The c^{HA} in SF varied with M_r ($P<0.0001$) and GROUP ($P<0.0001$), with an interaction ($P<0.0001$, **Fig. 4.1**). The total c^{HA} was decreased from ~2.5mg/mL by 47% for ACLT and 49% for SHAM at day 7, and by 26% for ACLT day 28. Both ACLT and SHAM day 7 groups contained decreased high-M_r HA (7000-2500kDa, $P<0.001$, **Fig. 4.1A, B**). By day 28, the ACLT group still contained less high-M_r HA ($P<0.01$), but also contained more lower-M_r (1000-50kDa) HA ($P<0.01$-0.05, **Fig. 4.1D-F**) than the NonOp group.

4.4.2 Residence Time of HA in SF

After washout and exogenous injection, the HA M_r-distribution showed endogenous replenishment of high-M_r HA, while lower-M_r HA was lost from SF, in particular at day 7 after ACLT. Rabbit SF normally contains mainly high M_r HA (>4000kDa) that, after washout, was replenished over time for both NonOp and ACLT joints (**Fig. 4.2 a-g**). After washout, HA with a M_r-distribution lower than the typical endogenous profile, was injected and resampled at $t=0^+$, showing a moderate dilution effect, but similar size distribution to the injection profile for both NonOp and ACLT joints (**Fig. 4.2 h-j**). Distributions determined at 1, 3, and 8hrs after injection showed M_r-dependent loss over time, with exacerbated loss occurring in ACLT joints 7d after surgery (**Fig. 4.2 k-v**).

The c^{HA} breakdown by M_r of each sample was determined to allow quantitative comparisons between surgical groups and time after surgery. After washout and injection (**Fig. 4.3A**), the HA distributions at $t=0^+$ were similar for NonOp and ACLT joints (P=0.82, **Fig. 4.3B**), diluted on average to ~60% injection concentration. The total c^{HA} by M_r bin was divided into the endogenous HA (**top, open bars**) and injected (**bottom, filled bars, Fig. 4.2C and D**), with the endogenous concentration mainly found in the 7000-2500kDa bin (**Fig. 4.3.C.i and D.i**). The injected HA varied with SURGERY (P<0.0001), DAY post-surgery (P<0.05), M_r (P<0.0001), and TIME post-injection (P<0.0001), with interactions of M_r*SURGERY (P<0.01), TIME*DAY (P<0.0001), and M_r*TIME (P<0.01). By 8hrs post-injection on day 7, c^{HA} in the 2500-1000kDa bin had dropped to 75% injection for NonOp compared to 37% for ACLT and 57% for SHAM groups (**Fig. 4.3.C.ii**) and in the 250-50kDa bin to 48% for NonOp compared to 24% for ACLT and 45% for SHAM groups (**Fig. 4.3.C.v**). However, by 8hrs post-injection on day 28 the differences between NonOp and ACLT were smaller, as HA concentration in the 2500-1000kDa bin had dropped to 85% injection for NonOp compared to 68% for ACLT (**Fig. 4.3.D.ii**) and in the 250-50kDa bin to 55% for NonOp and 43% for ACLT (**Fig. 4.3.D.v**).

The residence time of HA decreased with M_r and after surgery. Plotted as % of injected over sampling times, the increased loss for ACLT compared to SHAM and NonOp at day 7 are apparent (**Fig. 4.4A**), though by day 28 ACLT and NonOp are similar (**Fig. 4.4B**). The residence time constants, which describe the slope of the HA loss, by M_r-bin ranged from ~27hrs for the NonOp 2500-1000kDa bin to ~7hrs for the 250-50kDa bin, and were decreased at day 7 for all M_r after ACLT (by 64-75%) and in

the 2500-1000kDa bin for SHAM as well (by 41%) compared to NonOp (**Fig. 4.4C**), indicating a major effect of the ACLT and minor effect of the surgical procedure itself. By day 28, the ACLT time constants were similar to NonOp controls (P=0.39-0.50).

The M_r-dependence of HA loss for high-M_r HA was confirmed using FITC-HA. High-M_r FITC-labeled HA was cleared from the joint fluid slower than mid-range HA, while low-M_r HA was quickly lost (**Fig. 4.5**).

4.4.3 Synovium and Subsynovium Cell Density

ACLT surgery induced structural changes and increased cellular density in the synovium and subsynovium. The synovium thickness was increased at day 7, with weaker matrix staining than NonOp (**4.6.i-iii**). After surgery, the subsynovium of ACLT joints contained substantial cellular infiltration at day 7, including by CD4+ lymphocytes and CD11b+ macrophages (**Fig. 4.6.iv-vi**), and also evidence of neovascularization. Although the increased transport rates of HA out of the joint after ACLT appeared to be resolved by day 28, likely do to matrix molecule production, the cell infiltration of subsynovium was still apparent (**Fig. 4.6.iv**).

4.4.4 Serum HA Concentration

The c^{HA} in blood serum was also transiently increased after surgery. Treatment (normal, ACLT d7, SHAM d7, or ACLT d28) significantly affected serum HA content ($P<0.05$, **Fig. 4.7**). Serum HA concentration almost doubled from ~21ng/mL to ~41ng/mL in both ACLT and SHAM groups at day 7, before returning to ~22ng/mL at day 28.

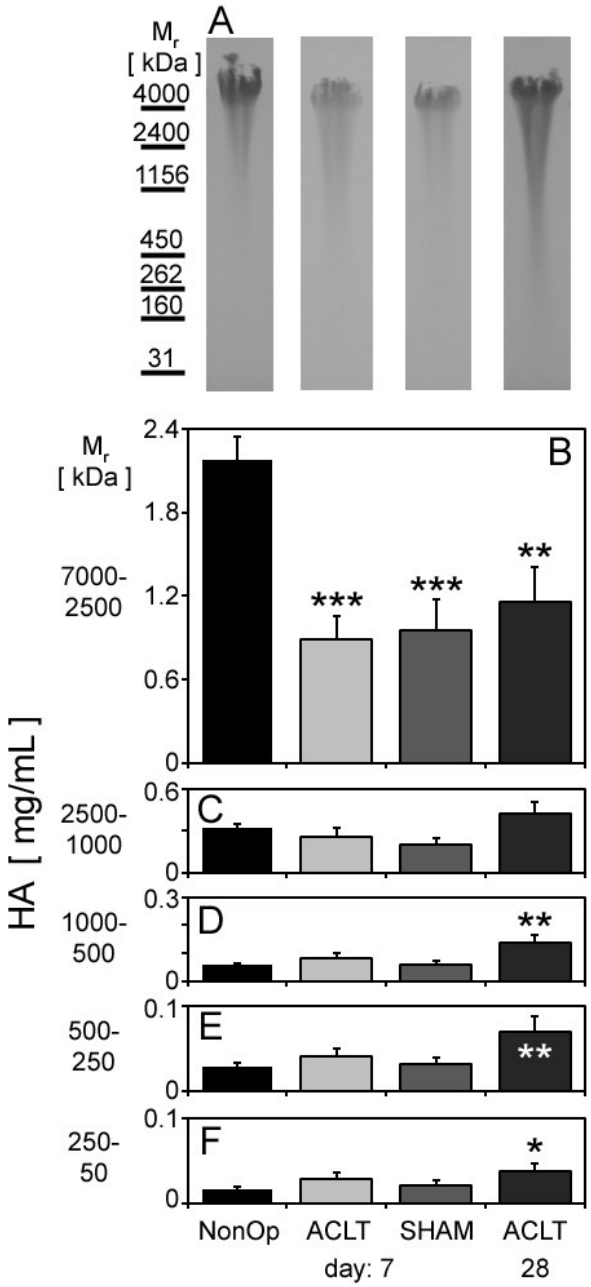

Figure 4.1: (**A**) HA Mr distribution in SF is altered after surgery. Quantification (**B-F**) showed decreased high-M_r HA is present at day 7 after ACLT or SHAM surgery. By day 28, in addition to decreased high-Mr, there is increased lower Mr HA present. *: P<0.05, **: P<0.01, ***: P<0.001.

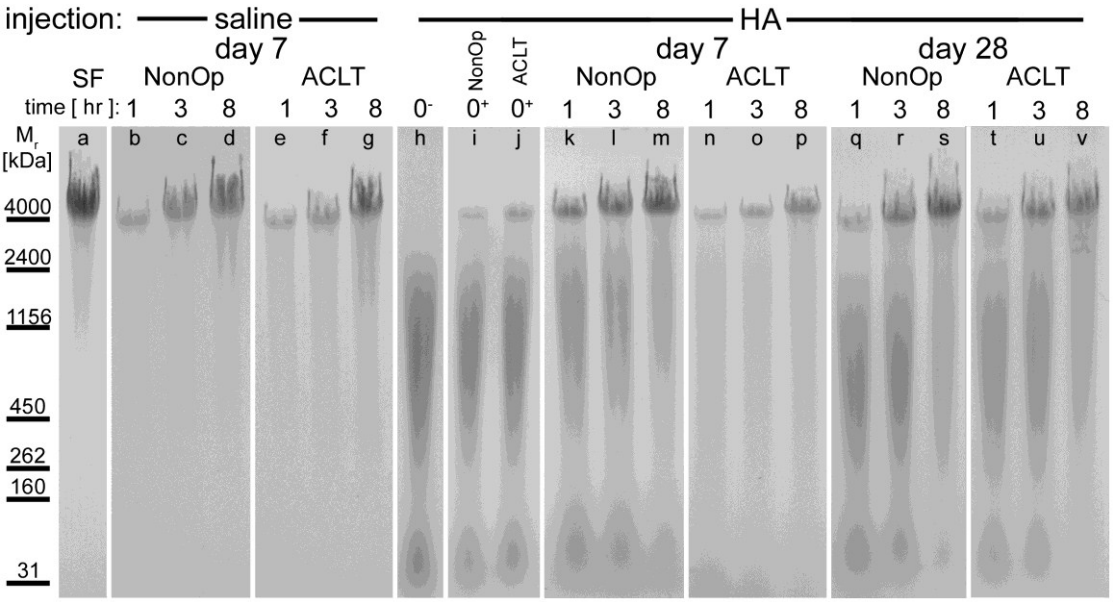

Figure 4.2: M_r distribution of HA in joint fluids sampled over time after saline lavage or HA injection for NonOp and ACLT rabbit knees. Replenishment of high-Mr HA occurred in all joints, likely due to secretion. Compared to NonOp controls, ACLT samples had less HA content at day 7, though this effect is lessened by day 28. HA loss from SF is M_r-dependent, with faster loss at lower M_r.

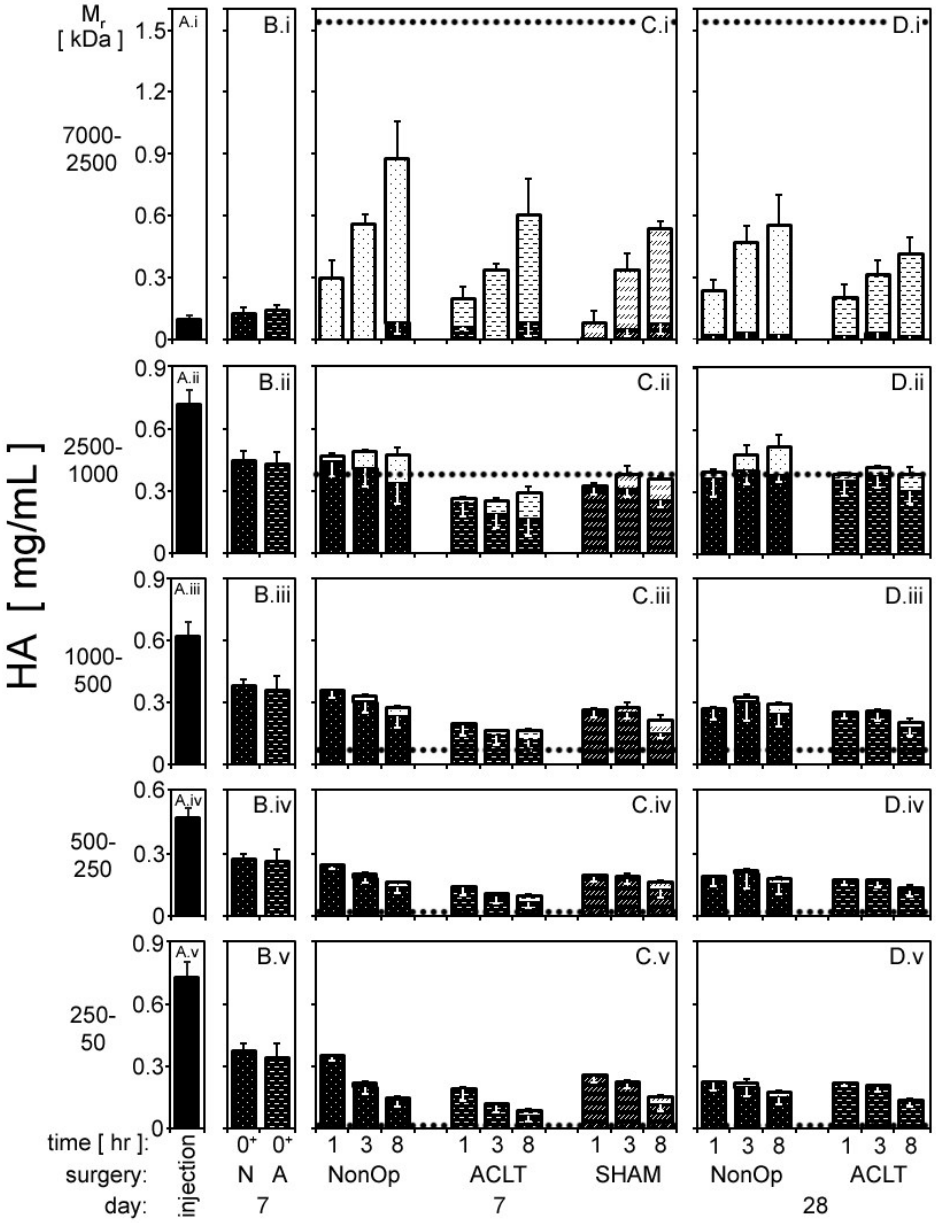

Figure 4.3: HA concentrations of various Mr bins in joint fluid samples over a time course after HA injection in NonOp, ALCT, or SHAM knees. Upper bars indicate endogenous replenishment, and lower bars indicate injected HA. Significant effects of surgery ($P<0.0001$), day post-surgery ($P<0.05$), M_r ($P<0.0001$), and time post-injection ($P<0.0001$) were determined.

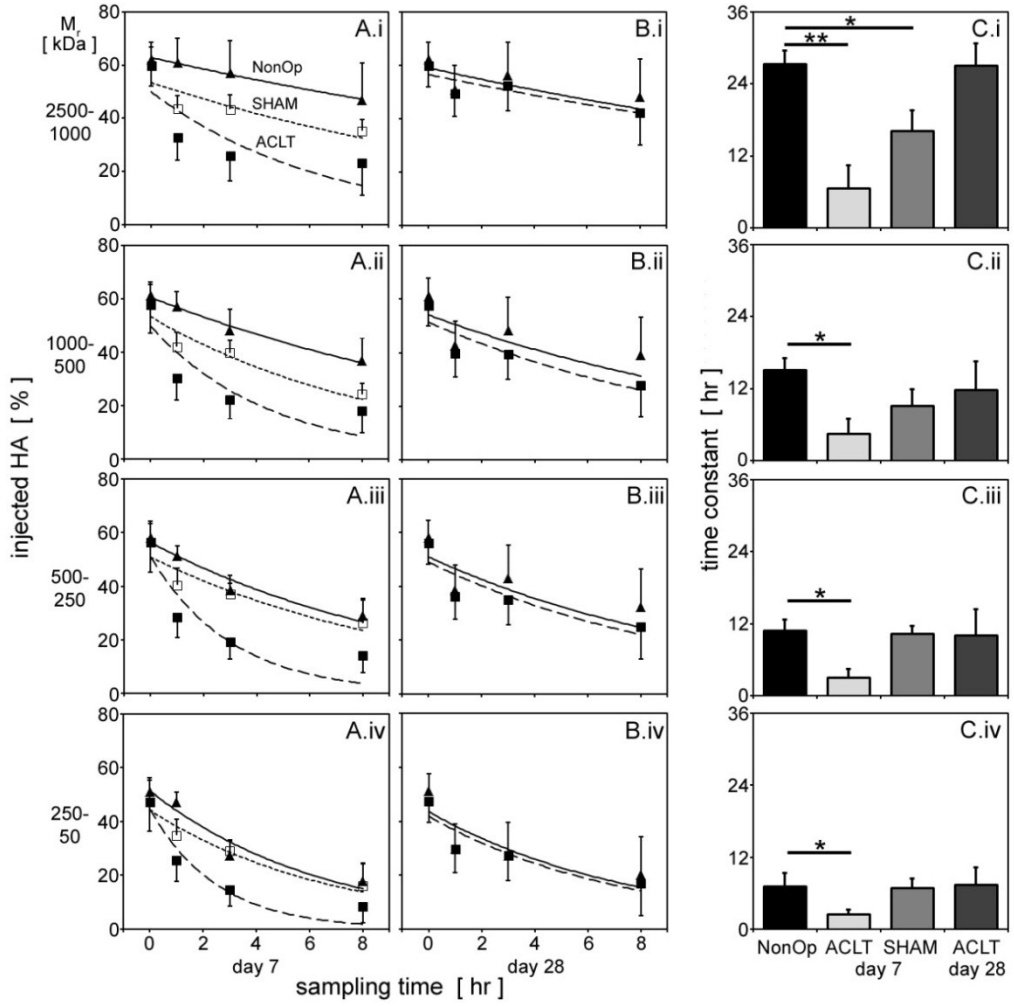

Figure 4.4: Residence time constants for HA increase with M_r, and are decreased at day 7 post-ACLT, though that decrease is recovered by day 28. SHAM controls were similar to NonOp at low M_r, and between ACLT and NonOp at higher M_r. *: $P<0.05$, **: $P<0.01$.

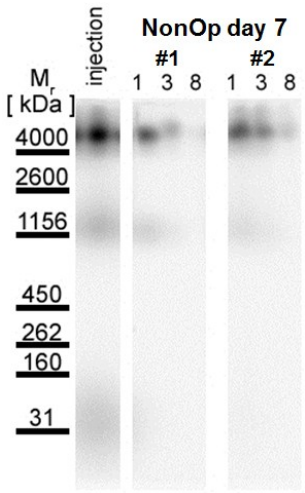

Figure 4.5: Example joint fluids after FITC-labeled HA injection in NonOp knees show M_r-dependent HA loss from SF even at high-M_r.

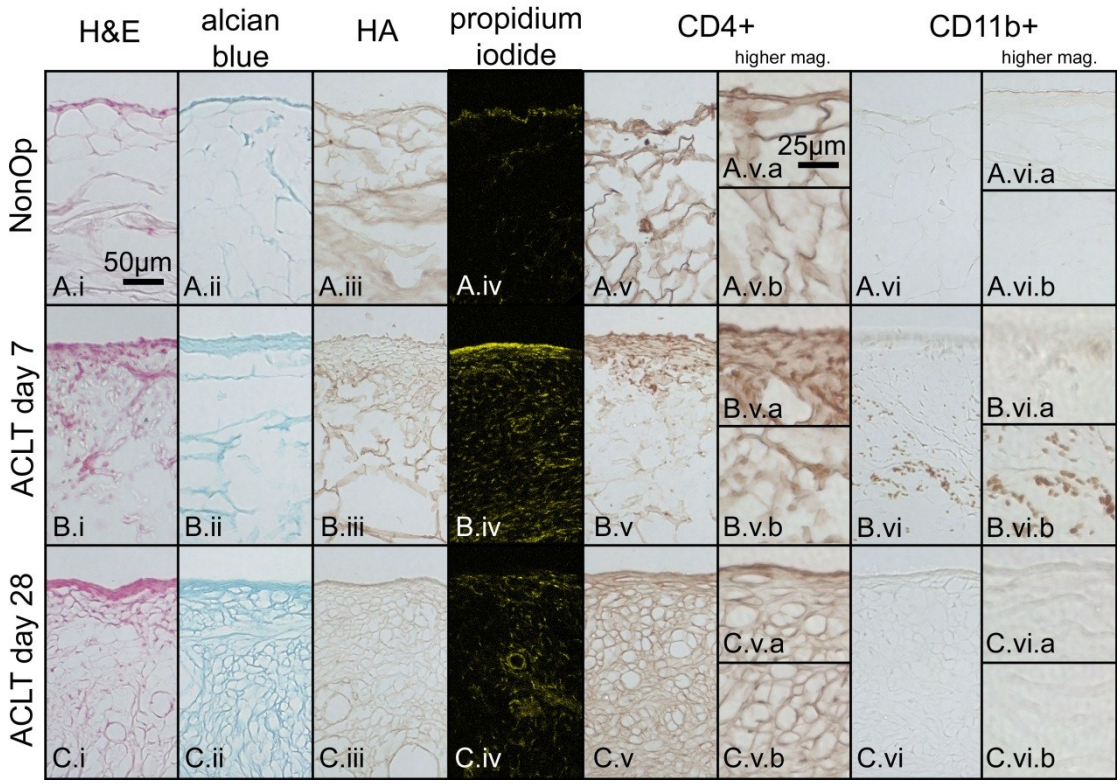

Figure 4.6: Histology of the structure and cellularity of synovium and subsynovium samples from (**A**) NonOp, (**B**) ACLT day 7, and (**C**) ACLT day 28. Sections were stained with H&E (**i**) and alcian blue (**ii**), or for HA (**iii**) to examine tissue structure, while others were stained with propidium iodide (**iv**) or for CD4 (**v**) and CD11b (**vi**) cell surface markers. Higher magnification images were taken at the synovium surface (**a**) or deep in the subsynovium (**b**).

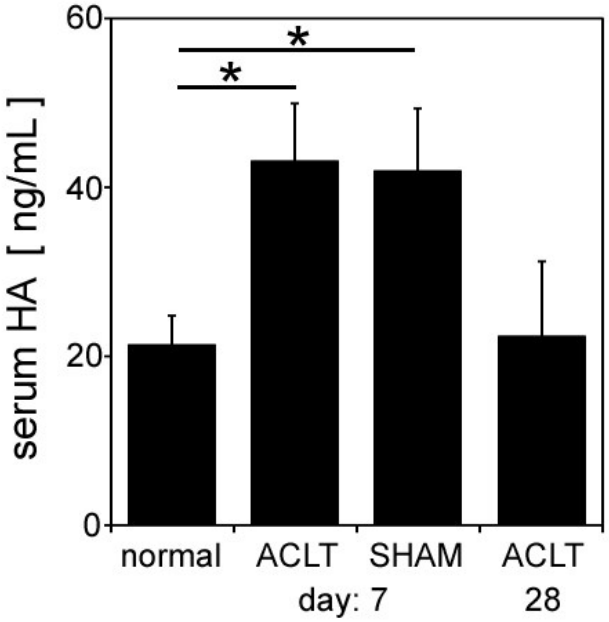

Figure 4.7: Serum concentration of HA is increased at day 7 after surgery for both ACLT and SHAM operations, but falls to normal levels by day 28. *: $P<0.05$.

4.5 Discussion

These results demonstrate that the residence time of HA in SF is transiently decreased after ACLT, suggesting a biophysical mechanism for the alterations in SF HA M_r distribution, and SF composition in general, after injury or during inflammation. The HA M_r-distribution shifted to lower M_r HA after surgery (**Fig. 4.1**). Direct sampling of SF over time after washout and injection indicated accumulation of high M_r species, while lower M_r HA diffused out of SF, especially at day 7 after ACLT (**Fig. 4.2**). Quantification of these gels confirmed the effects of HA M_r, surgery, day after surgery, and time after injection on HA loss from SF (**Fig. 4.3**). The time constants for HA residence in SF by M_r are consistent with previously reported times, and demonstrate an effect both of the surgical insult, as well as a more intense effect of ACLT itself in decreasing HA residence times (**Fig. 4.3, 4.4**). Synovium thickening and subsynovial cell infiltration after surgery (**Fig. 4.6**) likely decreases the resistance to HA loss through subsynovium to the lymphatics, while the systemic HA turnover via plasma concentration (**Fig. 4.7**), an additional measure of inflammation, was also increased at day 7. Together, these data suggest increased HA transport due to an inflammatory state as a biophysical mechanism underlying the loss of high-M_r HA from SF after injury and during inflammatory pathologies.

The *in vivo* data provide a self-consistent description of the transport of HA from SF, despite inherent limitations in this type of animal study. Animal numbers were limited, and neat SF was sampled repeatedly from individual knees. Although 26 rabbits and 52 knees were utilized, they were divided among 13 groups in order to

investigate the effects of surgery and time after surgery on HA transport. Despite limited sample numbers, sufficient power was achieved to show significant effects and confirm the hypothesis. In addition, endogenous noise in the high-M_r bins confounded the transport measurements, though FITC-labeling of HA confirmed similar transport trends as measured quantitatively for lower M_r bins (**Fig. 4.5**). Repeated sampling of the SF required multiple needle sticks through the joint capsule, which could have increased the HA loss from SF. However, the needle sampling did not appear to markedly affect HA loss, since large holes in synovium would have negated the M_r efflux dependence, which was not the case. Finally, homeostasis reflects loss through degradation, transport, and cellular phagocytosis. Although degradation and cellular uptake were not measured directly, the uniformity and concentration of high-M_r HA that accumulated after saline washout suggests the time-scale for degradation or uptake was longer than for diffusion, implying the data reported here were dominated by the diffusion effects.

The results are consistent with a biophysical mechanism explaining the shift to lower-M_r HA in SF after injury and during inflammatory pathologies (**Fig. 4.8**). Normally, the M_r-dependent residence time of HA in SF accompanied by the secretion of high-M_r HA leads to a steady-state, with SF containing mostly high-M_r HA (**Fig. 4.1**); low-M_r HA, created by HA turnover diffuses relatively quickly out of SF. After injury or during inflammation, the synovium becomes more permeable to HA (**Figs. 4.2-4.4**), likely due to cellular infiltration displacing and digesting the extracellular matrix barrier to molecular efflux through synovium, decreasing the residence time of high-M_r HA. Faster diffusive efflux of high-M_r HA, coupled with decreased secretion

rates and possibly increased degradation rates, would shift the steady-state M_r distribution to lower M_r, as observed experimentally. Although the cell infiltration was still present at day 28 (**Fig. 4.6**), the synovial matrix production in the meantime looks to have restored the extracellular matrix barrier, restoring residence times. In addition to major inflammatory events such as injury or during rheumatoid arthritis, this mechanism may also be responsible for altered SF composition in OA, where an inflammatory component is increasingly recognized [39].

Understanding the mechanisms leading to altered SF HA composition, such as altered transport rates due to inflammation, is important since SF function is determined by composition. Changes to the HA concentration and M_r in SF alter the biophysical properties of the fluid, including viscosity and viscoelastic properties [12, 37], as well as the lubrication function [36]. SF effusion is characteristic of inflammatory pathology, and increased plasma filtration rates into SF, which depend on SF hydrostatic pressure [19] and joint capsule strains [27] that vary with flexion, likely contribute to decreased HA concentration. In addition to HA, lubricant molecules secreted locally into SF, such as lubricin, likely also have decreased residence time in SF. A decreased barrier to diffusion out of SF also indicates decreased resistance to convective and diffusive molecular flux from plasma into SF. This may explain the increased concentration of higher M_r plasma proteins, including from the inter-α-trypsin inhibitor family, that are found in pathological SF [47, 48].

The transport mechanisms suggested by these results indicate potential avenues, and pitfalls, for therapeutic interventions. The M_r-dependent HA residence times in SF in NonOp and after ACLT provide an estimate of the residence time for

other proteoglycans and proteins in SF, and highlight the difficulty for localized retention of injected pharmaceuticals, especially during the inflammatory response phases following injury. The inflammatory state of the synovial lining may be a potential target for intervention to restore the normal homeostasis of SF. Early clinical intervention that decreases the synovial inflammatory response and restores lubrication following injury [1, 17] may be able to limit or retard the progression from injury to post-traumatic osteoarthritis.

This work investigated the state of transport of HA in the joint at various times after ACLT, demonstrating the M_r-dependent rate of HA loss likely due to inflammatory cell infiltration into the synovial and subsynovial joint capsule lining. Such altered transport rates help explain the altered HA content and general compositional changes in SF after injury and during inflammatory pathologies. In addition, these data describe the molecular conditions under which any pharmaceutical intervention must function, as well as suggest potential targets for clinical intervention.

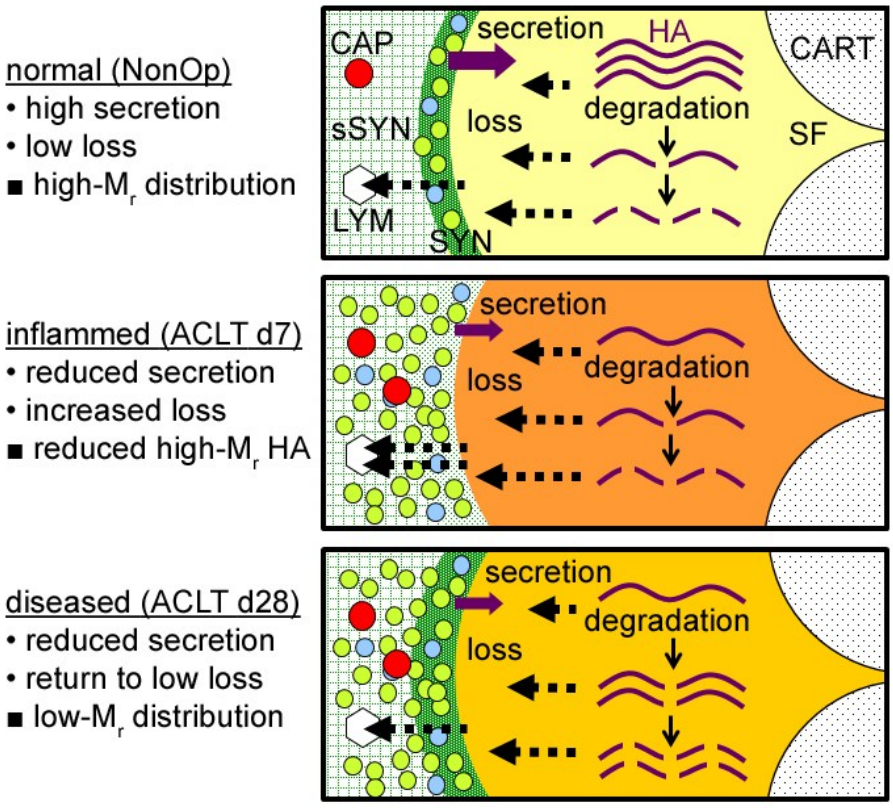

Figure 4.8: Schematic representation of the biophysical processes, including secretion, degradation, and loss, contributing to altered HA M_r distribution in pathological SF.

4.6 Acknowledgments

Chapter 4, in full, has been submitted to *Arthritis & Rheumatism*. The dissertation author was the primary author and thanks co-authors Justin C. Cheng, Bradley C. Hansen, Tomonori Yamaguchi, Koichi Masuda, and Robert L. Sah. This work was supported by grants from the National Institute of Arthritis, Musculoskeletal and Skin Diseases and a Ruth L. Kirschstein National Research Service Award predoctoral fellowship from the National Institute on Aging (for WJM).

4.7 References

1. Antonacci JM, Schmidt TA, Serventi LA, Cai MZ, Shu YL, Gastelum NS, Schumacher BL, McIlwraith CW, Sah RL: Effects of equine joint injury on boundary lubrication of articular cartilage by synovial fluid: role of hyaluronan. *Arthritis Rheum* (Accepted) Apr 19, 2012.

2. Antonas KN, Fraser JR, Muirden KD: Distribution of biologically labelled radioactive hyaluronic acid injected into joints. *Annals of the rheumatic diseases* 32:103-11, 1973.

3. Balazs EA: The physical properties of synovial fluid and the special role of hyaluronic acid. In: *Disorders of the Knee,* ed. by AJ Helfet, Lippincott Co., Philadelphia, 1974, 63-75.

4. Blewis ME, Nugent-Derfus GE, Schmidt TA, Schumacher BL, Sah RL: A model of synovial fluid lubricant composition in normal and injured joints. *Eur Cell Mater* 13:26-39, 2007.

5. Brown MP, Trumble TN, Plaas AH, Sandy JD, Romano M, Hernandez J, Merritt KA: Exercise and injury increase chondroitin sulfate chain length and decrease hyaluronan chain length in synovial fluid. *Osteoarthritis and cartilage / OARS, Osteoarthritis Research Society* 15:1318-25, 2007.

6. Brown TJ, Laurent UB, Fraser JR: Turnover of hyaluronan in synovial joints: elimination of labelled hyaluronan from the knee joint of the rabbit. *Experimental physiology* 76:125-34, 1991.

7. Chang DG, Iverson EP, Schinagl RM, Sonoda M, Amiel D, Coutts RD, Sah RL: Quantitation and localization of cartilage degeneration following the induction of osteoarthritis in the rabbit knee. *Osteoarthritis Cartilage* 5:357-72, 1997.

8. Coleman PJ, Scott D, Mason RM, Levick JR: Characterization of the effect of high molecular weight hyaluronan on trans-synovial flow in rabbit knees. *J Physiology* 514:265-82, 1999.

9. Coleman PJ, Scott D, Mason RM, Levick JR: Role of hyaluronan chain length in buffering interstitial flow across synovium in rabbits. *J Physiol* 526 Pt 2:425-34, 2000.

10. Dahl LB, Dahl IM, Engstrom-Laurent A, Granath K: Concentration and molecular weight of sodium hyaluronate in synovial fluid from patients with rheumatoid arthritis and other arthropathies. *Ann Rheum Dis* 44:817-22, 1985.

11. Decker B, Mc GW, Mc KB, Slocumb CH: Concentration of hyaluronic acid in synovial fluid. *Clin Chem* 5:465-9, 1959.

12. Fam H, Bryant JT, Kontopoulou M: Rheological properties of synovial fluids. *Biorheology* 44:59-74, 2007.

13. Fraser JR, Kimpton WG, Pierscionek BK, Cahill RN: The kinetics of hyaluronan in normal and acutely inflamed synovial joints: observations with experimental arthritis in sheep. *Semin Arthritis Rheum* 22:9-17, 1993.

14. Gomez JE, Thurston GB: Comparisons of the oscillatory shear viscoelasticity and composition of pathological synovial fluids. *Biorheology* 30:409-27, 1993.

15. Granger HJ, Taylor AE: Permeability of connective tissue linings isolated from implanted capsules; implications for interstitial pressure measurements. *Circ Res* 36:222-8, 1975.

16. Holley HL, Patton FM, Pigman W, Platt D: An electrophoretic study of normal and post-mortem human and bovine synovial fluids. *Arch Biochem Biophys* 64:152-63, 1956.

17. Jay GD, Elsaid KA, Zack J, Robinson K, Trespalacios F, Cha CJ, Chichester CO: Lubricating ability of aspirated synovial fluid from emergency department patients with knee joint synovitis. *J Rheumatol* 31:557-64, 2004.

18. Kaminski T, Siebrasse JP, Gieselmann V, Kubitscheck U, Kappler J: Imaging and tracking of single hyaluronan molecules diffusing in solution. *Glycoconj J* 25:555-60, 2008.

19. Knight AD, Levick JR: Pressure-volume relationships above and below atmospheric pressure in the synovial cavity of the rabbit knee. *J Physiol* 328:403-20, 1982.

20. Kushner I, Somerville JA: Permeability of human synovial membrane to plasma proteins. Relationship to molecular size and inflammation. *Arthritis Rheum* 14:560-70, 1971.

21. Laurent UB, Fraser JR, Engstrom-Laurent A, Reed RK, Dahl LB, Laurent TC: Catabolism of hyaluronan in the knee joint of the rabbit. *Matrix* 12:130-6, 1992.

22. Lee HG, Cowman MK: An agarose gel electrophoretic method for analysis of hyaluronan molecular weight distribution. *Anal Biochem* 219:278-87, 1994.

23. Levick JR: Permeability of rheumatoid and normal human synovium to specific plasma proteins. *Arthritis Rheum* 24:1550-60, 1981.

24. Levick JR: Microvascular architecture and exchange in synovial joints. *Microcirculation* 2:217-33, 1995.

25. Lindenhayn K, Heilmann HH, Niederhausen T, Walther HU, Pohlenz K: Elimination of tritium-labelled hyaluronic acid from normal and osteoarthritic rabbit knee joints. *Eur J Clin Chem Clin Biochem* 35:355-63, 1997.

26. Mazzucco D, Scott R, Spector M: Composition of joint fluid in patients undergoing total knee replacement and revision arthroplasty: correlation with flow properties. *Biomaterials* 25:4433-45, 2004.

27. McCarty WJ, Masuda K, Sah RL: Fluid movement and joint capsule strains due to flexion in rabbit knees. *J Biomech* 44:2761-7, 2011.

28. McDonald JN, Levick JR: Morphology of surface synoviocytes in situ at normal and raised joint pressure, studied by scanning electron microscopy. *Ann Rheum Dis* 47:232-40, 1988.

29. Myers SL, Brandt KD, Eilam O: Even low-grade synovitis significantly accelerates the clearance of protein from the canine knee. Implications for measurement of synovial fluid "markers" of osteoarthritis. *Arthritis Rheum* 38:1085-91, 1995.

30. Price FM, Levick JR, Mason RM: Changes in glycosaminoglycan concentration and synovial permeability at raised intra-articular pressure in rabbit knees. *J Physiol* 495 (Pt 3):821-33, 1996.

31. Price FM, Levick JR, Mason RM: Glycosaminoglycan concentration in synovium and other tissues of rabbit knee in relation to synovial hydraulic resistance. *J Physiol (Lond)* 495:803-20, 1996.

32. Ropes MW, Rossmeisl EC, Bauer W: The origin and nature of normal human synovial fluid. *J Clin Invest* 19:795-9, 1940.

33. Sabaratnam S, Arunan V, Coleman PJ, Mason RM, Levick JR: Size selectivity of hyaluronan molecular sieving by extracellular matrix in rabbit synovial joints. *J Physiol* 567:569-81, 2005.

34. Schmid K, Macnair MB: Characterization of the proteins of human synovial fluid in certain disease states. *J Clin Invest* 35:814-24, 1956.

35. Schmid K, Macnair MB: Characterization of the proteins of certain postmortem human synovial fluids. *J Clin Invest* 37:708-18, 1958.

36. Schmidt TA, Gastelum NS, Nguyen QT, Schumacher BL, Sah RL: Boundary lubrication of articular cartilage: role of synovial fluid constituents. *Arthritis Rheum* 56:882-91, 2007.

37. Schurz J, Ribitsch V: Rheology of synovial fluid. *Biorheology* 24:385-99, 1987.

38. Scott D, Coleman PJ, Mason RM, Levick JR: Glycosaminoglycan depletion greatly raises the hydraulic permeability of rabbit joint synovial lining. *Exp Physiol* 82:603-6, 1997.

39. Sellam J, Berenbaum F: The role of synovitis in pathophysiology and clinical symptoms of osteoarthritis. *Nat Rev Rheumatol* 6:625-35, 2010.

40. Simkin PA: Synovial permeability in rheumatoid arthritis. *Arthritis Rheum* 22:689-96, 1979.

41. Simkin PA: Physiology of normal and abnormal synovium. *Semin Arthritis Rheum* 21:179-83, 1991.

42. Simkin PA: Synovial perfusion and synovial fluid solutes. *Ann Rheum Dis* 54:424-8, 1995.

43. Sliwinski AJ, Zvaifler NJ: The removal of aggregated and nonaggregated autologous gamma globulin from rheumatoid joints. *Arthritis Rheum* 12:504-14, 1969.

44. Smith MM, Ghosh P: The synthesis of hyaluronic acid by human synovial fibroblasts is influenced by the nature of the hyaluronate in the extracellular environment. *Rheumatol Int* 7:113-22, 1987.

45. Vignon E, Bejui J, Mathieu P, Hartmann JD, Ville G, Evreux JC, Descotes J: Histological cartilage changes in a rabbit model of osteoarthritis. *J Rheumatol* 14S:104-6, 1987.

46. Wallis WJ, Simkin PA, Nelp WB: Protein traffic in human synovial effusions. *Arthritis Rheum* 30:57-63, 1987.

47. Yingsung W, Zhuo L, Morgelin M, Yoneda M, Kida D, Watanabe H, Ishiguro N, Iwata H, Kimata K: Molecular heterogeneity of the SHAP-hyaluronan complex. Isolation and characterization of the complex in synovial fluid from patients with rheumatoid arthritis. *The Journal of biological chemistry* 278:32710-8, 2003.

48. Yoshihara Y, Plaas A, Osborn B, Margulis A, Nelson F, Stewart M, Rugg MS, Milner CM, Day AJ, Nemoto K, Sandy JD: Superficial zone chondrocytes in normal and osteoarthritic human articular cartilages synthesize novel truncated forms of inter-alpha-trypsin inhibitor heavy chains which are attached to a chondroitin sulfate proteoglycan other than bikunin. *Osteoarthritis and cartilage / OARS, Osteoarthritis Research Society* 16:1343-55, 2008.

49. Yoshioka M, Coutts RD, Amiel D, Hacker SA: Characterization of a model of osteoarthritis in the rabbit knee. *Osteoarthritis Cartilage* 4:87-98, 1996.

CHAPTER 5:

CONTROL OF THE BIOPHYSICAL PROPERTIES OF HYALURONAN SOLUTIONS AND OSTEOARTHRITIC SYNOVIAL FLUID WITH INTER-ALPHA-TRYPSIN INHIBITOR HEAVY CHAINS

5.1 Abstract

Synovial fluid (SF) is an ultrafiltrate of plasma found in diarthrodial joints that allows for their low-friction articulation and normally contains high concentration and molecular mass (M_r) hyaluronan (HA). During joint pathologies, the concentration and molecular mass of HA and viscosity in SF is typically decreased. Pathological SF also contains higher concentrations of the inter-α-trypsin inhibitor (IαI) family, whose heavy chains (HC) modify HA. The hypothesis of this study was that the biophysical properties of HA solutions and osteoarthritic human SF samples (OA-hSF) can be altered by HC attachment. HA solutions and OA-hSFs were incubated with varying concentrations of IαI and the biophysical properties of the resulting samples were assessed. The results indicate HA binding proteins interactions account for a large portion (~20-70%) of OA-hSF viscosity, and HA concentration and M_r are also important determinants of viscosity. Incubation with IαI: 1) increased the viscosity of

HA solutions in a dose-dependent manner up to ~40% and the viscosity of OA-hSF by ~10%; 2) increased the hydrodynamic fluid pressure generated by HA solutions in a dose-dependent manner up to ~50% and OA-hSF by ~10%; and 3) decreased the membrane permeability to HA from HA solutions and OA-hSF by ~60%. The viscosity increase for HC·HA solutions was partially mitigated through reduction/alkylation, suggesting noncovalent HC-HC interactions contribute to the matrix stabilizing effects of HC attachment. These results suggest that HC attachment to HA alters the biophysical properties of HA-based solutions, including SF. The HC modification of HA could be used to tune HA solution properties for different biomedical applications, and may also allow for the clinical restoration of the biophysical properties of pathological SF..

5.2 Introduction

Synovial fluid (SF) is found in diarthrodial joints and contributes to their low-friction articulation. SF is an ultrafiltrate of plasma, filtered through the synovial intimal layer, synovium, with additional lubricants secreted by local cell populations, including synoviocytes [22, 32, 34] and chondrocytes [31]. The most abundant lubricant molecule in SF is hyaluronan (HA), a non-sulfated glycosaminoglycan of repeating disaccharides, normally present in high molecular mass (M_r) form (~4-6MDa) [3, 11, 25]. HA has long been considered as the primary contributor to the characteristic viscosity and viscoelasticity of SF [17]. In addition to being a major component of SF, HA on the surface of synovium provides substantial resistance to the outflow of fluid and macromolecules [9], helping to maintain the concentration of HA in SF.

During joint pathologies, such as rheumatoid arthritis, osteoarthritis (OA), and after joint injury, the composition and function of SF is altered. The HA concentration is typically decreased and the HA M_r-distribution shifts towards lower M_r species, especially after joint injury [7] and in rheumatoid arthritis [14, 19], leading to decreased viscosity [33]. Viscosity is an important determinant of the amount of pressure that can be supported by SF during "hydrodynamic mode" and "mixed mode" lubrication [18], which occurs in joints as opposing surfaces approach each other but before "boundary mode" lubrication of surfaces in contact [2]. In addition to decreasing viscosity, membrane permeability is decreased for lower M_r HA [5],

resulting in decreased HA residence time [8, 28] and possibly overall concentration in SF.

Pathological SF also contains higher proportions of protein-glycosaminoglycan-protein complexes, particularly from the inter-α-trypsin inhibitor (IαI) family, which modify HA. Human IαI is present in plasma at ~0.2-0.4mg/mL [4, 35] and consists of two heavy chains (HC), HC1 and HC2 [16], which are covalently linked to the chondroitin sulfate chain of a proteoglycan, bikunin [15]. HC molecules can covalently attach to HA via two sequential transesterification reactions, first from the donor IαI to an intermediate tumor necrosis factor-stimulated gene 6 (TSG-6) [36], and then from TSG-6·HC to HA, binding HC·HA and releasing free TSG-6 [27, 30]. HC·HA, also known as serum-derived hyaluronan-associated protein (SHAP·HA), is found in high concentration in inflamed tissues, including rheumatoid [24, 29, 37, 38] and osteoarthritic [24, 39] SF.

The binding of HCs to HA molecules alter their biochemical and biophysical properties, though only a few functional properties have been investigated. HC modification alters cell interactions with HA via CD44, as CD44+ leukocyte adhesion is enhanced for HC·HA compared to HA alone [41]. Non-covalent HC-HC interactions in HC·HA increase the structural stability of HA solutions, as in the case of HA-rich cumulus matrix expansion [42]. Such stabilization of HA matrices may be an important physiological response to inflammatory states [23, 40]. While the importance of HC·HA interactions in determining the biophysical properties of HA based solutions is clear and the HC·HA interactions have been recapitulated *in vitro* [10, 20], those properties have not yet been reported.

Thus, the hypothesis of this study was that the biophysical properties of HA solutions and osteoarthritic human SF samples (OA-hSF) can be altered by HC attachment. The objectives were to 1) determine the contributions HA binding proteins to OA-hSF viscosity, as well as the concentration and M_r-dependence of viscosity of HA solutions; 2) recapitulate the HC·HA interactions *in vitro*; and 3) determine the biophysical effects of the HC·HA interactions in HA solutions and OA-hSF, including on viscosity, fluid pressure generation, and membrane permeability to HA.

5.3 Materials and Methods

5.3.1 Study Design

The contributions of protein-based molecules and HA to SF viscosity were investigated. To determine the contributions of protein-based molecules to SF viscosity, the viscosity of OA SF samples were assessed with or without digestion with broad-spectrum serine protease, Proteinase K, and reduction and alkylation, processes that do not affect HA, but should digest most protein and disrupt tertiary and quaternary structure and minimize interactions of any remaining. The contributions of glycosaminoglycans, freed by proteoglycan core protein digestion, are assumed to be negligible compared to HA. To determine the contributions of HA to SF viscosity, solutions of HA at different concentration and M_r were prepared and the viscosity assessed.

The effects of HC modification of HA on the biophysical properties of HA solutions and OA SF were also investigated. IαI solutions were enriched from normal human plasma and incubated at various concentrations with TSG-6 and HA solutions of different molecular weights and OA SF. Reaction verification, in the form of HC·HA, indicated by high M_r (>260kDa) HC-positive bands that shift towards the expected size of HC (~90kDa) with hyaluronidase digestion, was assessed by Western blot. The biophysical properties of samples were assessed by determining solution viscosity, hydrodynamic fluid pressure, and membrane permeability to HA.

5.3.2 Synovial Fluid and Hyaluronan Solutions

Human SF was obtained clinically and solutions of different M_r and concentrations of HA were prepared from commercial sources. OA SF samples were obtained clinically (OA-hSF) from patients undergoing knee arthroplasty at the time of surgery, with IRB approval. OA-hSF samples were spun at 15,000g for 30min, and then the supernatant was aliquoted and stored at –80°C until use. Lyophilized HA of various weight-average molecular weights (51, 130, 500, 1000, 1680kDa, Lifecore Biomedical; Chaska, MN) were dissolved in phosphate buffered saline with 10mM $MgCl_2$ pH 7.4 (PBS) at 1 or 3mg/mL and were stored at 4°C for <1wk until use. Healon® (~4000kDa HA) was also purchased and similarly diluted in PBS. Solutions were allowed to mix overnight at 37°C before use to ensure uniformity of dilution.

5.3.3 Inter-α-trypsin Inhibitor Enrichment

Enriched solutions of IαI were prepared from human plasma. Anion exchange chromatography using DEAE Sepharose Fast Flow resin (GE Lifesciences; Piscataway, NJ) was performed on normal adult human plasma (Golden West Biologicals; Temecula, CA), with step gradients of 0.16, 0.23, 0.28, and 0.36M NaCl in phosphate buffer pH 6, as described previously [26]. The 0.23-0.28M fraction was concentrated using a 100kDa cutoff spin-filter at 3,000g. The retentate was diluted in PBS to $1/120^{th}$ the volume of plasma used, and contained 60mg/mL total protein, with ~10mg/mL IαI, as determined by BCA assay (Thermo Scientific; Waltham, MA), protein gel (6% tris-glycine, stain: GelCode Blue) and Western blot (Ab: polyclonal rabbit anti-human ITI-H1, Santa Cruz Biotechnology; Santa Cruz, CA). Solutions were stored at 4°C until for <1wk until use.

5.3.4 Sample Preparation

Samples of OA-hSF were prepared to determine the protein and proteoglycan contribution to SF viscosity. 500μL samples of OA-hSF were spiked with 10μL of PBS or 25μg/mL Proteinase K (Roche Applied Science; Indianapolis, IN) and incubated for 16hr at 37°C. An additional 5μL of PBS or 1M DL-dithiothreitol (DTT, Sigma-Aldrich; Saint Louis, MO) was added before incubation for 30min at 37°C. Finally, 50μL PBS or 0.55M iodoacetamide (IAA, Sigma) was added before incubation for 30min at 37°C.

Samples of HA and OA-hSF were prepared with or without IαI at various concentrations. HA solutions were diluted to the 2mg/mL with equivalent volumes of PBS or IαI. OA-hSFs were also slightly diluted (3% by volume, 15μL of solution in 500μL SF) with either PBS or IαI. Human recombinant TSG-6 (R&D Systems; Minneapolis, MN) was added to each sample at 0.6μg/mL, and the solutions were mixed and incubated for 16hrs at 37°C.

5.3.5 Reaction Verification

The HC to HA transfer reaction was verified by Western blot. Samples of 2mg/mL 1680kDa HA with 6mg/mL IαI were prepared as described above and then separated on a sephacryl 400-HR (Sigma) gel permeation column. The fraction of interest was collected from K_{AVG}=0-0.2, isolating the high M_r species. Portions of this eluate were incubated with hyaluronidase (from *Streptomyces* hyalurolyticus, MP Biomedical; Solon, OH) for 0, 10, 100, or 1000min at 37°C. Samples were then run on

a 6% tris-glycine gel (Life Technologies; Grand Island, NY) and either i) fixed in 25% isopropanol and stained in Stainsall (Sigma), or ii) blotted to PVDF and probed for HC1 using ITI-H1 (Santa Cruz Biotechnologies).

5.3.6 Viscosity and Fluid Pressurization

The viscosity of sample solutions was determined at various shear rates. A cone/plate viscometer (DV-III Ultra, Brookfield Engineering; Middleboro, MA) was used to determine the viscosity of 0.5mL samples at shear rates of 10, 30, 100, 300, 1000, and 1500 1/s. Low shear rate data are omitted for low viscosity samples that did not generate enough torque to give accurate viscosity values at those shear rates.

The pressure generated by samples during parallel-plate hydrodynamic lubrication was determined. A parallel-plate setup was created by positioning a 6.8mm diameter flat-tipped cylindrical stainless-steel pin 1mm above a flat stainless steel surface on a Dynastat mechanical testing system (Northern Industrial Services; Cohoes, NY). The gap was filled with 60μL of sample, and the gap height reduced to 70μm. The gap height was oscillated for 10 cycles at 20Hz with peak displacement amplitude of 50μm and velocity of ~6.2mm/s, while the pressure generated in the fluid in opposition to compaction was monitored with a 250g load cell (Honeywell; Columbus, OH). These parameters were chosen to simulate the hydrodynamic lubrication regime. The loads measured at peak velocity were divided by pin area and reported as pressures.

5.3.7 Hyaluronan Membrane Permeability

The permeability of membranes to HA in HA solutions and OA-hSF with or without IαI was assessed using a custom diffusion chamber. Two single-chamber blocks were machined from acrylic such that a membrane could be sandwiched between them, sealed with o-rings, and the blocks secured using stainless steel screws with wing nuts. The equal 0.75mL chambers were separated by a 100nm pore size polycarbonate track-etched membrane (GE Healthcare; Piscataway, NJ), slightly larger than synovial membrane's estimated pore size of ~50nm [28], and with a 0.245cm^2 surface area for diffusion. The 'source' chamber was filled with 0.25mL of sample, and the 'buffer' chamber with 0.25mL PBS. Samples of 25µL were taken from both chambers at 24 and 48hr and tested for HA concentration using an HA assay (R&D Systems). The slope of HA mass vs time for each sample was used to compute membrane permeability as:

$$P_{HA} = \frac{dM_{HA}}{dt}\frac{1}{Ac^0_{HA}} \qquad \text{(Equation 1)}$$

where P is the permeability, M the mass of HA in the buffer chamber, A the surface area for diffusion, and c^0 the initial HA concentration in the 'source' chamber.

5.3.8 Statistical Analysis

The data are presented as mean±SEM for n=2-4 samples of HA solutions and n=4 donors of OA-hSF. The effects of shear rate and protein digestion/denaturation on viscosity of OA-hSFs were assessed by 2-way repeated measures ANOVA. The fixed effects of M_r and concentration and repeated effect of shear rate on HA solution

viscosity were assessed by 3-way repeated measures ANOVA. The fixed effect of IαI concentration and repeated effect of shear rate on HA solutions, and the repeated effects of IαI concentration and shear rate on OA-hSFs were assessed by 2-way repeated measures ANOVAs. The fixed effect of IαI concentration on fluid pressure of HA solutions was assessed by 1-way ANOVA with Tukey posthoc tests, and the effect of IαI addition on fluid pressure of OA-hSF was assessed by paired t-test. Finally, the effects of IαI addition on permeability were assessed by t-test and paired t-tests for HA solutions and OA-hSFs, respectively. Significance was set as $P<0.05$ and statistical analyses were performed using Systat 10.2 (Systat Software Inc., Chicago, IL).

5.4 Results

5.4.1 Contributions of Hyaluronan Binding Proteins to Viscosity

Proteins and proteoglycans account for a large portion of OA-hSF viscosity. The viscosity of OA-hSF varied with shear rate ($P<0.0001$) and protein digestion and denaturation ($P<0.05$), with interaction ($P<0.0001$). Digestion and denaturation of protein-based molecules decreased the viscosity by 20-70%, with the largest effects at low shear rates (**Fig. 5.1**).

The viscosity of HA solutions increased with concentration and M_r. The viscosity of HA solutions varied with shear rate ($P<0.0001$), M_r ($P<0.0001$), and concentration ($P<0.0001$), with interactions between shear rate*M_r ($P<0.0001$) and shear rate*concentration ($P<0.001$). The concentration and shear rate-dependencies were more pronounced at higher M_r (**Fig. 5.2A, B**).

5.4.2 HC Transfer to HA

The transfer of HC1 from IαI to HA was verified by Western blot. High M_r products of the HA and IαI incubation from the S400 column were incubated with hyaluronidase for varying lengths of time, leading to partial or full digestion of the HA, as indicated by the Stainsall gel (**Fig. 5.3, left panel**). HC1-reactivity was assessed by Western blot (**Fig. 3, right panel**). Without HA digestion, two main low mobility bands suggest the presence of high M_r HC·HA, and unreacted IαI. With partial HA digestion, HC1 reactivity appears in a number of discrete bands and as

diffuse staining. After full HA digestion, the diffuse staining is replaced with a large band at ~90kDa, the expected value of HC1.

5.4.3 Viscosity of HA Solutions and OA-hSF After IαI Incubation

Incubation with IαI increased the viscosity of HA solutions in a dose-dependent manner. The viscosity of HA solutions of both 4000 and 1680kDa varied with shear rate ($P<0.0001$) and IαI incubation ($P<0.01$, **Fig 5.4A**). IαI incubation increased the viscosity of both M_r HA solutions over all shear rates (e.g for 4000kDa HA at $10s^{-1}$ from 143 to 242cP) up to ~40% (**Fig. 5.4B**).

IαI incubation also increased the viscosity of OA-hSF. The viscosity of OA-hSF varied with shear rate ($P<0.0001$) and IαI ($P<0.05$). The viscosity increase was shear rate-dependent, increasing from 161 to 223cP or ~40% at low shear rates and from 12.6 to 13.4cP or ~6% at high shear rates (**Fig. 5.4D**).

5.4.4 Fluid Pressure During Lubrication Flow

Incubation with IαI increased the fluid pressure generated by HA solutions during lubrication flow in a dose-dependent manner. Fluid pressure varied with IαI ($P<0.0001$), with each IαI concentration different than the others ($P<0.001$-0.05, **Fig. 5.5**), and increasing the pressure from 520 to 790Pa, or by up to ~50%. IαI incubation also increased the fluid pressure generated by OA-hSF. Fluid pressure increased from 660 to 721Pa, or by ~10% with IαI ($P<0.05$, **Fig. 5.5**).

5.4.5 Membrane Permeability to HA and HC·HA

The permeability of membranes to HA from HA solutions and OA-hSF decreased with addition of IαI. Permeability values for the 100nm pore size membrane to HA in HA solutions were significantly lower ($P<0.05$) after incubation with IαI, decreasing from 50 to 19 $x10^{-8}$ cm/s, or by 63% (**Fig. 5.6**). The permeability of HA from OA-hSF samples was also lower after IαI treatment ($P<0.05$), decreasing from 12 to 4.4 $x10^{-8}$ cm/s, or by ~64% (**Fig. 5.6**).

5.4.6 HC-HC Interactions

The increased viscosity of HA solutions after HC modification was partially mitigated by reduction and alkylation. The viscosity of HA solutions varied with treatment (HA vs HA+IαI vs HA+IαI+R/A, $P<0.0001$) and shear rate ($P<0.0001$), with an interaction ($P<0.0001$, **Fig. 5.7A**). While incubation with IαI increased the viscosity of HA solutions by ~51-63%, R/A treatment reduced the increase to ~21-33% (**Fig. 5.7B**), with a more pronounced mitigation at lower shear rates.

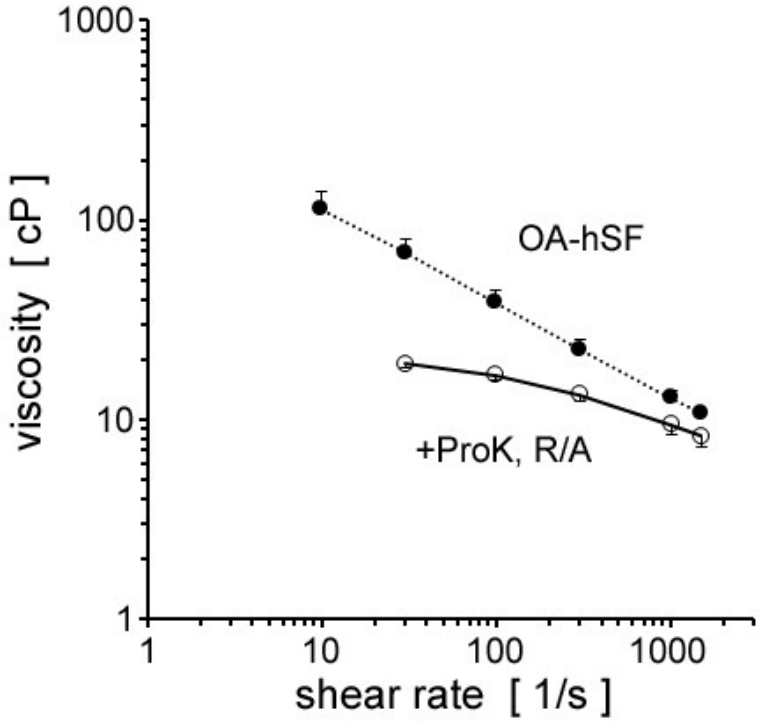

Figure 5.1: HA binding proteins account for 20-70% of the viscosity of OA-hSF. Significant effects of shear rate ($P<0.0001$), protein digestion and denaturation ($P<0.05$), and the interaction between them ($P<0.0001$). n=4 donors tested.

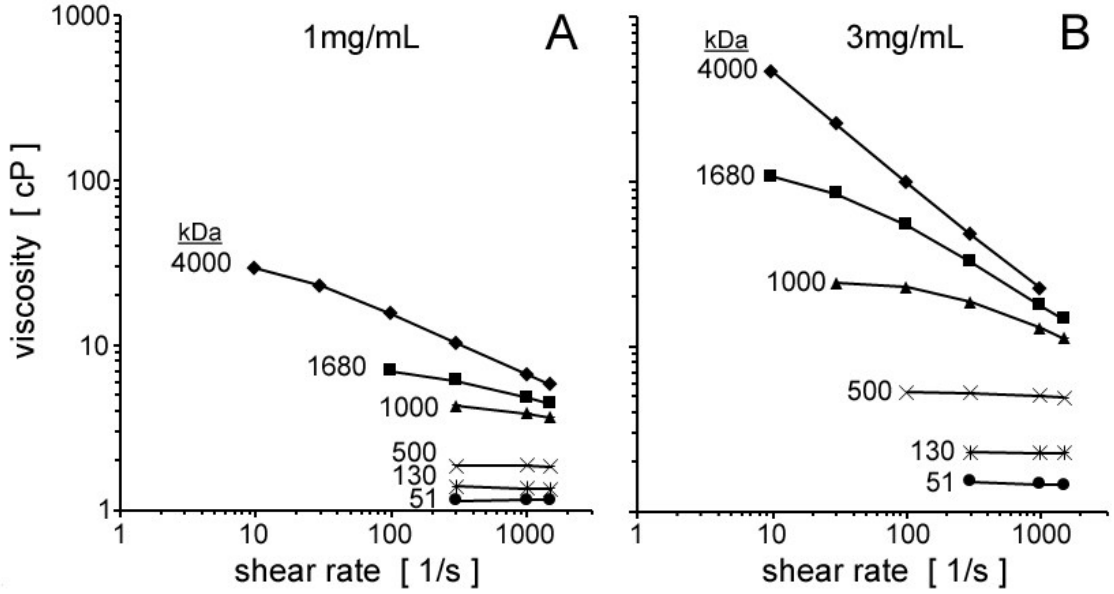

Figure 5.2: The viscosity of HA solutions is increased with concentration and M_r. Significant effects of M_r ($P<0.0001$), concentration ($P<0.0001$), shear rate (0.0001), shear rate*M_r ($P<0.0001$), and shear rate*concentration ($P<0.001$). n=4 HA solutions.

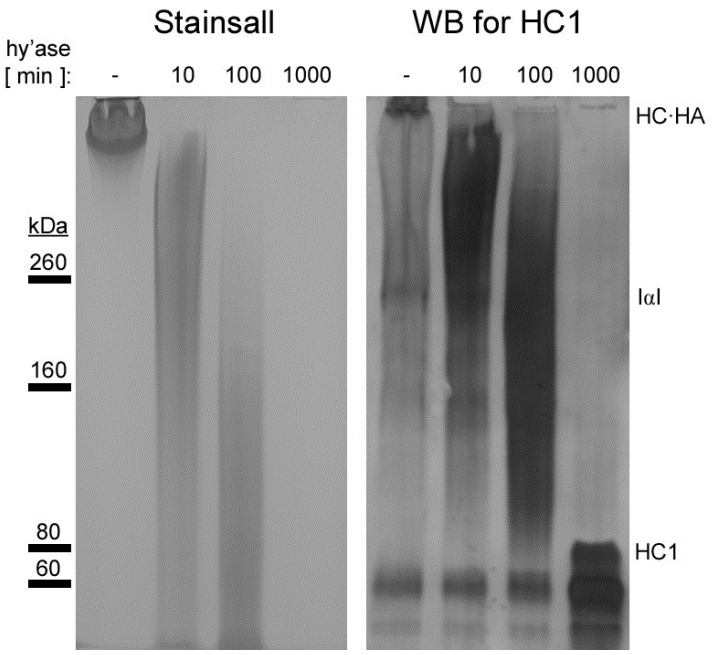

Figure 5.3: Stainsall gel and Western blot indicating the presence of HC1 attached to HA. Left panel: Stainsall gel showing high molecular weight HA that is digested with increasing exposure to hyaluronidase. Right panel: Western blot for HC1 showing a high molecular weight band and a second band, likely unreacted IαI, before hyaluronidase digestion. With partial digestion, HC1-reactive discrete bands as well as a smear of reactivity are visible. After full digestion, discrete bands are still visible, but the reactive smear has shifted to the expected ~90kDa for HC1.

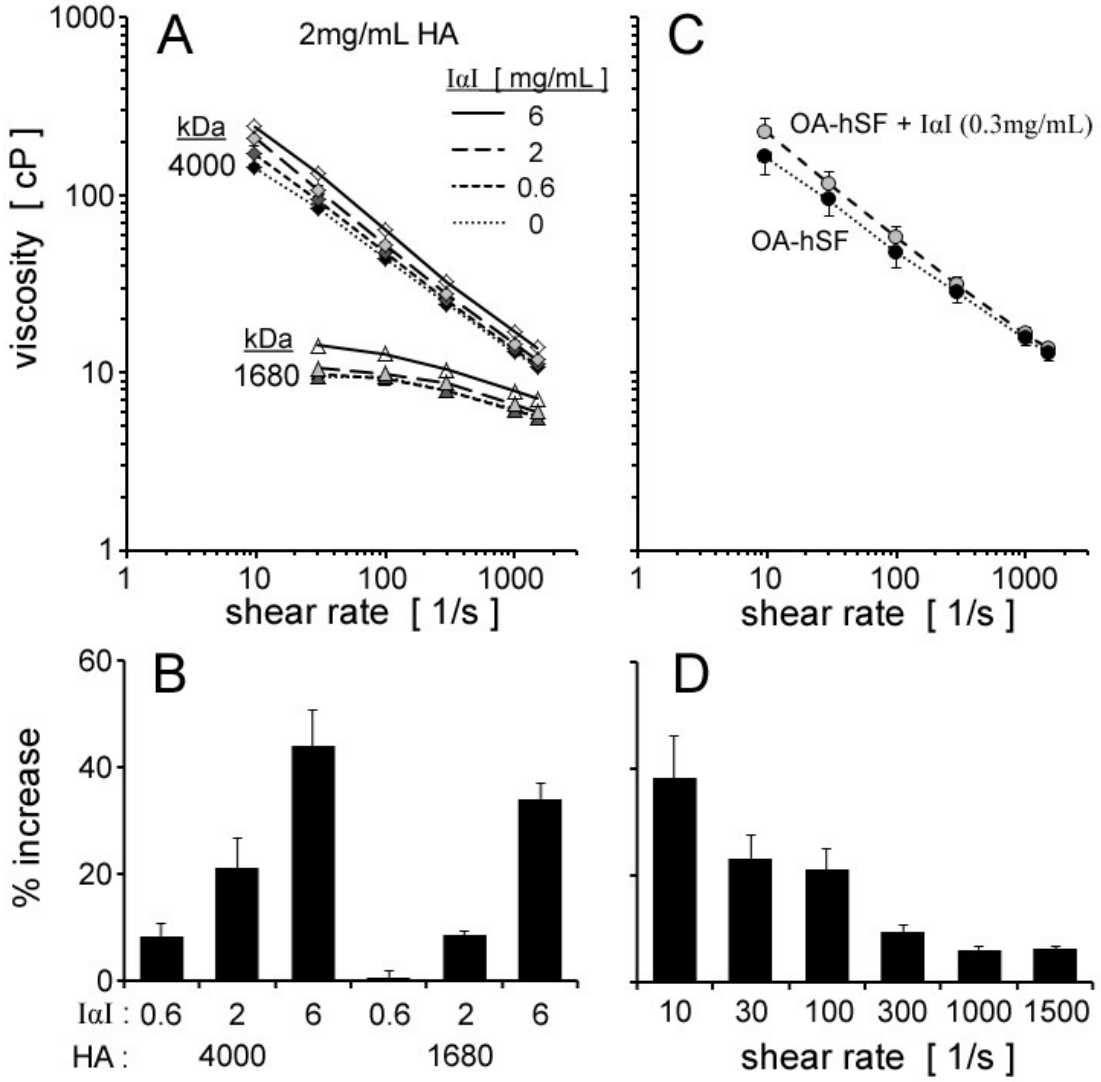

Figure 5.4: HA incubation with IαI increases the solution viscosity. Viscosity increased for both molecular weights of HA in a dose-dependent manner (**A**), with an average increase of ~40% at 6mg/mL IαI (**B**). OA-hSF displayed similar trends, with IαI increasing viscosity (**C**) in a shear rate-dependent manner (**D**). Effects of shear rate ($P<0.0001$) and IαI ($P<0.05$) were significant for both HA solutions and for OA-hSF. n=2-4 HA samples, n=4 OA-hSF donors.

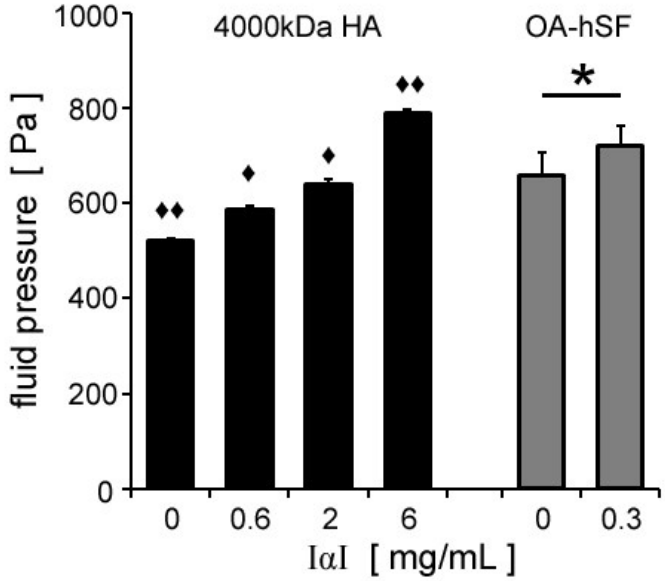

Figure 5.5: HA incubation with IαI increases the fluid pressure generated during lubrication flow. HA of 4000kDa at 2mg/mL or OA-hSF were incubated with IαI and tested for fluid pressure generated during lubrication flow for a 70µm gap width moving at 6.2mm/s. ♦: $P<0.05$, ♦♦: $P<0.01$ vs all others. *: $P<0.05$. n=3 HA solutions, n=4 OA-hSF donors.

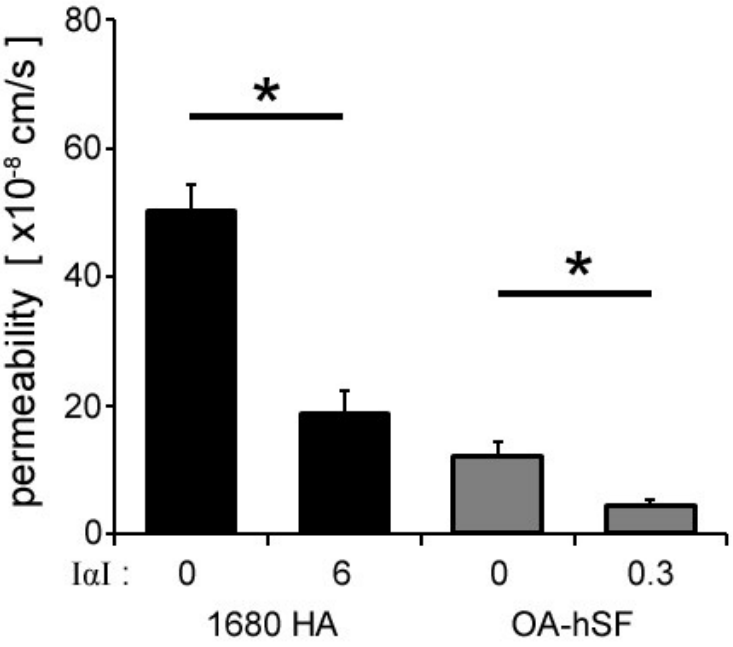

Figure 5.6: Membrane permeability to HC-HA complexes is lower than to HA alone. After reaction with IαI, membrane permeability decreased by ~63% ($P<0.05$) for HA solutions and ~64% ($P<0.05$) for OA-hSF. n=2 HA solutions, n=3 OA-hSF donors.

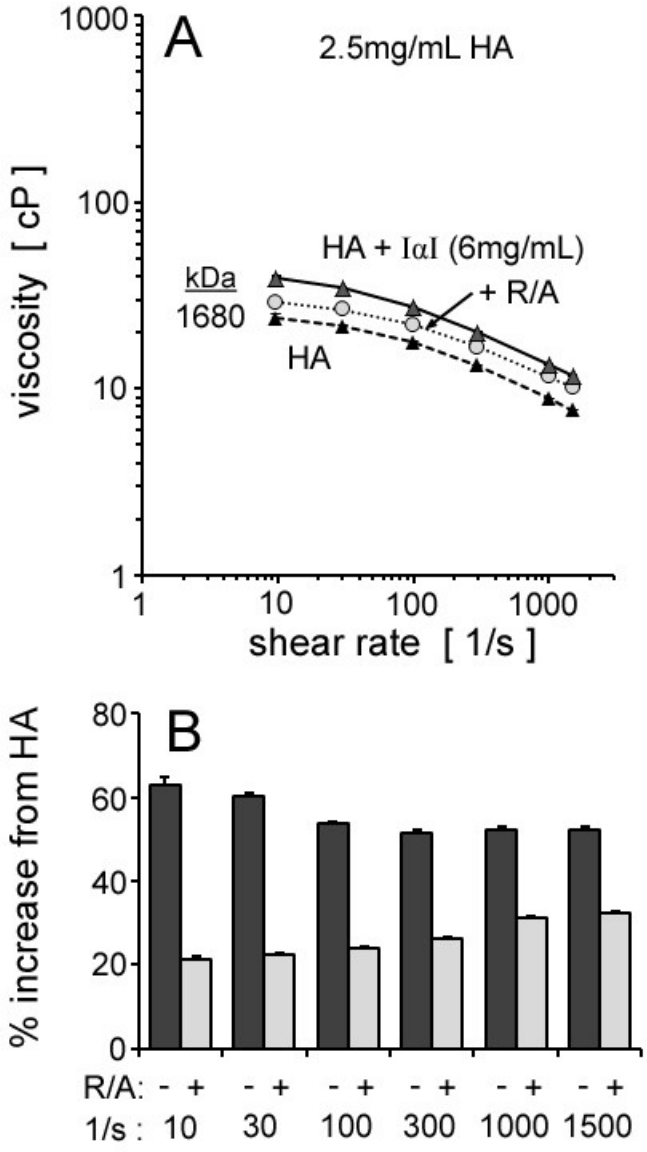

Figure 5.7: Modification of HA with HCs increases the solution viscosity partially due to noncovalent HC-HC interactions that are disrupted with reduction and alkylation. Significant effects of treatment, shear rate, and treatment*shear rate interaction ($P<0.0001$).

5.5 Discussion

These results demonstrate that HC modification of HA alters the biophysical properties of HA-based solutions, including SF. While HA binding protein interactions in SF (**Fig. 5.1**) and the concentration and M_r of HA (**Fig. 5.2**) contribute to viscosity, further attachment of HC to HA (**Fig. 5.3**) can be used to control HA-based solutions' biophysical properties. HC modification increases viscosity (**Fig. 5.4**) and hydrodynamic lubrication pressures (**Fig. 5.5**), and decreases the membrane permeability of HA (**Fig. 5.6**), due to non-covalent interactions (**Fig. 5.7**) between the HCs. This reaction could be used to create HA solutions with tunable biophysical properties, as well as treat pathological joints by restoring the biophysical functions of SF.

These *in vitro* experiments provide proof-of-principle for the control of biophysical properties of HA solutions and SF by modifying HA with HCs. Reconstitution of HC·HA was achieved *in vitro* to control the amount of HC attachment via IαI concentration. Additional studies to determine similar physical properties of HC·HA extracted from physiological tissues would complement the current approach. The biophysical parameters investigated here were tailored to the functions of SF, including physiologically relevant shear rates, hydrodynamic velocity, and membrane pore size, though expanding those ranges, utilizing additional testing modalities, and further molecular analysis of the number of HC modifications and how they correlate with biophysical properties would be of interest.

The altered biophysical properties of HC·HA are likely attributable to both static and dynamic HC-HC interactions, as well as the stereological tangling effects of adding side chains. Electron microscopy studies of IαI indicate the HCs consist of a sphere-like globular domain of ~11nm diameter, and a thin linear chain region of ~15.5nm [6]. In HC·HA, the globular domains of the HC side chains appear to interact, and this interaction can be partially mitigated with reduction/alkylation (**Fig. 5.7**), possibly explaining the aggregation of HA [38]. This mitigation was shear rate dependent with less mitigation at higher shear rates, consistent with a view that both HC-HC interactions (dominant at low shear rates), as well as stereological molecular tangling (dominant at high shear rates), In addition to static HC-HC interactions that stabilize the HA matrix and may allow for the formation of higher order HA organization into fibrils or cables [12, 13], the presence of HCs alters the dynamic matrix properties as well. The viscosity increases reported in the current study (**Fig. 5.4**) are likely due to transient HC-HC interactions that increase the fluid's internal friction and therefore viscosity. Such interactions would also explain the increased fluid pressure during hydrodynamic lubrication testing and the decreased membrane permeability.

The HC modification of HA could be used as an adjustable property of HA solutions, along with concentration and M_r, to tune properties for different biomedical applications. HA gels are used clinically for a variety of situations, including joint pain, dry eye syndrome, healing skin wounds, and for cosmetic enhancements. The biophysical properties needed for each application differ and are typically determined by HA concentration, M_r, and degree of cross-linking. HC·HA modification could

provide a biomimetic alternative to chemical cross-linking or additional controllable dimension to achieve the desired properties. Functionalization of the globular ends of HC may also be possible, allowing for a physiologically compatible HA modification reaction that could be used for a wide array of biomaterials for tissue engineering [1].

Exploiting the transesterification reactions that produce HC·HA may allow for the clinical restoration of the biophysical properties of pathological SF. *In vitro* treatment of OA-hSF with physiologic concentrations of IαI resulted in modest increases in viscosity and fluid pressure and decreased membrane permeability (**Figs. 5.4-5.6**); intraarticular injection of exogenous IαI and TSG-6 to increase HC modification of native HA may be an effective clinical intervention to restore normal SF function. Further study of the in vivo biophysical effects in an animal model would be an appropriate next step. The modification of HA with HCs has also been reported to decrease HA susceptibility to degradation by oxygen derived free radicals [21]. This combination of decreased membrane permeability and potential resistance to free radical degradation point to a longer residence time for HC·HA in the joint, a limitation of current HA injectable therapies. Stabilization of the HA layer associated with synovium in the joint by HC·HA would increase resistance to fluid and macromolecular outflow and could further increase the residence time of lubricant molecules in SF.

The results of this study demonstrate that the biophysical properties of HA solutions and SF can be controlled by the modification of HA using HCs from IαI. While the biochemistry of the reaction is well-understood, these data demonstrate the importance of the physical properties of HC·HA at different concentrations in

physiological solutions. The IαI dose-dependence of the HA solution properties and the physiologically compatible reaction conditions that result in HC·HA suggest utility for the reaction in generating native HA biomaterials as well as for a clinical intervention in pathological joints.

5.6 Acknowledgments

Chapter 5, in full, will be submitted to *The Journal of Biological Chemistry*. The dissertation author was the primary author and thanks co-authors Justin C. Cheng, William D. Bugbee, and Robert L. Sah. This work was supported by grants from the National Institute of Arthritis, Musculoskeletal and Skin Diseases and a Ruth L. Kirschstein National Research Service Award predoctoral fellowship from the National Institute on Aging (for WJM).

5.7 References

1. Allison DD, Grande-Allen KJ: Review. Hyaluronan: a powerful tissue engineering tool. *Tissue engineering* 12:2131-40, 2006.

2. Ateshian GA: The role of interstitial fluid pressurization in articular cartilage lubrication. *Journal of biomechanics* 42:1163-76, 2009.

3. Balazs EA: The physical properties of synovial fluid and the special role of hyaluronic acid. In: *Disorders of the Knee,* ed. by AJ Helfet, Lippincott Co., Philadelphia, 1974, 63-75.

4. Becker A, Sandson J: The source of the inter-alpha trypsin inhibitor in pathologic hyaluronateprotein. *Arthritis and rheumatism* 14:764-6, 1971.

5. Blewis ME, Lao BJ, Jadin KD, McCarty WJ, Bugbee WD, Firestein GS, Sah RL: Semi-permeable membrane retention of synovial fluid lubricants hyaluronan and proteoglycan 4 for a biomimetic bioreactor. *Biotechnol Bioeng* 106:149-60, 2009.

6. Blom AM, Morgelin M, Oyen M, Jarvet J, Fries E: Structural characterization of inter-alpha-inhibitor. Evidence for an extended shape. *The Journal of biological chemistry* 274:298-304, 1999.

7. Brown MP, Trumble TN, Plaas AH, Sandy JD, Romano M, Hernandez J, Merritt KA: Exercise and injury increase chondroitin sulfate chain length and decrease hyaluronan chain length in synovial fluid. *Osteoarthritis and cartilage / OARS, Osteoarthritis Research Society* 15:1318-25, 2007.

8. Brown TJ, Laurent UB, Fraser JR: Turnover of hyaluronan in synovial joints: elimination of labelled hyaluronan from the knee joint of the rabbit. *Experimental physiology* 76:125-34, 1991.

9. Coleman PJ, Scott D, Mason RM, Levick JR: Role of hyaluronan chain length in buffering interstitial flow across synovium in rabbits. *J Physiol* 526 Pt 2:425-34, 2000.

10. Colon E, Shytuhina A, Cowman MK, Band PA, Sanggaard KW, Enghild JJ, Wisniewski HG: Transfer of inter-alpha-inhibitor heavy chains to hyaluronan by surface-linked hyaluronan-TSG-6 complexes. *The Journal of biological chemistry* 284:2320-31, 2009.

11. Dahl LB, Dahl IM, Engstrom-Laurent A, Granath K: Concentration and molecular weight of sodium hyaluronate in synovial fluid from patients with rheumatoid arthritis and other arthropathies. *Ann Rheum Dis* 44:817-22, 1985.

12. Day AJ, de la Motte CA: Hyaluronan cross-linking: a protective mechanism in inflammation? *Trends in immunology* 26:637-43, 2005.

13. de la Motte CA, Hascall VC, Drazba J, Bandyopadhyay SK, Strong SA: Mononuclear leukocytes bind to specific hyaluronan structures on colon mucosal smooth muscle cells treated with polyinosinic acid:polycytidylic acid: inter-alpha-trypsin inhibitor is crucial to structure and function. *The American journal of pathology* 163:121-33, 2003.

14. Decker B, Mc GW, Mc KB, Slocumb CH: Concentration of hyaluronic acid in synovial fluid. *Clin Chem* 5:465-9, 1959.

15. Enghild JJ, Thogersen IB, Cheng F, Fransson LA, Roepstorff P, Rahbek-Nielsen H: Organization of the inter-alpha-inhibitor heavy chains on the chondroitin sulfate originating from Ser(10) of bikunin: posttranslational modification of IalphaI-derived bikunin. *Biochemistry* 38:11804-13, 1999.

16. Enghild JJ, Thogersen IB, Pizzo SV, Salvesen G: Analysis of inter-alpha-trypsin inhibitor and a novel trypsin inhibitor, pre-alpha-trypsin inhibitor, from human plasma. Polypeptide chain stoichiometry and assembly by glycan. *The Journal of biological chemistry* 264:15975-81, 1989.

17. Fam H, Bryant JT, Kontopoulou M: Rheological properties of synovial fluids. *Biorheology* 44:59-74, 2007.

18. Gleghorn JP, Bonassar LJ: Lubrication mode analysis of articular cartilage using Stribeck surfaces. *J Biomech* 41:1910-8, 2008.

19. Gomez JE, Thurston GB: Comparisons of the oscillatory shear viscoelasticity and composition of pathological synovial fluids. *Biorheology* 30:409-27, 1993.

20. He H, Li W, Tseng DY, Zhang S, Chen SY, Day AJ, Tseng SC: Biochemical characterization and function of complexes formed by hyaluronan and the heavy chains of inter-alpha-inhibitor (HC*HA) purified from extracts of human amniotic membrane. *The Journal of biological chemistry* 284:20136-46, 2009.

21. Hutadilok N, Ghosh P, Brooks PM: Binding of haptoglobin, inter-alpha-trypsin inhibitor, and alpha 1 proteinase inhibitor to synovial fluid hyaluronate and the influence of these proteins on its degradation by oxygen derived free radicals. *Annals of the rheumatic diseases* 47:377-85, 1988.

22. Jay GD, Britt DE, Cha CJ: Lubricin is a product of megakaryocyte stimulating factor gene expression by human synovial fibroblasts. *J Rheumatol* 27:594-600, 2000.

23. Jiang D, Liang J, Noble PW: Hyaluronan as an immune regulator in human diseases. *Physiol Rev* 91:221-64, 2011.

24. Kida D, Yoneda M, Miyaura S, Ishimaru T, Yoshida Y, Ito T, Ishiguro N, Iwata H, Kimata K: The SHAP-HA complex in sera from patients with rheumatoid arthritis and osteoarthritis. *The Journal of rheumatology* 26:1230-8, 1999.

25. Mazzucco D, Scott R, Spector M: Composition of joint fluid in patients undergoing total knee replacement and revision arthroplasty: correlation with flow properties. *Biomaterials* 25:4433-45, 2004.

26. Michalski C, Piva F, Balduyck M, Mizon C, Burnouf T, Huart JJ, Mizon J: Preparation and properties of a therapeutic inter-alpha-trypsin inhibitor concentrate from human plasma. *Vox sanguinis* 67:329-36, 1994.

27. Rugg MS, Willis AC, Mukhopadhyay D, Hascall VC, Fries E, Fulop C, Milner CM, Day AJ: Characterization of complexes formed between TSG-6 and inter-alpha-inhibitor that act as intermediates in the covalent transfer of heavy chains onto hyaluronan. *The Journal of biological chemistry* 280:25674-86, 2005.

28. Sabaratnam S, Arunan V, Coleman PJ, Mason RM, Levick JR: Size selectivity of hyaluronan molecular sieving by extracellular matrix in rabbit synovial joints. *J Physiol* 567:569-81, 2005.

29. Sandson J, Hamerman D, Schwick G: Altered properties of pathological hyaluronate due to a bound inter-alpha trypsin inhibitor. *Transactions of the Association of American Physicians* 78:304-13, 1965.

30. Sanggaard KW, Sonne-Schmidt CS, Jacobsen C, Thogersen IB, Valnickova Z, Wisniewski HG, Enghild JJ: Evidence for a two-step mechanism involved in the formation of covalent HC x TSG-6 complexes. *Biochemistry* 45:7661-8, 2006.

31. Schmid T, Soloveychik V, Kuettner K, Schumacher B: Superficial zone protein (SZP) from human cartilage has lubrication activity. *Trans Orthop Res Soc,* 26:178, 2001.

32. Schumacher BL, Hughes CE, Kuettner KE, Caterson B, Aydelotte MB: Immunodetection and partial cDNA sequence of the proteoglycan, superficial zone protein, synthesized by cells lining synovial joints. *J Orthop Res* 17:110-20, 1999.

33. Schurz J, Ribitsch V: Rheology of synovial fluid. *Biorheology* 24:385-99, 1987.

34. Smith RC, Rutherford OM: The role of metabolites in strength training. I. A comparison of eccentric and concentric contractions. *Eur J Appl Physiol Occup Physiol* 71:332-6, 1995.

35. Steinbuch M, Loeb J: Isolation of an alpha2-globulin from human plasma. *Nature* 192:1196, 1961.

36. Wisniewski HG, Burgess WH, Oppenheim JD, Vilcek J: TSG-6, an arthritis-associated hyaluronan binding protein, forms a stable complex with the serum protein inter-alpha-inhibitor. *Biochemistry* 33:7423-9, 1994.

37. Wisniewski HG, Hua JC, Poppers DM, Naime D, Vilcek J, Cronstein BN: TNF/IL-1-inducible protein TSG-6 potentiates plasmin inhibition by inter-

alpha-inhibitor and exerts a strong anti-inflammatory effect in vivo. *Journal of immunology* 156:1609-15, 1996.

38. Yingsung W, Zhuo L, Morgelin M, Yoneda M, Kida D, Watanabe H, Ishiguro N, Iwata H, Kimata K: Molecular heterogeneity of the SHAP-hyaluronan complex. Isolation and characterization of the complex in synovial fluid from patients with rheumatoid arthritis. *The Journal of biological chemistry* 278:32710-8, 2003.

39. Yoshihara Y, Plaas A, Osborn B, Margulis A, Nelson F, Stewart M, Rugg MS, Milner CM, Day AJ, Nemoto K, Sandy JD: Superficial zone chondrocytes in normal and osteoarthritic human articular cartilages synthesize novel truncated forms of inter-alpha-trypsin inhibitor heavy chains which are attached to a chondroitin sulfate proteoglycan other than bikunin. *Osteoarthritis and cartilage / OARS, Osteoarthritis Research Society* 16:1343-55, 2008.

40. Zhuo L, Hascall VC, Kimata K: Inter-alpha-trypsin inhibitor, a covalent protein-glycosaminoglycan-protein complex. *The Journal of biological chemistry* 279:38079-82, 2004.

41. Zhuo L, Kanamori A, Kannagi R, Itano N, Wu J, Hamaguchi M, Ishiguro N, Kimata K: SHAP potentiates the CD44-mediated leukocyte adhesion to the hyaluronan substratum. *The Journal of biological chemistry* 281:20303-14, 2006.

42. Zhuo L, Yoneda M, Zhao M, Yingsung W, Yoshida N, Kitagawa Y, Kawamura K, Suzuki T, Kimata K: Defect in SHAP-hyaluronan complex causes severe female infertility. A study by inactivation of the bikunin gene in mice. *The Journal of biological chemistry* 276:7693-6, 2001.

CHAPTER 6:

CONCLUSIONS

The studies presented in the preceding chapters were undertaken with the general motivation of contributing to understanding synovial fluid physiology, particularly the homeostasis of HA in SF, and were designed to determine 1) SF movement and joint capsule strain due to flexion, 2) the rheological and biomechanical properties of mixtures of SF and blood, 3) the mechanisms of lubricant homeostasis in normal and injured joints, and 4) the molecular determinants of the biophysical properties of SF and to utilize them to control those properties in solutions of HA and in OA SF. In this chapter, the main findings of these studies are summarized and discussed, and future directions for research are suggested.

6.1 Summary of Findings

Flexion of the knee alters the distribution of SF within the joint cavity and the joint capsule undergoes varying amounts of strain based on location (**Chapter 2**). A method for measuring the location and volume of fluid within an intact joint capsule through radiopaque imaging on a μCT scanner was developed. With increasing SF volume, or effusion, as occurs during many joint pathologies, fluid preferentially accumulates in the anterior lateral portion of the joint space, for knees at 60° flexion. Increasing flexion from 30 to 90° shifted ~20% of the fluid from the anterior

compartments to the posterior compartments. Analogous *in vivo* measurements made using a planar digital X-ray system showed similar fluid movement as the *ex vivo* μCT data. Steel suture was used in conjunction with radiopaque fluid to create fiducial markers within the joint capsule at 6 locations around the patella, and their relative locations were determined at different levels of flexion. Planar joint capsule principal strains were ~100% (tension) in the proximal-distal direction and ~–40% (shortening) in the circumferential direction relative to the femur axis and 30° flexion strain state, indicating a Poisson's ratio of ~0.4 for the capsule.

During acute trauma and in certain cartilage repair procedures, hemarthrosis, or introduction of blood into the joint, leads to mixtures of blood and SF with unique rheological properties (**Chapter 3**). A thromboelastograph-like test was designed to monitor the tensile strength of the blood/SF mixtures during clotting. The initial stages of blood coagulation were not affected by dilution with SF or saline, dilution with SF altered the coagulation torque profile over time, resulting in a decreased maximum torque generation. Clot mechanical stiffness was decreased with SF dilution by 42-90%, while fluid permeability increased 41-468 fold, both depending on mixture ratio. Compared to diluting with saline, SF had a smaller effect on the mechanical properties of the clots formed. High molecular weight HA from SF retained its molecular weight during the clotting process, likely contributing to the structure of the clot.

The biophysical mechanisms that determine the residence time of HA in the SF of knee joints after ACL transection were investigated using an in vivo rabbit model (**Chapter 4)**. The pseudo steady-state M_r distribution of HA in SF was altered after surgery, with a loss of high-M_r HA by day 7 for ACLT and SHAM groups, and a shift

towards a lower-M_r distribution of HA at day 28. In addition, the total HA concentration was decreased by ~50% at day 7 and 26% at day 28. After saline washout of the joints, SF was replenished with high-M_r HA over time, likely through endogenous secretion. However, the secretion rates were diminished for ACLT and SHAM groups at day 7, and for the ACLT group at day 28. The efflux of HA from the joint was assessed through joint washout and injection of polydisperse exogenous HA. Directly after injection and joint flexion, at time 0^+, the distribution of HA was similar to that injected, though diluted to ~60% by concentration. Sampling over time indicated that HA loss from the SF occurred in a M_r-dependent manner, and the loss was increased at day 7 after ACLT, but not by day 28. The residence time of HA by M_r was similarly decreased by 70% for ACLT day 7 from a NonOp value of ~27hrs for 1000-2500kDa HA. Compared to the NonOp joint tissues, ACLT subsynovium was highly cellular and showed evidence of neovascularization at days 7 and 28.

Finally, the molecular determinants of the biophysical properties of SF were elucidated, and heavy chain binding was utilized to control those properties in solutions of HA and in OA SF (**Chapter 5**). While the HA concentration and M_r are major contributors to SF viscosity, the importance of HA binding proteins to OA SF viscosity was demonstrated, with protein removal resulting in decreases of viscosity by 20-70%, depending on shear rate. Modification of HA with inter-α-inhibitor heavy chains increased the viscosity of HA solutions in a dose-dependent manner up to 40% and the viscosity of OA SF by ~10%; increased the fluid pressure generated by HA solutions in a dose-dependent manner up to ~50% and OA SF by ~10%, and decreased the membrane permeability to HA from HA solutions and OA SF by ~60%.

6.2 Discussion

Major contributions of this work include to understanding: (1) the structural physiology of the joint, (2) molecular homeostasis in SF, (3) the effects of injury on joints, and (4) clinical implications for joint disease.

6.2.1 Structural Physiology of the Joint

Flexion of the knee shifts SF from the anterior to the posterior regions of the joint cavity (**Chapter 2**). While the anatomical structure of the joint cavity, with its distinct though interconnected bursae, has been appreciated for over a century [11], a detailed description of the location and movement of SF within the joint cavity with flexion had not been reported. A case report where radiopaque dye was injected into human knees and imaged via X-ray showed general motion of fluid from anterior to posterior with flexion, but did not give quantitative description of fluid movement [20]. Given that ~20% of the anterior fluid shifts to the posterior bursae with flexion (**Figs. 2.3-2.5**), and assuming about half of the moving fluid mixes with the , approximately 5 cycles of flexion and extension would be needed to fully mix the SF within the joint.

Dilution of SF with blood, as occurs during joint hemarthrosis, results in clotted material that forms the initial repair environment of the joint (**Chapter 3**). After intra-articular fracture or microfracture of a focal cartilage defect, blood from the bone fracture that likely contains hematopoietic stem cells mixes with SF and clots, providing the cellular source of fibrous repair tissue [21, 25]. In addition to the

cellular component, the clotted mixtures provide a physical structure with distinct properties (**Fig. 3.4 and 3.5**) depending on the amount of SF present.

The viscosity of SF is determined not only by the HA concentration and molecular weight, but also by the HA binding proteins, including inter-α-inhibitor heavy chains (**Chapter 5**). The biophysical properties of SF depend on the fluid composition, with HA concentration and molecular weight typically thought to determine the viscosity [9]. However, HA binding proteins [6], notably inter-α-inhibitor heavy chains, account for 20-70% of the viscosity (**Fig. 5.1**) of OA SF. Although normal SF contains ~2% protein bound to HA compared to ~10% in pathological SF [23], the magnitude of the viscosity effect suggests that HA binding proteins may play a role out of proportion to their concentration in determining the biophysical properties of normal SF as well.

6.2.2 Molecular Homeostasis in SF

Joint capsule strains due to flexion in the joint (**Chapter 2**) are important mechanical cues that help regulate synoviocyte HA secretion. While articulation of *in vivo* joints [13] and synoviocyte cell culture on flexible plates with imposed strains [22] results in increased HA synthesis, the *in vivo* strains experienced by synovium have not been reported. This work measured the joint capsule strains (**Fig. 2.7**), which translate into the strains in synovium through the local tissue architecture (**Fig. 2.8**). Articulation, which increases articular pressure and convective outflow from SF that may lead to molecular loss, also induces strain in the joint capsule and synovium, increasing HA secretion by synoviocytes.

Fluid movement and mixing within the joint (**Chapter 2**) also has implications for the molecular homeostasis of SF. Without normal articulation, SF composition will not be well-mixed, and its composition, and therefore function, will vary based on location. Convective flow from plasma, synoviocyte secretion rates, and even diffusive loss to lymphatics may be location-dependent due to the local bursae geometry [11] influencing intra-articular hydrostatic pressure [17], the cellularity of synovium in the region [4], and the density of lymphatic vessels[18] acting as diffusion sinks. In addition, a lack of mixing will limit the exchange of information between cell types via molecular signaling through growth factors and cytokines [12].

The secretion and diffusive loss of HA from SF are altered during joint pathology (**Chapter 4**), and these biophysical mechanisms likely also apply to other joint molecules. The secretion rates and loss of HA from SF were M_r-dependent and were decreased and increased, respectively, by joint inflammation (**Fig. 4.2-4.4, 4.6**). The self-consistent description of the biophysical mechanisms (**Fig. 4.8**) that lead to the altered steady-state SF HA composition (**Fig. 4.1**), may also apply to lubricants, such as lubricin, proteins, such as inter-α-trypsin inhibitor, and small signaling molecules. A shift to lower-M_r HA may result in decreased outflow buffering by the polarized HA layer that normally forms at the intra-articular face of synovium [5], which would further increase molecular and fluidic outflow.

The concentrations and molecular size distributions of HA and proteins in SF have important implications for its biophysical properties (**Chapter 5**). The increased concentration of inter-α-trypsin inhibitor observed in inflamed joints may be a direct result of the general increase in synovial permeability to molecules during

inflammation (**Fig. 4.4**). Inter-α-trypsin inhibitor is ~260kDa [29] (**Fig. 5.3**), suggesting that joint inflammation may have a large effect on its synovial permeability, explaining its abundant concentration in inflammatory SF [16, 24, 26, 28, 29].

6.2.3 Effects of Injury on Joints

The effects of hemarthrosis in the mechanical properties of SF (**Chapter 3**) provide an *in vitro* model of the materials that form after intra-articular fraction and microfracture. Though traumatic injury often leads to degenerative joint changes that cause post-traumatic osteoarthritis [3], the physical properties of the initial repair mixture of blood and SF (**Fig. 3.4 and 3.5**) had not been reported. The mechanical properties of repair material likely alter the cartilage mechanics surrounding a defect [27], and appropriate repair material may be able to delay the post-traumatic degenerative cartilage changes.

Inflammation of the joint is an important aspect of many major joint diseases, and has clear effects on the SF composition (**Chapter 4**) and function. Although the ACLT model, which is ostensibly an injury model that develops into post-traumatic OA with time, was used, the characteristic synovial inflammation observed (**Fig. 4.6**) suggests that similar results may be obtained from other inflammatory models. Intermittent inflammatory flare-ups during OA and circadian inflammation in rheumatoid arthritis may be accompanied by temporary losses of SF high-M_r HA and lubrication function.

Pathological SF displays altered biophysical properties due to its composition (**Chapter 5**). OA SF typically displays an HA distribution shifted towards lower-M_r HA [2, 7, 10] (**Fig. 4.1**), which would lead to large changes in the viscosity compared to normal SF. While the viscosity of OA SF is indeed less than normal [9], the less-than-expected difference may be due to increases in OA SF viscosity due to the increased concentration of inter-α-inhibitor heavy chains.

6.2.4 Clinical Implications for Prevention and Treatment of Joint Disease

Fluid volumetric distribution and movement in the knee (**Chapter 2**), especially during effusion, is associated with joint pain, with the nociception possibly originating from joint capsule strain. Patients typically maintain knees with effusion at 30-60° flexion, with pain and intra-articular fluid pressure increasing during further flexion [8, 15]. The nociception of such joint pain may originate in the capsule, as joint capsule strain has been correlated with afferent nerve impulses in an animal model [19]. Flexion would cause proximal-distal elongation and circumferential contraction (**Fig. 2.7**), and shift fluid from the anterior to the posterior bursae (**Fig. 2.3**), either of which may trigger the nociception.

The increased, M_r-dependent molecular loss from SF after injury (**Chapter 4**) suggests potential intervention strategies and pitfalls. The increased molecular loss during inflammation highlights the difficulty for localized retention of injected pharmaceuticals, especially during an acute injury. Early clinical intervention that decreases the synovial inflammatory response and restores lubrication following

injury[1, 14] may be able to limit or retard the progression from injury to post-traumatic osteoarthritis.

The methods to control the biophysical properties of OA SF investigated (**Chapter 5**) could lead to clinical interventions to restore lubricating function of diseased SF. The increases in viscosity, hydrodynamic fluid pressurization, and membrane permeability (**Figs. 5.4-5.6**) provide proof-of-concept for the approach of manipulating the biophysical function to OA SF. Alternative HA binding proteins could potentially be used, including synthetic or functionalized proteins, to promote beneficial physical or cellular responses.

6.3 Future Directions

6.3.1 Joint Capsule and Synovium Biomechanics

The fluid movement and joint capsule strains presented here could be expanded with additional work on diseased joints and synovium biomechanics. Joint capsule tissue may undergo significant changes in structure and function during joint pathologies such as OA and rheumatoid arthritis that would be reflected in the strains experienced with flexion. Using a similar setup as described (**Chapter 2**), rabbit knees with experimentally induced OA or other inflammatory joint pathology could be tested for fluid movement and capsule strain and compared to the normal joint values reported here. Human living or cadaver knees could also be investigated using MRI imaging. In addition, the effects of aging on capsule strains may be of particular interest as tissues tend to be able to undergo less elastic deformation with age.

The macroscopic capsule strains reported here set up work at the cellular level investigating synovium biomechanics and mechanotransduction. How the capsule strains translate into the strains experienced by cells in synovium could be investigated using a biaxial test setup that allows for the tracking of cells. Normal or pathological living synovium with underlying joint capsule bathed in media could be stretched to the strain values reported here (**Fig. 2.7**), and the resulting cellular strains identified by cell tracking methods. The effects of cellular and matrix structural components on strains could be determined by antibody staining for specific molecules, e.g. actin, collagen, or laminin. In addition, the secretion of molecules into the bathing media could be correlated with the stretch protocol.

6.3.2 In vivo Cartilage Defect Repair

The *in vitro* mechanical properties of blood and SF mixtures investigated here could be expanded by analyzing the repair tissue in an *in vivo* model of cartilage defect repair, including the mechanical properties of endogenously created blood and SF mixtures and their effects on the surrounding cartilage tissue mechanics. A large animal (e.g. goat or horse) focal cartilage defect model would allow for a clinically relevant defect, and after animal euthanasia, the defect with repair material and surrounding cartilage tissue would be harvested to perform *ex vivo* mechanical testing. Alternatively, in vivo mechanical testing using contrast agents and μCT may be possible.

6.3.3 Lubricant Homeostasis

The lubricant homeostasis work presented here could be expanded to include additional molecules of interest and pathologies, and also potential clinical interventions. Measuring the secretion, loss, and accumulation of lubricin, in normal and pathological joints would be of special interest to the field of joint lubrication. Given the importance of HA binding proteins (**Chapter 5**), determining the convective flux of inter-α-trypsin inhibitor molecules from plasma in normal and pathological joints would be of interest. In addition to the arthritic pathologies discussed, the aging of joints may have significant consequences for the secretion and loss of molecules in SF, especially if coupled with altered structure-function relationships in joint tissues, such as joint capsule and synovium.

The biophysical mechanisms regulating molecular homeostasis in SF investigated here (**Chapter 4**) suggest potential clinical interventions that could be tested in a translational model. Early intervention to decrease the inflammatory state of the joint after injury by joint lavage and SF supplementation could be tested using the rabbit model described here. In addition, gene therapy techniques that attempt to increase synoviocyte matrix or anti-inflammatory cytokine production or to inhibit inflammatory signaling molecules may be of interest to study in a translational model.

6.3.4 Restoration of the Biophysical Properties of SF

The *in vitro* effects of inter-α-trypsin inhibitor heavy chains on OA SF presented here could be expanded by testing in a translational model. The biophysical effects of modifying HA with heavy chains (**Fig. 5.4-5.6**) could be tested in vivo by first examining whether the reaction occurs in the living joint environment. Normal rabbits could receive an intra-articular injection of pre-mixed inter-α-trypsin inhibitor with TSG-6, and the SF from the joints analyzed over a time course to verify the reaction occurred and to determine the time-course of altered SF biophysical properties. Depending on the duration of action, a series of multiple injections or preparation step where undesirable HA binding proteins are first removed from native SF before inter-α-trypsin inhibitor injection, may be necessary. After determining the time-course and duration of effects on SF, the efficacy of altered SF in preventing post-traumatic degenerative tissue changes could be examined by looking for early degenerative changes in cartilage and the inflammatory state of synovium.

6.4 References

1. Antonacci JM, Schmidt TA, Serventi LA, Cai MZ, Shu YL, Gastelum NS, Schumacher BL, McIlwraith CW, Sah RL: Effects of equine joint injury on boundary lubrication of articular cartilage by synovial fluid: role of hyaluronan. *Arthritis Rheum* (Accepted) Apr 19, 2012.

2. Brown MP, Trumble TN, Plaas AH, Sandy JD, Romano M, Hernandez J, Merritt KA: Exercise and injury increase chondroitin sulfate chain length and decrease hyaluronan chain length in synovial fluid. *Osteoarthritis and cartilage / OARS, Osteoarthritis Research Society* 15:1318-25, 2007.

3. Buckwalter JA, Brown TD: Joint injury, repair, and remodeling: roles in post-traumatic osteoarthritis. *Clin Orthop Relat Res*:7-16, 2004.

4. Castor CW: The microscopic structure of normal human synovial tissue. *Arthritis and rheumatism* 3:140-51, 1960.

5. Coleman PJ, Scott D, Mason RM, Levick JR: Role of hyaluronan chain length in buffering interstitial flow across synovium in rabbits. *J Physiol* 526 Pt 2:425-34, 2000.

6. Day AJ, Prestwich GD: Hyaluronan-binding proteins: tying up the giant. *The Journal of biological chemistry* 277:4585-8, 2002.

7. Decker B, Mc GW, Mc KB, Slocumb CH: Concentration of hyaluronic acid in synovial fluid. *Clin Chem* 5:465-9, 1959.

8. Eyring EJ, Murray WR: The Effect of Joint Position on the Pressure of Intra-Articular Effusion. *J Bone Joint Surg Am* 46:1235-41, 1964.

9. Fam H, Bryant JT, Kontopoulou M: Rheological properties of synovial fluids. *Biorheology* 44:59-74, 2007.

10. Gomez JE, Thurston GB: Comparisons of the oscillatory shear viscoelasticity and composition of pathological synovial fluids. *Biorheology* 30:409-27, 1993.

11. Gray H. Anatomy of the human body. In: WH Lewis, ed. 20 ed. Philadelphia: Lea & Febiger; 1918.

12. Hui AY, McCarty WJ, Masuda K, Firestein GS, Sah RL: A systems bIology approach to synovial joint lubrication in health, injury, and disease. *Wiley Interdiscip Rev Syst Biol Med* 4:15-37, 2012.

13. Ingram KR, Wann AK, Angel CK, Coleman PJ, Levick JR: Cyclic movement stimulates hyaluronan secretion into the synovial cavity of rabbit joints. *J Physiol* 586:1715-29, 2008.

14. Jay GD, Elsaid KA, Zack J, Robinson K, Trespalacios F, Cha CJ, Chichester CO: Lubricating ability of aspirated synovial fluid from emergency department patients with knee joint synovitis. *J Rheumatol* 31:557-64, 2004.

15. Jayson MI, Dixon AS: Intra-articular pressure in rheumatoid arthritis of the knee. 3. Pressure changes during joint use. *Ann Rheum Dis* 29:401-8, 1970.

16. Kida D, Yoneda M, Miyaura S, Ishimaru T, Yoshida Y, Ito T, Ishiguro N, Iwata H, Kimata K: The SHAP-HA complex in sera from patients with rheumatoid arthritis and osteoarthritis. *The Journal of rheumatology* 26:1230-8, 1999.

17. Levick JR: The influence of hydrostatic pressure on trans-synovial fluid movement and on capsular expansion in the rabbit knee. *J Physiol* 289:69-82, 1979.

18. Levick JR: An analysis of the effect of synovial capillary distribution upon trans-synovial concentration profiles and exchange. *Q J Exp Physiol* 69:289-300, 1984.

19. Lu Y, Chen C, Kallakuri S, Patwardhan A, Cavanaugh JM: Neurophysiological and biomechanical characterization of goat cervical facet joint capsules. *J Orthop Res* 23:779-87, 2005.

20. Menschik A: Die Synoviapumpe des Kniegelenkes. *Z Orthop Ihre Grenzgeb* 114:89-94, 1976.

21. Mithoefer K, Williams RJ, 3rd, Warren RF, Potter HG, Spock CR, Jones EC, Wickiewicz TL, Marx RG: Chondral resurfacing of articular cartilage defects in the knee with the microfracture technique. Surgical technique. *J Bone Joint Surg Am* 88 Suppl 1 Pt 2:294-304, 2006.

22. Momberger TS, Levick JR, Mason RM: Hyaluronan secretion by synoviocytes is mechanosensitive. *Matrix Biol* 24:510-9, 2005.

23. Sandson J, Hamerman D, Schwick G: Altered properties of pathological hyaluronate due to a bound inter-alpha trypsin inhibitor. *Trans Assoc Am Physicians* 78:304-13, 1965.

24. Sandson J, Hamerman D, Schwick G: Altered properties of pathological hyaluronate due to a bound inter-alpha trypsin inhibitor. *Transactions of the Association of American Physicians* 78:304-13, 1965.

25. Steadman JR, Rodkey WG, Rodrigo JJ: Microfracture: surgical technique and rehabilitation to treat chondral defects. *Clin Orthop Relat Res*:362-9, 2001.

26. Wisniewski HG, Hua JC, Poppers DM, Naime D, Vilcek J, Cronstein BN: TNF/IL-1-inducible protein TSG-6 potentiates plasmin inhibition by inter-alpha-inhibitor and exerts a strong anti-inflammatory effect in vivo. *Journal of immunology* 156:1609-15, 1996.

27. Wong BL, Sah RL: Effect of a focal articular defect on cartilage deformation during patello-femoral articulation. *J Orthop Res* 28:1554-61, 2010.

28. Yingsung W, Zhuo L, Morgelin M, Yoneda M, Kida D, Watanabe H, Ishiguro N, Iwata H, Kimata K: Molecular heterogeneity of the SHAP-hyaluronan complex. Isolation and characterization of the complex in synovial fluid from patients with rheumatoid arthritis. *The Journal of biological chemistry* 278:32710-8, 2003.

29. Yoshihara Y, Plaas A, Osborn B, Margulis A, Nelson F, Stewart M, Rugg MS, Milner CM, Day AJ, Nemoto K, Sandy JD: Superficial zone chondrocytes in normal and osteoarthritic human articular cartilages synthesize novel truncated forms of inter-alpha-trypsin inhibitor heavy chains which are attached to a chondroitin sulfate proteoglycan other than bikunin. *Osteoarthritis and cartilage / OARS, Osteoarthritis Research Society* 16:1343-55, 2008.

APPENDIX A:

AN ARTHROSCOPIC DEVICE TO ASSESS ARTICULAR CARTILAGE DEFECTS AND TREATMENT WITH A HYDROGEL

A.1 Abstract

The hydraulic resistance R across osteochondral tissue, especially articular cartilage, decreases with degeneration and erosion. Clinically useful measures to quantify and diagnose the extent of cartilage degeneration and efficacy of repair strategies, especially with regard to pressure maintenance, are still developing. The hypothesis of this study was that hydraulic resistance provides a quantitative measure of osteochondral tissue that could be used to evaluate the state of cartilage damage and repair. The aims were to (1) develop a device to measure R in an arthroscopic setting, (2) determine whether the device could detect differences in R for cartilage, an osteochondral defect, and cartilage treated using a hydrogel ex vivo, and (3) determine how quickly such differences could be discerned. The apparent hydraulic resistance of defect samples was ~35% less than intact cartilage controls, while the resistance of hydrogel-filled groups were not statistically different than controls, suggesting some restoration of fluid pressurization in the defect region by the hydrogel. Differences in hydraulic resistance between control and defect groups were apparent after 4s. The

results indicate that the measurement of R is feasible for rapid and quantitative functional assessment of the extent of osteochondral defects and repair. The arthroscopic compatibility of the device demonstrates the potential for this measurement to be made in a clinical setting.

A.2 Introduction

Articular cartilage is a load-bearing connective tissue at the ends of long bones in synovial joints that facilitates low-friction, low-wear joint articulation. The load-bearing ability of cartilage is dependent on the presence of a large aggregating proteoglycan, aggrecan, in the matrix [4]. Aggrecan is highly negatively charged due to its numerous sulfated glycosaminoglycan (GAG) side chains, and the charge density of these sulfated GAG moieties creates a swelling pressure in the interstitial fluid of cartilage that resists compression [19]. The permeability, or ease of fluid flow through cartilage, is inversely related to the tissue charge density [17], and is low in normal tissue [6], which is essential for fluid pressurization. Interstitial fluid pressurization supports most of the load that cartilage receives, shielding the solid matrix from excessive strain [26].

While permeability has traditionally been reported for individual materials, such as articular cartilage, related variables such as hydraulic resistance are needed to describe complex multi-tissue structures. Permeability, or specific permeability, typically refers to the constant K in Darcy's empirical law [15, 27]. Hydraulic resistance R is similar, though inversely related to permeability

$$R=\left(\frac{\Delta P}{Q}\right),\ K=\frac{\mu L}{A}\left(\frac{Q}{\Delta P}\right),\ K'=k_p=\frac{Q/A}{\Delta P/L}=\frac{L}{A}\left(\frac{Q}{\Delta P}\right),\ K''=c=\frac{1}{A}\left(\frac{Q}{\Delta P}\right), \qquad \text{(Eqs. 1-4)}$$

with viscosity μ, flow rate Q, fluid path-length L, pressure P, and cross-sectional area A. Less specific forms of permeability have been defined, including hydraulic permeability k_p or hydraulic conductivity K', and hydraulic conductance c. The use of

the less specific definitions, c or R, is appropriate when multi-tissue structures are used, such as osteochondral tissue [13], as K and k_p are typically defined for individual materials.

The hydraulic resistance across osteochondral tissue, especially articular cartilage, decreases with degeneration and erosion. Progressive degeneration and erosion of articular cartilage that can occur with osteoarthritis (OA) has been correlated with decreased hydraulic resistance [1]. In addition, focal defects, which are commonly observed in the knees of symptomatic patients during arthroscopy [8, 12], are discrete areas of cartilage erosion that also likely have reduced hydraulic resistance. Differences in the hydraulic resistance of osteochondral tissue with normal, partially, and fully eroded cartilage have also been reported [13]. Such decreases in hydraulic resistance will diminish the ability of cartilage to maintain fluid pressurization, leading to larger strains on the cartilage matrix and likely to further degeneration [19, 30, 31].

Different repair strategies for cartilage defects are being investigated, though only a limited number address the need for immediate restoration of interstitial fluid pressurization. Defect repair strategies include arthroscopic procedures, such as microfracture [25]; soft tissue grafts [5]; osteochondral grafts of autogenic [11] or allogenic source material [9]; cell transplantation with or without a scaffold, including autologous cell implantation [3] and mesenchymal stem cells; and synthetic and natural scaffolds. Interstitial fluid pressurization, and load-bearing capacity, is typically restored with the osteochondral graft techniques, and for certain scaffold implants, such as high concentration formulations of poly-(ethylene glycol) with high

stiffness (similar to cartilage stiffness) and low permeability [16, 23], while most cell-based techniques make use of a scaffold that is initially less stiff than normal cartilage.

Clinically useful measures to diagnose the extent of cartilage degeneration and efficacy of repair strategies are limited, especially with regard to pressure maintenance. Imaging modalities have typically been used to diagnose cartilage degeneration and defects, including plain film x-ray attenuation, magnetic resonance imaging (MRI), computed tomography (CT), and visual observation during arthroscopy. Though these methods alone have limited quantitative ability, contrast-enhanced MRI, used clinically [14], and CT, used in small animal models [22, 32], can allow for the determination of spatial maps of charge density in cartilage, an indirect measure of hydraulic resistance, though the resolution of MRI techniques widely available clinically lags behind what is reported in academia. Cartilage degeneration detection using optical coherence tomography has also recently been reported [7]. Arthroscopic instruments for the determination of stress-strain behavior or electrical impedance, from which hydraulic resistance could be inferred, have been suggested [2, 21, 28], but are not yet in clinical practice in the United States. A device allowing the direct perfusion-based measurement of hydraulic resistance in an arthroscopic setting has not yet been described.

Thus, the hypothesis of this study was that hydraulic resistance provides a quantitative measure of osteochondral tissue that could be used to evaluate the state of cartilage damage and treatment. The aims were to (1) develop a device to assess hydraulic resistance in an arthroscopic setting, (2) determine whether the device could detect differences in hydraulic resistance for cartilage, an osteochondral defect, and a

defect treated with a low permeability hydrogel, and (3) determine how quickly such differences could be discerned.

A.3 Materials and Methods

A.3.1 Study Design

An arthroscopic probe was used to measure the hydraulic resistance of osteochondral tissue *ex vivo*. Ten osteochondral blocks were harvested from the medial and lateral femoral condyles of 5 adult bovine knees, with 1 block per condyle. Samples were wrapped in gauze soaked with PBS with protease inhibitors (PBS+PI: 1mM phenylmethanesulfonyl fluoride, 2mM disodium ethylenediamine tetraacetate, 5mM benzamidine-HCl, and 10mM N-ethylmaleimide) and stored at -20°C until testing. The hydraulic resistance of each block was tested in a single location on the load-bearing, posterior face of the condyle on (1) intact cartilage, (2) after drilling an osteochondral defect, and (3) after filling the defect with a photopolymerized hydrogel.

A.3.2 Arthroscopic Probe Device Design and Testing

A prototype for a potentially arthroscopically-deliverable probe tip that sealed against normal cartilage or the cartilage surface surrounding a defect to allow the measurement of hydraulic resistance was fabricated and calibrated. The probe consisted of a cylindrical silicone rubber cap (8mm height by 15mm inner diameter by

1.4mm thick) glued on a flat silicone rubber donut (18mm outer, 10mm inner diameter by 1.0mm thick) with a silicone rubber disc (23mm diameter by 2.0mm thick) glued to the closed end. A 3mm diameter hole was punched in the side of the cap, and a stainless steel tube (4.5mm outer diameter by 0.13mm thick) adhered inside silicone tubing (3.8mm inner diameter by 1.0mm thick) was secured to this hole, creating a single compartment space (Fig. A.1). The range of pressures the probe could withstand without collapse was tested against intact cartilage and the probe dimensions were tested by passing it through an 8mm diameter stainless steel tube to simulate a standard arthroscopic cannula (typical inner diameter range of 4.5-8mm).

Using this device, R was measured. A perfusion apparatus consisting of a syringe pump and pressure transducer was assembled and calibrated. A 20mL plastic syringe was filled with phosphate buffered saline (PBS) and place in a syringe pump (Harvard PHD 2000; Harvard Apparatus, Holliston, MA). The syringe was connected to the stainless steel tube of the probe device and to a pressure sensor (DP15 Low Pressure Sensor; Validyne Engineering, Northridge, CA) using stiff tubing. The pressure sensor was calibrated to confirm linearity between 0 and 344kPa.

The hydraulic resistance of each sample with intact cartilage, after creation of a defect, and after hydrogel polymerization was measured using the device and setup described. The tissue blocks and device were submerged in a bath of PBS. The device was placed against the sample surface, held in place with a clamp, a weight (~0.5N normal force) was placed on top of the probe tip, and the pressure was recorded for 20s without flow, and then for 40s after the flow was initiated at a rate of 167 mm3 s-1. Once the flow was initiated, the negative pressure generated inside the probe tip

was sufficient to maintain the probe position against the sample surface and the normal force was removed. After testing the intact samples, 10mm diameter by 4mm deep defects were created through the cartilage and into the subchondral bone, though not into the cancellous bone, using a drill press while irrigating with PBS, and retested. The device was placed directly over the defect, enclosing it within the probe tip such that the outer edge of the probe tip was completely surrounding the defect site and the inner edge was within the defect region. Finally, the defects were filled with poly-(ethylene glycol) diacrylate hydrogel (30%w/v, Synthasome Inc, La Jolla, CA) [23] that was adhered to the surrounding articular cartilage and bone by tissue initiated photopolymerization [29] using an A4000 series UV light source (EXFO, Mississauga, Canada), and samples retested. Each sample was tested 3 times in each condition. The hydraulic permeability of 3mm thick samples of hydrogel were assessed *in vitro* by direct perfusion as $3.4\pm0.8 \times 10^{-14}$ [m2 Pa-1 s-1] (n=3), slightly more permeable than the range of 1×10^{-16} to 2×10^{-15} [m2 Pa-1 s-1] reported for cartilage [17, 18, 20], and much less permeable than subchondral bone $\sim1\times10^{-10}$ [m2 Pa-1 s-1] [13].

A.3.3 Data Reduction and Curve Fitting

Experimental data were reduced and fit to a model equation to determine the hydraulic resistance and compliance parameters. For each trial, pressure values were normalized to the average pressure recorded over 5s before initiation of flow. The zero time point was set as the point where the pressure increased over 3 standard deviations from the baseline average. The three trials for each condition of pressure versus time

data were averaged at each time point. The experimental setup was modeled as a parallel RC lumped parameter circuit with a current source (Fig. 2), assuming the hydraulic resistance through the sample was the dominant resistance R [kPa s mm-3], the total system compliance C [mm3 kPa-1], flow rate Q [mm3 s-1], pressure P [kPa], and time t [s]. Averaged P versus time data sets were fit to the solution equation

$$(-P) = QR\left(1 - \exp\left[-\frac{t}{R \cdot C}\right]\right) \qquad \text{(Eq. 5)}$$

to estimate R for each trial and a single, global C value using an ordinary least square error nonlinear regression (Excel 2003, Microsoft Corporation, Redmond, WA).

A.3.4 *Statistical Analysis*

Data are presented as mean±SEM for n=10 samples. A 2-way repeated measures ANOVA was used to determine the effects of tissue condition (intact, defect, hydrogel) and time (t=1, 2, 4, 8, 16, 32s) on measured pressure. A 1-way ANOVA was used to determine the fixed effect of condition (intact, defect, hydrogel) on hydraulic resistance. When significant effects were determined, $p<0.05$, differences between groups were assessed with Tukey post-hoc tests.

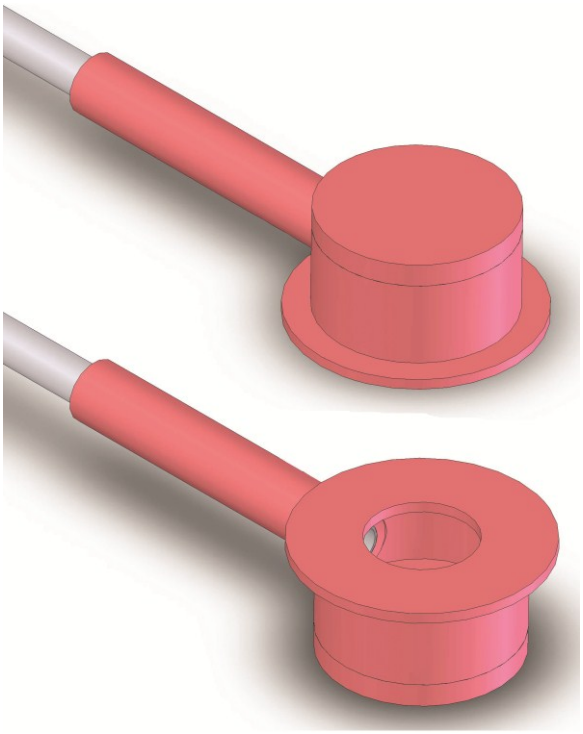

Figure A.1: Schematic representation of the arthroscopic probe device in an isometric view from the top and bottom.

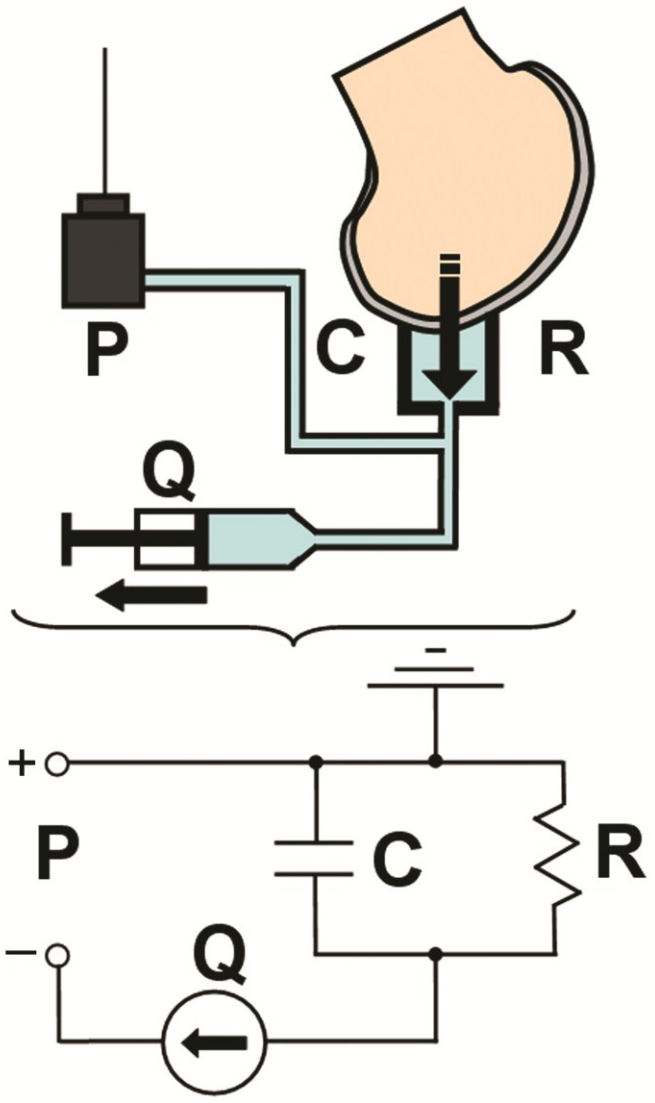

Figure A.2: The experimental setup was modeled as a parallel RC lumped parameter circuit with hydraulic resistance R, the total system compliance C, flow rate Q, and pressure P.

A.4 Results

The arthroscopic probe device sealed against the cartilage surface upon initiation of flow and the resulting pressures were measured for samples with intact cartilage, defects, and hydrogel-filled defects. The device was able to seal against the cartilage surface and maintain pressures over 344kPa. The lateral walls and top of the cylindrical silicone rubber cap deformed for ~5s with increasing pressure, resulting in an approximately 15% decrease in cap volume before stabilization.

The pressure versus time data revealed differences between the pressure responses from samples with intact cartilage, defects, and hydrogel-filled defects. Pressure varied with cartilage condition (intact, defect, or hydrogel; $p<0.001$) and time after initiation of flow ($p<0.0001$), with an interaction effect ($p<0.0001$). Differences in pressure between the intact and defect groups were significant at all times from 4 to 32s ($p<0.0001$-0.05, Fig. A.3). The pressure response from the hydrogel-filled defects was not statistically different than the unfilled defects at 4 and 8s, but was different than the unfilled defects, and not different than the intact cartilage, at 16 and 32s.

The best-fit parameters for hydraulic resistance also showed differences between the intact cartilage, defects, and hydrogel-filled defects. R varied significantly with cartilage condition ($p<0.00001$, Fig. A.4), with the best fit value for system compliance of 26.4 mm3 kPa-1. On average, R_{defect} values were 35% less than $R_{cartilage}$ values ($p<0.0001$), and 31% less than R_{gel} values ($p<0.001$), while R_{gel} values were not significantly different than $R_{cartilage}$ values ($p=0.75$).

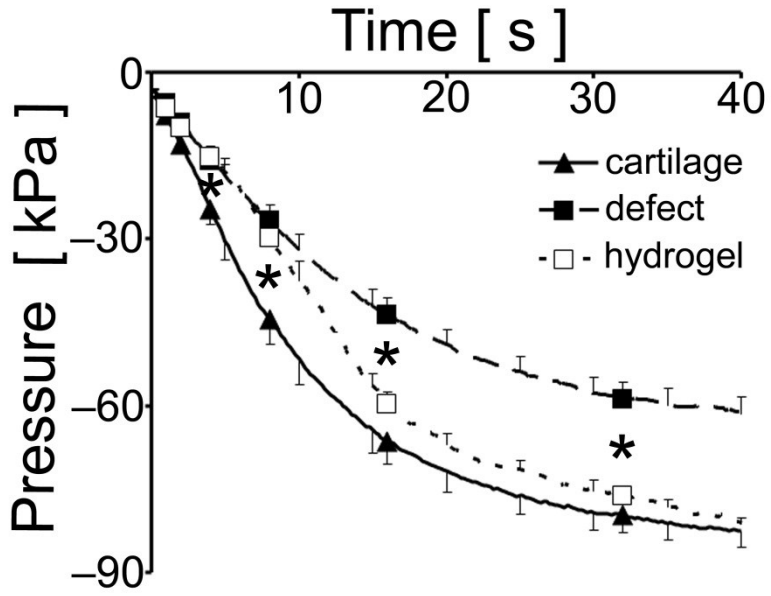

Figure A.3: Pressure vs. time curves for intact cartilage, osteochondral defects, and defects filled with hydrogel, n=10. Triangle and square markers indicate the 1, 2, 4, 8, 16, and 32s time points that were analyzed. *: $p<0.05$ difference between groups above and below the asterisk.

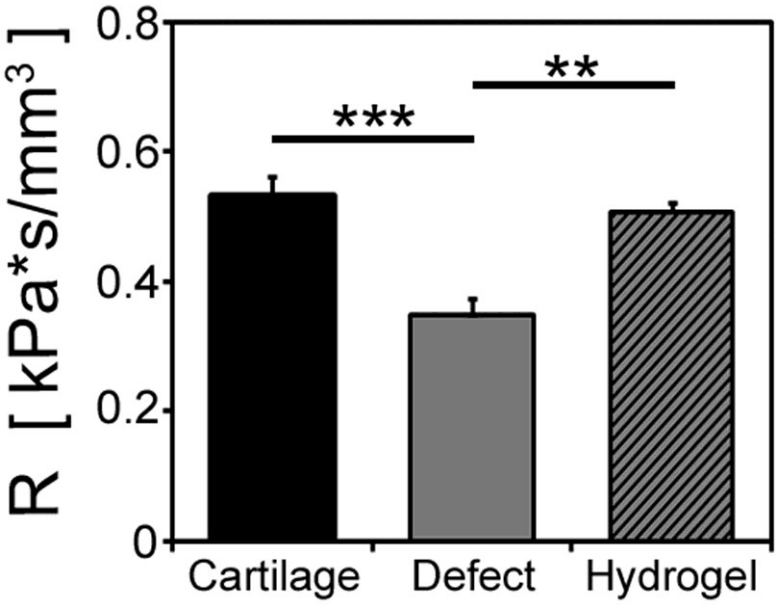

Figure A.4: Best-fit values of resistance (R) at a compliance (C) of 26.4 mm3 kPa-1 for intact cartilage, osteochondral defects, and defects filled with hydrogel, n=10. **: $p<0.001$, ***: $p<0.0001$.

A.5 Discussion

The results indicate that the measurement of hydraulic resistance is feasible for rapid and quantitative functional assessment of osteochondral defects and treatments. The magnitude of pressure generated against the samples with an intact cartilage surface was significantly higher than that generated against the samples with an osteochondral defect (**Fig. A.3**), indicating a loss of hydraulic resistance (**Fig. A.4**) that was apparent after a few seconds. The application of the hydrogel to the defects increased the magnitude of pressure generated compared to the defect samples at longer times (**Fig. A.3**), while the hydraulic resistance value was increased to levels similar to those measured for intact cartilage (**Fig. A.4**).

The differences in hydraulic resistance measured between conditions are a proof of concept using a prototype device for the idea of an arthroscopic probe to quantify local regions of cartilage degeneration and abnormal fluid communication between the intraarticular space and bone. The defects created were severe, such as could be found in intraarticular fractures or significantly advanced osteoarthritis with wear of the subchondral bone, where the defects are visible. Additional experiments could be performed to determine whether finer differences in hydraulic resistance can be assessed, such as in normal osteochondral tissue depleted of GAG and osteoarthritic tissue with sites of grade II or III degeneration (Modified Outterbridge Scale), using the current device, or after varying device design parameters to increase the resolution.

The ability of the device to resolve finer differences, including cartilage fibrillation or partial- or full-thickness erosion, on a reasonable time-scale depends on several device and setup properties, including stiffness of the probe material and volume of the chamber. The system compliance and sample resistance determine the sensitivity of the probe and time constant, and, along with the flow rate, the pressure magnitudes obtained. A lower system compliance would increase the sensitivity of the device, as a smaller deformation of the stiffer probe tip would increases the fluid pressure generated. In addition, the increase in fluid flow due to degenerate or eroded cartilage compared to healthy cartilage may be masked by flow associated with the system compliance. The current compliance of ~26 mm3 kPa-1 could be significantly reduced by increasing the stiffness of the probe material and decreasing the probe chamber volume, as well as by reducing any compliance in the pressure sensor and syringe, increasing the sensitivity of the device. Thus, additional work could be done to increase the sensitivity of the device and to characterize the ability of the probe to reveal partial defects.

The hydraulic resistance values measured here are apparent values for osteochondral tissue that could be useful to determine the extent of cartilage erosion. While the values of hydraulic resistance measured using this device are several orders of magnitude less than those that could be calculated for articular cartilage alone based on previously reported hydraulic permeability values from direct perfusion measurements [17, 18, 20], the comparison between intact and damaged cartilage, including assessing whether a fluidic short circuit through intact cartilage or any defect treatment implant exists, is the intended purpose of the device. Determining a

resistance value similar to cartilage indicates that there is some fluid pressurization in the defect area, and that there is minimal abnormal fluid flow in that region between the intraarticular space and the bone. Direct perfusion experiments to determine the hydraulic permeability of cartilage are technically difficult, requiring tens of hours for fluid pressurization before running time and controls for tissue deformation with pressure among other challenges, making their clinical utility limited. By determining the apparent hydraulic resistance, this device and measurement procedure was able to determine differences between intact cartilage and defects in tens of seconds, instead of hours.

The arthroscopic compatibility of the device design and short time constant demonstrate the potential for this measurement to be made in a clinically useful setting. The design of the actual instrument for this purpose, instead of the prototype described here, would need to have a method for ensuring no portion of the device could detach and become a loose body in the joint and would be tested using standard arthroscopic tools The device materials were chosen such that the cap portion could be temporarily deformed to pass through a standard arthroscopy cannula with an 8mm inner diameter, allowing for its use in an arthroscopic setting. The time constant τ

$$\tau = R \cdot C \qquad \text{(Eq. 6)}$$

is a reasonable estimate of the time over which pressure would need to be collected in order to have data covering a significant portion of the pressure curve. The time constants for determination of the pressure curve averaged 14.1±0.8s for intact cartilage, 9.2±0.7s for cartilage with a defect, and 13.4±0.3s for a defect filled with hydrogel. Obtaining data beyond the initial few seconds, at which point absolute

differences in pressure were already significantly different between intact and defect samples (**Fig. A.3**), is necessary to fit the data to the model equation, as the initial slope at t=0 is independent of R, as shown by taking the derivative of Eq. 5 with respect to time

$$\left.\frac{d(-P)}{dt}\right|_{t=0} = \frac{Q}{C} \qquad \text{(Eq. 7)}$$

With only approximately 20s necessary for data collection (~5s of no flow, and ~15s with flow), and negative pressure holding the device in place after a brief push, the time that would be added to an arthroscopic surgery to obtain a quantitative measurement of damage to a local region of cartilage is a reasonable tradeoff.

The increased hydraulic resistance following application of the hydrogel suggests there was some restoration of fluid pressurization function at the defect area. The shape of the pressure curve for the hydrogel samples suggests that there is more compliance in the hydrogel than in cartilage, as the pressures generated were different in magnitude from intact samples and similar to the defect samples up until 8s (**Fig. A.3**). After that time, the pressures transitioned to become similar to the intact samples, with significantly higher hydraulic resistance than the defect samples, indicating that some hydraulic resistance had been restored to the defect. Cartilage repair strategies that restore the fluid pressurization, such as the high concentration formulation of photopolymerized PEG hydrogel with high stiffness and low permeability used here, have the advantage of allowing the load-bearing functions of the tissue to resume, while reducing the exaggerated loads on the surrounding tissue that occur with regions of low stiffness.

Further experimentation could be performed to determine the effects of the negative pressure that is generated on the cartilage and bone. Articular cartilage normally experiences fluid pressurization during loading, with estimates of physiological magnitudes of pressure up to 20MPa [24], depending on joint, type of activity, body weight, and location, among other factors, which is about 50 times higher than the pressures used here. Positive hydrostatic pressures of 2.5MPa applied for 20s stimulate matrix synthetic rates of chondrocytes [10], indicating that even short procedures may affect chondrocyte metabolism, though negative pressures may have different effects than hydrostatic pressure. Investigating whether chondrocyte viability is altered by the portion of the device that seals to the cartilage surface would also be important.

The results of this study demonstrate the potential use of measuring hydraulic resistance as a diagnostic tool, and describe a practical device that could be used to make such measurements. While this data provides a proof of principle, additional work determining how fine of degradative changes can be discerned and characterizing the effects of a similar procedure on bone and cartilage *in vivo* could be performed. Such a device allows for a quantitative assessment of the fluid pressurization ability of articular cartilage that can be used in the arthroscopic setting to complement and extend current diagnostic tools.

A.6 Acknowledgments

Appendix A, in full, is reproduced from the *Annals of Biomedical Engineering*, volume 39, number 4, p. 1306-12, 2011 with permission of the authors, as authors retain copyright with Springer, Inc. The dissertation author was the primary author and thanks co-authors Anna Luan, Priya Sundaramurthy, Caryn Urbanczyk, Atal Patel, Jacob Hahr, Mohammad Sotoudeh, Anthony Ratcliffe, and Robert L. Sah. This work was supported by grants from the National Institutes of Health and an award to UCSD from the Howard Hughes Medical Institute through the HHMI Professors Program (for RLS). The authors would like to thank the UCSD Senior Design course BENG 187.

A.7 References

1. Armstrong CG, Mow VC: Variations in the intrinsic mechanical properties of human articular cartilage with age, degeneration, and water content. *J Bone Joint Surg Am* 64-A:88-94, 1982.

2. Athanasiou K, Constantinides G: Arthroscopic indenter, U.S. Patent #5433215, Board of Regents, University of Texas System, 1995.

3. Brittberg M, Lindahl A, Nilsson A, Ohlsson C, Isaksson O, Peterson L: Treatment of deep cartilage defects in the knee with autologous chondrocyte transplantation. *N Engl J Med* 331:889-95, 1994.

4. Buckwalter JA, Mankin HJ: Articular cartilage. Part I: tissue design and chondrocyte-matrix interactions. *J Bone Joint Surg Am* 79-A:600-11, 1997.

5. Carranza-Bencano A, Garcia-Paino L, Armas Padron JR, Cayuela Dominguez A: Neochondrogenesis in repair of full-thickness articular cartilage defects using free autogenous periosteal grafts in the rabbit. A follow-up in six months. *Osteoarthritis Cartilage* 8:351-8, 2000.

6. Chen AC, Bae WC, Schinagl RM, Sah RL: Depth- and strain-dependent mechanical and electromechanical properties of full-thickness bovine articular cartilage in confined compression. *J Biomech* 34:1-12, 2001.

7. Chu CR, Williams A, Tolliver D, Kwoh CK, Bruno S, 3rd, Irrgang JJ: Clinical optical coherence tomography of early articular cartilage degeneration in patients with degenerative meniscal tears. *Arthritis Rheum* 62:1412-20, 2010.

8. Curl WW, Krome J, Gordon ES, Rushing J, Smith BP, Poehling GG: Cartilage injuries: a review of 31,516 knee arthroscopies. *Arthroscopy* 13:456-60, 1997.

9. Görtz S, Bugbee WD: Allografts in articular cartilage repair. *J Bone Joint Surg Am* 88:1374-84, 2006.

10. Hall AC, Urban JPG, Gehl KA: The effects of hydrostatic pressure on matrix synthesis in articular cartilage. *J Orthop Res* 9:1-10, 1991.

11. Hangody L, Kish G, Karpati Z, Szerb I, Udvarhelyi I: Arthroscopic autogenous osteochondral mosaicplasty for the treatment of femoral condylar articular defects. A preliminary report. *Knee Surg Sports Traumatol Arthrosc* 5:262-7, 1997.

12. Hjelle K, Solheim E, Strand T, Muri R, Brittberg M: Articular cartilage defects in 1,000 knee arthroscopies. *Arthroscopy* 18:730-4, 2002.

13. Hwang J, Bae WC, Shieu W, Lewis CW, Bugbee WD, Sah RL: Increased hydraulic conductance of human articular cartilage and subchondral bone plate with progression of osteoarthritis. *Arthritis Rheum* 58:3831-42, 2008.

14. Kim YJ, Jaramillo D, Millis MB, Gray ML, Burstein D: Assessment of early osteoarthritis in hip dysplasia with delayed gadolinium-enhanced magnetic resonance imaging of cartilage. *J Bone Joint Surg Am* 85-A:1987-92, 2003.

15. Levick JR: Flow through interstitium and other fibrous matrices. *Q J Exp Physiol* 72:409-37, 1987.

16. Li Q, Wang J, Shahani S, Sun DD, Sharma B, Elisseeff JH, Leong KW: Biodegradable and photocrosslinkable polyphosphoester hydrogel. *Biomaterials* 27:1027-34, 2006.

17. Maroudas A: Physicochemical properties of cartilage in the light of ion exchange theory. *Biophys J* 8:575-95, 1968.

18. Maroudas A, Bullough P: Permeability of articular cartilage. *Nature* 219:1260-1, 1968.

19. Maroudas AI: Balance between swelling pressure and collagen tension in normal and degenerate cartilage. *Nature* 260:808-9, 1976.

20. McCutchen CW: The frictional properties of animal joints. *Wear* 5:1-17, 1962.

21. McPherson R, Shrive N, Damson E, Frank C, Lhenen F, Schachar N: Tissue softness probe, U.S. Patent #5701913, University Technologies International Inc., 1997.

22. Palmer AW, Guldberg RE, Levenston ME: Analysis of cartilage matrix fixed charge density and three-dimensional morphology via contrast-enhanced microcomputed tomography. *Proc Natl Acad Sci U S A*, 2006.

23. Riley SL, Dutt S, de la Torre R, Chen AC, Sah RL, Ratcliffe A: Formulation of PEG-based hydrogels affects tissue-engineered cartilage construct characteristics. *J Mater Sci Mater Med* 12:983-90, 2001.

24. Rushfeldt PD, Mann RW, Harris WH: Improved techniques for measuring in vitro the geometry and pressure distribution in the human acetabulum--I. ultrasonic measurement of acetabular surfaces, sphericity and cartilage thickness. *J Biomech* 14:253-60, 1981.

25. Sledge SL: Microfracture techniques in the treatment of osteochondral injuries. *Clin Sports Med* 20:365-77, 2001.

26. Soltz MA, Ateshian GA: Experimental verification and theoretical prediction of cartilage interstitial fluid pressurization at an impermeable contact interface in confined compression. *J Biomech* 31:927-34, 1998.

27. Swartz MA, Fleury ME: Interstitial flow and its effects in soft tissues. *Annu Rev Biomed Eng* 9:229-56, 2007.

28. Treppo S, Grodzinsky A, Quan E, Frank E, Bombard E, Breslau D: Arthroscopic impedance probe to detect cartilage degeneration, U.S. Patent #6856834, Massachusetts Institute of Technology, 2005.

29. Wang D, Williams CG, Yang F, Elisseeff JH: Enhancing the tissue-biomaterial interface: Tissue-initiated integration of biomaterials. *Adv Func Mat* 14:1152-59, 2004.

30. Wong BL, Bae WC, Chun J, Gratz KR, Lotz M, Sah RL: Biomechanics of cartilage articulation: effects of lubrication and degeneration on shear deformation. *Arthritis Rheum* 58:2065-74, 2008.

31. Wong BL, Sah RL: Effect of a focal articular defect on cartilage deformation during patello-femoral articulation. *J Orthop Res*, 2010.

32. Xie L, Lin AS, Guldberg RE, Levenston ME: Nondestructive assessment of sGAG content and distribution in normal and degraded rat articular cartilage via EPIC-muCT. *Osteoarthritis Cartilage*, 2009.

APPENDIX B:

THE PROTEOGLYCAN METABOLISM OF ARTICULAR CARTILAGE IN JOINT-SCALE CULTURE

B.1 Abstract

Understanding and controlling chondrocyte and cartilage metabolism in osteochondral tissues may facilitate ex vivo maintenance and application, both for allografts and tissue-engineered grafts. The hypothesis of this study was that maintenance of chondrocyte viability and sulfated glycosaminoglycan (sGAG) content in the articular cartilage of joint-scale osteochondral fragments is temperature- and metabolism-dependent. The aims were to assess, for adult goat joints, the effects of incubation temperature (37 vs 4°C) on cartilage chondrocyte viability and tissue matrix content and mechanical function, and the effects of temperature and cellular biosynthesis on sGAG release. Chondrocyte viability was maintained with 37°C incubation for 28d, but decreased by ~30% with 4°C incubation. Concomitantly, with 37°C incubation, cartilage sGAG was depleted by ~52% with the lost sGAG predominantly unable to aggregate with hyaluronan, whereas collagen content, tissue thickness, and tissue stiffness were maintained. The depletion of sGAG was diminished by slowing metabolism, with 4°C decreasing release by ~79% compared to 37°C incubation, and cycloheximide inhibition of cell metabolism at 37°C decreasing

release by ~47%. These results indicate that the articular cartilage of joint-scale grafts have enhanced chondrocyte viability by incubation at 37°C, but may need anabolic stimuli or catabolic inhibitors to maintain sGAG content.

B.2 Introduction

The repair of articular cartilage defects using osteochondral allografts and autografts is one option for functional restoration, though the procedures are limited by a lack of donor tissue. Cartilage repair and replacement treatments are typically used for small and large cartilage defects that have not yet progressed to the point where prosthetic joint replacement is recommended [13, 31]. The shortage of available donor tissue [1] has stimulated tissue engineering efforts to generate large, appropriately-shaped, joint-scale osteochondral fragments [15, 20, 21, 57, 58]. Allografts are currently stored at the joint scale, so that the properties of cartilage in such stored allografts provide the standard for large tissue-engineered constructs.

The effects of storage conditions on cadaveric donor tissue have typically been studied using small osteochondral cores at 4°C, although studies suggest that joint-scale storage at 37°C may be beneficial. Tissue banks currently store tissue as large osteochondral fragments at 4°C in proprietary media with 10% serum. Studies of storage conditions have typically examined small osteochondral cores as a model system [3, 28, 39, 40, 44, 53] at 4°C in media with 10% serum, with only a few studies addressing the practical storage in joint-scale fragments [59, 60]. Cartilage tissue structure, cell viability, and proteoglycan (PG) metabolism can be maintained in explant culture at 37°C in certain media formulations [8, 16, 17], but have only recently been investigated in the context of allograft storage, using small cores [36].

Viable chondrocytes are necessary for long term function of osteochondral grafts, and the viability of chondrocytes in cultured cartilage is affected by incubation

media, temperature, and configuration (**Table B.1**). In small osteochondral cores, chondrocyte viability is higher with the addition of serum to the culture medium at 4°C [38, 39] and also with 37°C compared to 4°C incubation [8, 38]. Chondrocyte viability at 4°C follows similar trends in joint-scale osteochondral fragments as in small cores, with significant loss of viability over several weeks [59, 60], although quantitative viability results at 37°C at the joint scale have not yet been reported.

Understanding and controlling chondrocyte metabolism in different tissue configurations facilitates *ex vivo* maintenance of cartilage, and may be useful for storage of allografts and osteochondral tissue. While the collagen content of cartilage explants and osteochondral cores remain relatively stable during tissue culture, sulfated glycosaminoglycan (sGAG) content can be markedly influenced by metabolic stimuli in the culture medium, such as serum which promotes biosynthesis of aggrecan [4, 7, 16], the major compressive load-bearing component of cartilage [6]. The first globular domain of aggrecan mediates its association with hyaluronan (HA) [48], stabilizing it within the cartilage matrix. Cleavage of aggrecan can disrupt this association with HA, increasing the release of sGAG from cartilage. Aggrecan metabolism and maintenance is important for tissue function, as tissue stiffness has been correlated with sGAG content [2, 34, 55]. The metabolism of sGAG in cartilage is mediated by biosynthetically active chondrocytes, as inhibition of cell biosynthesis with cycloheximide (CX) diminishes both the synthesis and the degradation of aggrecan [7, 23, 46]. In the joint-scale configuration of intact bovine calf sesamoid bones, cartilage sGAG metabolism is affected by both static [24, 25] and dynamic [26,

27] loading. The modulation of sGAG metabolism in mature cartilage at the joint-scale with 37°C incubation remains to be investigated.

Thus, the hypothesis of this study was that maintenance of chondrocyte viability and matrix content and release of sGAG in the articular cartilage of joint-scale osteochondral fragments are temperature- and metabolism-dependent. The specific aims were to assess the effects of adult goat joint-scale culture temperature (37 vs 4°C) and duration (fresh, 12d, or 28d) on articular cartilage chondrocytes (viability and DNA content) and tissue matrix (sGAG and collagen contents, sGAG distribution, and stiffness), and the effects of temperature (37 vs 4°C) and cellular biosynthesis (±CX) on matrix depletion (sGAG release rate and aggregatability with HA).

Table B.1: Osteochondral and joint-scale culture: effects of temperature and duration on chondrocyte viability.

		Conditions				
Tissue	*Age*	T (°C)	*Days*	*FBS*	*Viability*	*Reference*
Small osteochondral core	Mature	4	28	—	37–32%	11
			21–44	10%	50–84%	21
Joint-scale fragment[a]	Mature	4	28–60	10%	50–77%	15,16
Small osteochondral core	Mature	37	25	—	90–100%	17
Joint-scale fragment	Inmature	37	1	5%	—	36
	Mature	37	10	10%	Viable	31
			28	10%	—	

[a]Typical tissue bank incubation configuration and condition.
FBS, fetal bovine serum.

B.3 Materials and Methods

B.3.1 Experimental Design

A total of 42 distal humeri, harvested bilaterally from 22 adult goats were used. The humeri harvested bilaterally were always used for different experimental conditions. In particular, 18 humeri from different goats were used as fresh controls. The remaining 24 humeri were used for various incubation conditions. (The 4 out of the 24 humeri that were harvested bilaterally from 2 goats were used for different incubation conditions.) This allowed efficient usage of the available animal tissue. Groups included: (1) fresh controls (n=18) or joints incubated for (2) 12d (n=6) or (3) 28d (n=5) at 37ºC without CX, for (4) 28d (n=4) at 4ºC without CX, for 7d at 4ºC then 7d at 37ºC (4/37) (5) without CX (n=3) or (6) with CX (n=3), or for (7) 14d at 37ºC with CX (n=3) (Fig. B.1A). Although the goats were of two types, Boer males (16) and mixed-breed females (6), they were of similar age and joint size, with average cartilage thicknesses of (mean±SD) 0.35±0.05mm and 0.34±0.05mm and average surface areas of 12.5±2.5cm^2 and 11.2±0.9cm^2, respectively. In addition, 'type' had no significant effect on the outcome variables described below (P=0.18-0.86). The left and right limbs were divided as evenly as possible into each group, with either the same number of left and right limbs in each group or at most 1 more left or right limb in groups with an odd number of samples.

B.3.2 Harvest and Culture

Distal humeri were aseptically isolated, affixed to the lid of a bioreactor, and suspended in media. Thoracic limbs were received on wet ice within 24 hours of animal sacrifice. Elbow joints [12] were aseptically isolated essentially as described previously [33]. Briefly, the mid-diaphyses of the radius and ulna were exposed and transected. The bone marrow was removed and the cavities were rinsed with 3% hydrogen peroxide and then with phosphate buffered saline (PBS) with 100Units/mL penicillin, 100μg/mL streptomycin, and 0.25μg/mL fungizone (PSF). The distal humerus was exposed, separated from the radius and ulna, and soft tissue, including the periosteum on the diaphysis, was removed. Each humerus was suspended in a 250mL polycarbonate jar functioning as a bioreactor, with a stainless steel bolt affixed to the lid and attached to the diaphysis with bone cement (Osteobond, Zimmer Inc.) by filling the diaphysis with ~10mL of wet cement, inserting the bolt, and allowing the cement to set for 15min. For incubation at 37°C, the bioreactor lids were modified to allow gas exchange via 0.45μm filters. Each bioreactor was filled with medium, the secured with a lid, and placed at 4 or 37°C. 100mL of medium were used per bioreactor (low-glucose Dulbecco's modified Eagle's medium, 10m*M* HEPES, 0.1m*M* non-essential amino acids, 0.4m*M* L-proline, 2m*M* L-glutamine, PSF, and 25ug/mL ascorbic acid) (DMEM+) supplemented with 10% fetal bovine serum (FBS), and also with 0.5mM CX to inhibit biosynthesis [46] in certain studies. The lid with suspended distal humerus was screwed on to the bioreactor base (Fig. B.1B), and incubated at 37˚C within a humidified environment at 5% CO_2 or at 4°C for the appropriate durations. For joints incubated at 4°C, the closed container effectively maintained the CO_2 environment since the bicarbonate-dependent pH of the spent incubation medium

was 7.40±0.05. The media was changed twice per week and spent medium was collected and stored at -20˚C until processing.

B.3.3 Joint Surface Area

Joint surface area was estimated from geometries determined from photographs and a scaling factor determined from three-dimensional (3D) surface scanning of selected samples. Photographs of the articulating face of the distal humerus of all joints were taken before core isolation with a digital camera. The width of the humeral head, as well as the diameters of the medial and lateral edges, was measured using ImageJ (NIH). The shape of the humeral head was approximated as a truncated hemi-cone with half of the circumferential face corresponding to the surface area of cartilage, as calculated from the diameters and width. To determine a scaling factor between geometrical measures and cartilage surface area, three joint surfaces were scanned in 3D (3D Desktop Scanner, NextEngine Inc.), and cartilage surface areas were determined directly from 3D reconstructions (ScanStudio, NextEngine). The difference between surface area estimated from the geometrical estimate and the direct measurement was 6.6±3.2%. Thus, surface area was estimated routinely by the geometrical estimate scaled up by 1.066.

B.3.4 Isolation of Osteochondral Cores for Analysis

After harvest or incubation, 8 3.2mm diameter osteochondral cores were isolated with the articular cartilage intact and samples were prepared for analysis of viability and histology or for analysis of stiffness and biochemistry. Cores were

isolated from 4 proximal (P1-4) and 4 distal (D1-4) sites spanning the medial to lateral margin of the distal humerus (Fig. B.1C) using a custom stainless steel coring bit under constant irrigation with PBS with PSF kept at 4°C. Cores from 3 positions (D1, D4, P3) were placed in DMEM+ with 10% FBS for 1-2hrs until viability staining and analysis. The cores from the remaining 5 positions were rinsed in PBS with protease inhibitors (1mM phenylmethanesulfonyl fluoride, 2mM disodium ethylenediamine tetraacetate, 5mM benzamidine-HCl, and 10mM N-ethylmaleimide) (PBS+PI), for 1hr at 4°C and then stored at -20°C until further processing.

B.3.5 Viability and Histology

Cores from 3 positions (D1, D4, and P3) were bisected axially with a razor blade and one half was analyzed for chondrocyte viability. The half-cores were stained with Live/Dead® (Molecular Probes, Inc.) and the *en face* and vertical profiles were imaged at 10x with a fluorescence microscope (Eclipse TE300, Nikon). Images were analyzed using a custom image processing routine in MATLAB® v7.5 to determine the percent of live cells. The vertical profile was divided into superficial, middle, and deep zones each comprising 15, 30, and 55% of the total thickness based on cellular morphological features. Since the superficial zone contained only 1-3 layers of cells, viability estimates from vertical profiles were variable due to the low number of cells visualized in each field of view (mean±SD: 49±21cells). Instead, the viability of the chondrocytes in the superficial zone was determined from *en face* views, which provided a larger numbers of cells in each field of view (601±156cells).

The second half of each core was prepared for histology and stained with Toluidine blue. The half-cores were fixed in 4% paraformaldehyde in PBS for ~1wk at 4°C and then decalcified in 1mL of PBS with 15% EDTA on a rocker at room temperature. The EDTA solution was changed every other day for ~3wks to allow decalcification. The decalcified cores were cryostat sectioned at 10μm, stained with 0.04% Toluidine blue, and imaged at 10x magnification.

B.3.6 Core Diameter, Thickness, and Indentation Stiffness

Cores from the remaining 5 positions (D2, D3, P1, P2, and P4) were analyzed for diameter and thickness. The diameter of each core was measured using calipers (Mitutoyo). For cartilage thickness, images were captured at 0, 60, and 120° around the perimeter of the core, thickness measured from the images (ImageJ) at 3 locations per angle, and the average of the 9 measurements was used.

The short-time indentation stiffness was determined. Samples were compressed at the articular surface by 20% of cartilage thickness at a rate of 0.1mm/s (over <1s) with a plane-ended, impermeable, 400μm diameter indenter tip and the load was measured using a mechanical testing apparatus (v500cs, BioSyntech Canada Inc). The tip was held at maximum displacement for 0.5s, the load recorded, and test repeated at three sites 400μm apart on each core. The average load for each core was divided by the indentation depth to determine the indentation stiffness.

B.3.7 DNA, Collagen, and sGAG Content

After indentation testing, the cartilage was analyzed for content of DNA, collagen, and sGAG .For each core, cartilage was removed from the bone, solubilized with proteinase K at 60°C for 16hrs, and the portions of the digests were analyzed for DNA by the PicoGreen dye binding assay [30], sulfated sGAG by the dimethylmethylene blue dye binding assay [11], and collagen by p-dimethylaminobenzaldehyde detection of hydroxyproline [61]. The hydroxyproline content was converted to collagen content using a mass ratio of 7.25 collagen to hydroxyproline [19, 35]. Biochemical measures were normalized to core surface area to allow comparison between sGAG in the tissue and released to the media. Portions of the spent media were also analyzed for sGAG content and normalized to joint surface area per day, as passive loss of cleaved sGAG molecules from cartilage matrix in explants is a surface area-dependent phenomenon [5]. Total sGAG in the culture system was calculated by summing the mass of sGAG in the spent media over the culture duration normalized to joint surface area, and adding that to the average sGAG per surface area in the cores, scaled up to the joint surface area.

B.3.8 Aggregation of sGAG in Conditioned Media with HA

The size and aggregatability with hyaluronan (HA) of sGAG in conditioned media and from freshly extracted controls were analyzed using gel electrophoresis. Pooled samples of conditioned media from the initial days in culture of joints incubated at 37°C were concentrated to ~1μg/μl sGAG with a 100kDa filter. As a control sample, cartilage was harvested from 1 adult goat distal humerus and sGAG was extracted [18] (with an extraction efficiency of 97%). The ability of aggrecan in

the spent media and in the cartilage extract control to aggregate with HA was analyzed by the addition of 5% (w/w) Healon and 5% (w/w) link protein (LP), isolated from bovine calf cartilage [52]. Samples were dissociated by dialyzing against 4M GuHCl, 0.1M NaAc pH 6.8 overnight at 4°C. Then samples were allowed to associate by dialysis against 0.1M NaAc pH 6.8, for 24hr at 4°C. Subsequently, as a control for association mediated by HA, portions of each sample were incubated with *Streptomyces* hyaluronidase (10units/mL in 0.1M NaH_2PO_4, 0.15M NaCl, pH 6) overnight at 37°C to digest HA. Sample volumes with an equivalent of 10μg of sGAG were electrophoresed in TAE pH 8 in a 1% agarose gel, fixed, stained in 0.2% (w/v) Alcian blue 8GX, 3% acetic acid, 0.05M $MgCl_2$, pH 2 [56], destained, and imaged.

B.3.9 Statistics

Data are presented as mean ± SEM. The effects of incubation condition (fresh control, 12d at 37°C, 28d at 37°C or 28d at 4°C) and position (P3, D1, and D4) on *en face*, middle, and deep zone viabilities, and remaining positions (P1, P2, P4, D2, D3) on cartilage thickness and stiffness, and DNA, sGAG and COL contents were determined by 2-way ANOVA with condition as a fixed effect and position as a repeated measure. Because humeri were distributed amongst the various experimental conditions, with no two humeri from the same animal being used for the same condition, the statistical model did not attempt to account for animal donor effects. Viability data were arcsine transformed to improve normality [51]. The effects of incubation condition (4°-CX, 4/37°-CX, 4/37°+CX, 37°-CX, or 37°+CX) and day (0:3.5:28) on sGAG in the media samples were determined by 2-way ANOVA with

condition as a fixed effect and day as a repeated measure on $\log_{10}$ transformed data to improve homoscedasticity [51]. Tukey post hoc comparisons were performed to compare groups when significant differences ($P<0.05$) were detected between conditions. Statistical analyses were performed using Systat 10.2 (Systat Software Inc.).

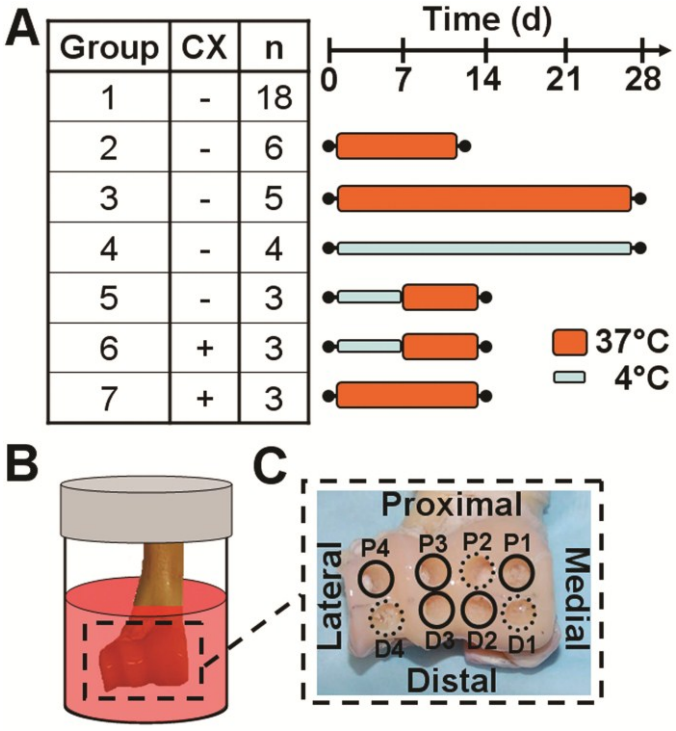

Figure B.1: Schematic diagrams of **(A)** experimental groups, **(B)** joint-scale bioreactor setup, and **(C)** core isolation locations from the distal humerus.

B.4 Results

B.4.1 Viability

Chondrocyte viability was high in the *en face* view and middle zone of fresh controls and joints incubated at 37°C, but lower in joints incubated at 4°C, while no effect of condition was observed in the deep zone (**Fig. B.2**). Quantitative analysis was consistent with these observations, with a significant effect of incubation condition on viability in the *en face* ($P<0.05$) and middle zone ($P<0.05$), though not in the deep zone ($P=0.98$). A significantly lower % of viable cells were present in joints incubated at 4°C in the *en face* profile (62%) compared to all other groups (86-95%, **Fig. B.3A**, $P<0.05$) and in the middle zone (52%) compared to fresh controls (84%) and joints incubated for 28d at 37°C (88%, **Fig. B.3B**, $P<0.05$).

B.4.2 Thickness and Stiffness

Cartilage thickness varied slightly with incubation condition, though stiffness was not detectably affected. Average distal humerus cartilage thickness ranged from approximately 0.3 to 0.4mm, and varied slightly, but significantly with incubation condition ($P<0.01$). There were no differences between the thickness of fresh controls and any incubation condition (**Fig. B.4A**, $P=0.14$-0.24), but slight differences between the 12d at 37°C group and 28d at 37°C ($P<0.01$) and 28d at 4°C ($P<0.05$) groups. Average cartilage indentation stiffness ranged from approximately 2.4 to 2.8N/mm and did not vary with incubation condition (**Fig. B.4B**, $P=0.98$).

B.4.3 DNA and Collagen Content

DNA and collagen contents of the cartilage digests were not affected by incubation condition. DNA content averaged 18.8±1.2μg/cm^2 and was not affected by incubation condition (P=0.12). Collagen content averaged 5.3±0.4mg/cm^2 and was not affected by incubation condition (P=0.75). The trends for DNA and collagen contents normalized to volume, 603±38μg/cm^3 and 169±13mg/cm^3 respectively, were generally similar (P=0.06, 0.30).

B.4.4 sGAG Content and Distribution

sGAG content was decreased in joints incubated at 37°C compared to fresh controls. sGAG content was significantly affected by incubation condition (P<0.001). sGAG content was significantly lower (~35%) in joints incubated for 12d at 37°C compared to fresh controls (P<0.01) and compared to 4°C incubated joints (**Fig. B.4C**, P<0.01), and also lower (~52%) in joints incubated for 28d at 37°C compared to fresh control (**Fig. B.4C**, P<0.001) and compared to 4°C incubated joints (P<0.001). The same trends were observed when normalizing core sGAG mass to tissue volume instead of area, with a fresh control average of 49.1±2.4mg/cm^3.

Representative histological sections of cartilage from cores isolated for fresh control, 28d at 37°C and 28d at 4°C showed typical cartilage morphology and an intact surface (**Fig. B.5**). Qualitatively, the staining intensity overall was similar in fresh controls and joints incubated at 4°C, though slightly less intense at 4°C (**Fig. B.5A vs B.5C**). However, the staining intensity was decreased overall, and

particularly in the deep zone of sections of joints incubated for 28d at 37°C (**Fig. B.5B**).

B.4.5 Quantity and Aggregatability of sGAG Released into the Medium

The amount of sGAG released into the medium varied with incubation condition ($P<0.01$) and by day ($P<0.001$). sGAG released during incubation without CX at 4°C was significantly lower at all time points than at 37°C (**Fig. B.6A, open triangles vs open circles,** $P<0.001$-0.05). sGAG released during incubation for 7d at 4°C then 7d at 37°C without CX was low and no different than other 4°C data at 3.5d ($P=0.42$) and 7d ($P=0.46$), but there was a trend for it to be higher than other 37°C data at 10.5d ($P=0.07$) and it was significantly higher at 14d ($P<0.05$, **Fig. B.6A, open squares**). The addition of CX to the 4/37°C condition resulted in a decrease in the amount of sGAG released compared to without CX, starting with a tendency for a 55% decrease at 10.5d ($P=0.61$) that became a significant 60% decrease at 14d ($P<0.05$, **Fig. B.6A, filled vs open squares**). Within each incubation condition, the amount of sGAG released varied by day (**Fig. B.6A**, $P<0.001$-0.01), except for 37°C with CX ($P=0.11$). The sGAG released during 7 days for each group, over 0-7d (**Fig. B.6B**) and over 7-14d (**Fig. B.6C**), normalized to the sGAG release from the 37°C without CX group from 0-7d, illustrated the effects of CX and temperature.

Total sGAG in the culture system, defined as sGAG in the tissue plus that in the medium, summed over the incubation duration, did not vary with incubation condition ($P=0.16$), whereas the relative % remaining in the tissue did vary with incubation condition (**Fig. B.7**, $P<0.001$). The % left in the tissue was significantly

lower for joints incubated 28d at 37°C than all other groups (34% vs 60-83%, $P<0.001$), and significantly higher for joints incubated 28d at 4°C than all other groups ($P<0.001$-0.05), except for joints incubated 14d at 4/37°C+CX ($P=0.58$). The addition of CX to the media of joints incubated for 12-14d at 37°C resulted in an increased fraction (73 vs 59%) of sGAG remaining in the tissue ($P<0.001$), just as it resulted in an increased fraction of sGAG (78 vs 64%) for joints incubated for 14d at 4/37°C ($P<0.01$).

Differences in PG size and aggregatability between sGAG in 37°C conditioned medium and that from freshly extracted cartilage were apparent from gel electrophoretic analysis. Compared to the sGAG of freshly extracted cartilage (**Fig. B.8, lane 1**), the major band of sGAG from the 37°C conditioned media (**Fig. B.8, lane 4**) had a higher electrophoretic mobililty and an additional, highly mobile band was visible, indicative of lower molecular weight sGAG molecules. sGAG in the control extract was able to aggregate with HA and LP, as indicated by the shift of the major sGAG band to a lower mobility position (**Fig. B.8, lane 2**). This shift depended on intact HA, as digestion of the extract+HA+LP sample with hyaluronidase resulted in a band distribution (**Fig. B.8, lane 3**) similar to control extract alone (**Fig. B.8, lane 1**). In contrast, the mobility of the sGAG in the 37°C conditioned medium was not affected by the addition of HA and LP or digestion of HA (**Fig. B.8, lanes 4-6**).

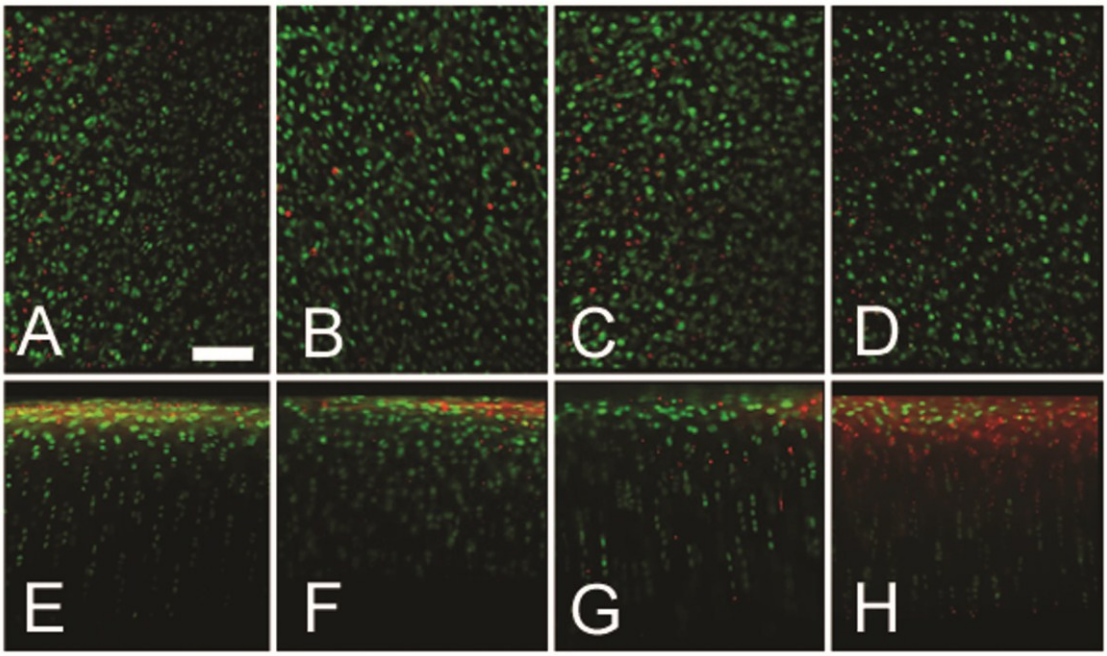

Figure B.2: Osteochondral cores were analyzed for chondrocyte viability by LIVE/DEAD® fluorescence staining in the *en face* **(A-D)** and vertical **(E-H)** profiles. Representative images of cores from fresh control **(A,E)**, 12d 37°C **(B,F)**, 28d 37°C **(C,G)**, and 28d 4°C **(D,H)** are shown. Scale bar: 100μm.

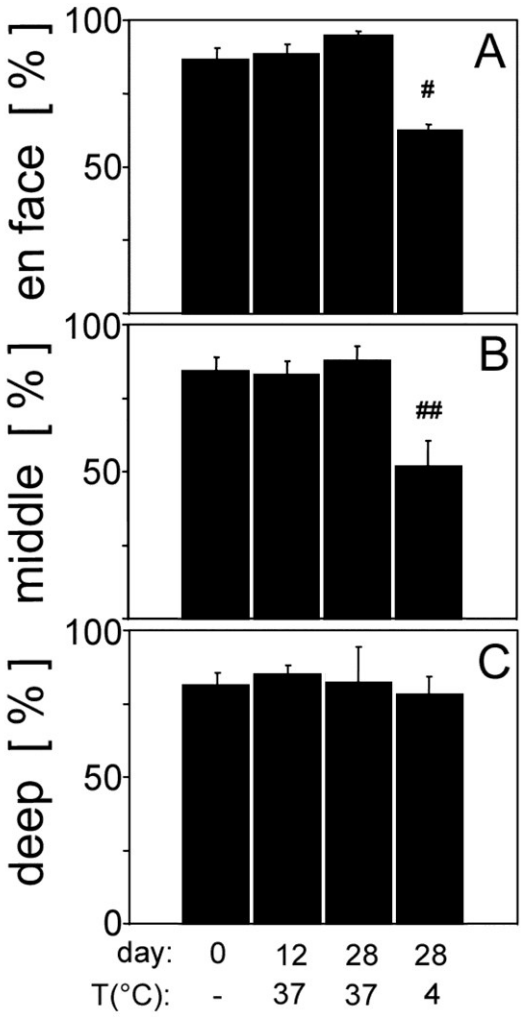

Figure B.3: Fluorescent LIVE/DEAD® images were analyzed for % viable chondrocytes in the *en face* profile **(A)** and the middle **(B)** and deep **(C)** zones of the vertical profile from fresh control, 37°C at 12d, 37°C at 28d, and 4°C. # indicates significantly less than all other bars ($P<0.05$), ## indicates significantly less than fresh control and 37°C at 28d groups ($P<0.05$).

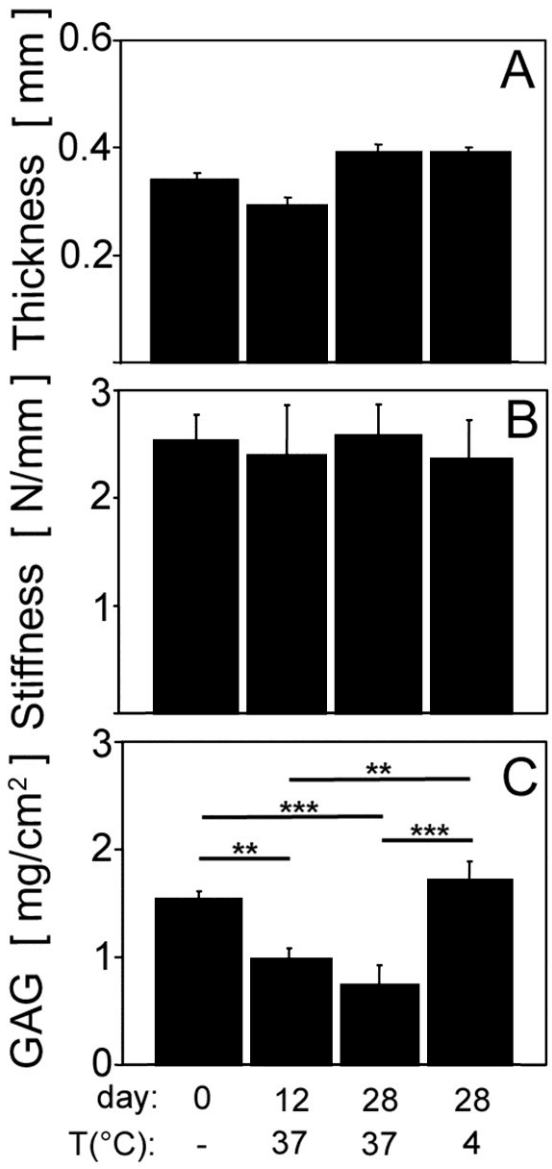

Figure B.4: Osteochondral cores from fresh control, 37°C at 12d, 37°C at 28d, and 4°C were analyzed for thickness **(A)**, indentation stiffness **(B)**, and sGAG content **(C)**. ** indicates $P<0.01$, *** indicates $P<0.001$.

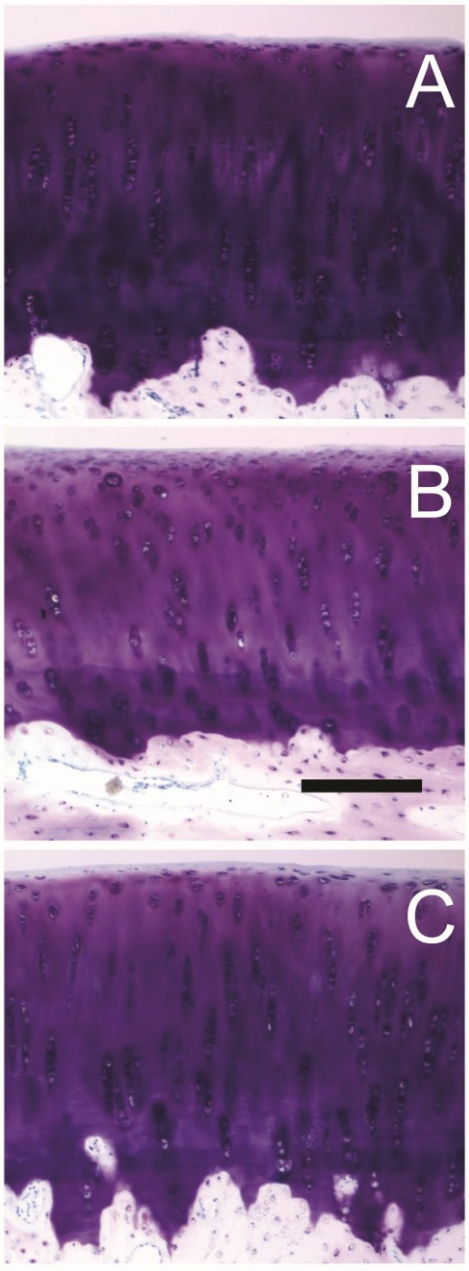

Figure B.5: Sections of osteochondral cores from fresh control **(A)**, 28d 37°C **(B)**, and 28d 4°C **(C)** were prepared and stained with Toluidine Blue. Scale bar: 200μm.

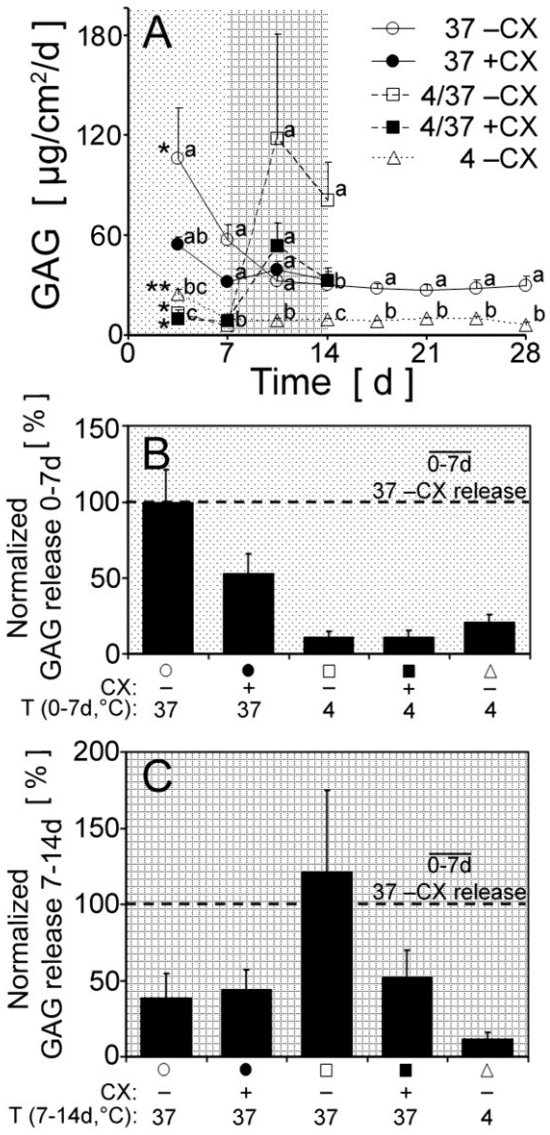

Figure B.6: Conditioned media sGAG content. Joints were incubated with (filled) or without (open) 0.5 mM CX at 4°C, 37°C, or for 7d at 4°C and then 7d at 37°C (4/37°C) **(A)**. Within each time point, letters (a,b,c) designate significantly different groups ($P<0.05$), with a shared letter indicating no difference. *: initial time point not different from 2nd point, but different from the remaining time points ($P<0.05$), **: initial time point different from the remaining time points ($P<0.05$). Average sGAG release for each group over 0-7d **(B)** and 7-14d **(C)** were normalized to the sGAG release from the 37 –CX group from 0-7d to emphasize differences due to CX and temperature.

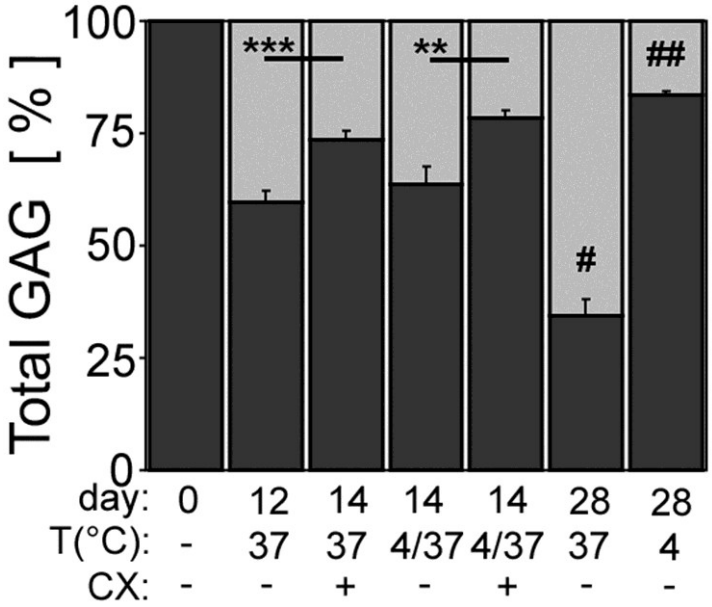

Figure B.7: % of total sGAG content ($sGAG_{tissue}$ + $sGAG_{media}$) detected in the core digests (dark grey) and cumulative amount in the media summed over the incubation period (light grey). Incubation time, temperature (4/37 indicates 1wk at 4°C then 1wk at 37°C), and the presence or absence of 0.5mM cycloheximide (CX) are indicated. **: P<0.01; ***: P<0.001; #: different than all other groups, P<0.001; ##: different than all other groups (P<0.001-0.05) except 14d at 4/37 with CX (P=0.58).

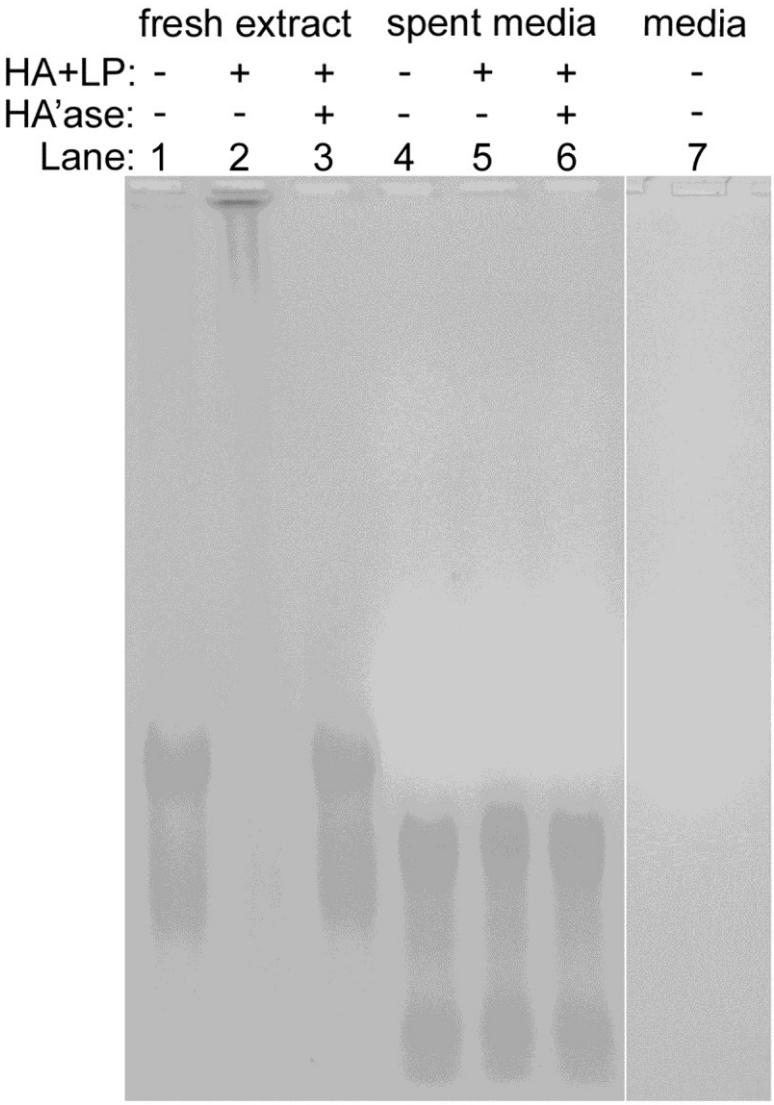

Figure B.8: Fresh extract controls and spent media (day 3.5 at 37°C) samples with or without HA and link protein and hyaluronidase were separated on a 1% agarose gel and stained with Alcian blue.

B.5 Discussion

The results of this study demonstrate that many properties of articular cartilage can be maintained during incubation at 37°C in a joint-scale configuration, although sGAG content is affected in a metabolism-dependent manner. The viability of chondrocytes was maintained during incubation at 37°C, while 4°C incubation led to a loss in viability (**Figs. B.2, B.3A, B.3B**), while still maintaining tissue thickness and stiffness (**Fig. B.4A, B.4B**), and DNA and collagen contents, suggesting that osteochondral tissue stored for use in allograft procedures may benefit in terms of viability from 37°C storage. More sGAG was depleted from the tissue and released during incubation at 37°C compared to 4°C (**Figs. B.4C, B.5-B.7**), and the release was partially cell-mediated (**Fig. B.6**). The released sGAG macromolecules were smaller than controls and their inability to aggregate with HA (**Fig. B.8**) indicate that the sGAG lost was likely actively cleaved from the tissue matrix. For allograft storage and tissue-engineered grafts at the joint-scale in the conditions used here, there may be a trade-off between higher cell viability with 37°C incubation, but loss of matrix sGAG content.

A limitation of working at the joint-scale is that each sample requires intensive preparation, limiting the number of samples that can be obtained in a given amount of time. In the present study, multiple small samples were taken across the joint surface to account for regional variation. In addition, analyzing the entire joint surface for biochemical contents was impractical as it would require accurately removing a thin layer of cartilage from the entire irregularly shaped joint surface. Thus, sample values

were scaled to joint area to estimate properties of the full joint surface, assuming the values for individual cores were collectively representative of the entire joint. Experiments at the joint-scale may be best suited for translational studies after preliminary studies at a smaller (e.g., tissue) scale. Still, despite the variability between animals and limited sample numbers, there were clear differences in viability, tissue sGAG content, and sGAG released to the medium between incubation conditions.

The increased viability in 37°C vs 4°C storage suggests that allograft tissue stored at 37°C may have improved long term function. Graft retrieval studies after recipient death have identified donor tissue cells or their progeny remaining in the repaired cartilage defect 29yrs after the surgical procedure [22]. While preservation of the tissue structure is important to the allograft procedure as it allows immediate restoration of the weight-bearing function of the defected region, the tissue matrix will eventually degrade without the presence of living cells synthesizing matrix constituents [9, 10]. Thus, maintaining the viability of allograft tissue is likely critically important for the long-term success of a tissue grafting procedure. While the release of sGAG from the tissue in 37°C incubation reported here is not ideal for the goal of tissue preservation, the increased viability of chondrocytes in the tissue stored at 37°C vs 4°C is likely more important to long term graft success.

The initial bolus release of sGAG from cartilage during the first few days in 37°C and experimental modulation of that release (**Fig. B.6**) suggest that a cell-mediated process is responsible for aggrecan cleavage in and release from the cartilage of such cultures. A product of chondrocytes may cleave aggrecan directly or activate

proteinases already present in the matrix. Likely candidates mediating such aggrecan cleavage include the MMP and ADAMTS families [37, 49] and reactive oxygen species (ROS) [41, 54], such as hydrogen peroxide [42, 43]. MMP and ADAMTS enzymes cleave the interglobular domain of aggrecan at various locations [48], resulting in large PG fragments unable to aggregate with HA. The inability of the sGAG fragments lost to the media to aggregate with HA (**Fig. B.8**) suggests these fragments lack this first globular domain, consistent with the likely cleavage sites, though exposure of PG aggregates to hydrogen peroxide also generates large sGAG fragments that are unable to interact with HA [42]. The difference in magnitude of sGAG release at 37°C vs 4°C and the delay of the large bolus release by 7d in the joints incubated for 7d at 4°C and then moved to 37°C indicate that the molecules participating in sGAG cleavage do not simply diffuse away while they are inactive. Further analysis is needed to clarify the mechanism of aggrecan degradation and release from cartilage in the joint-scale culture configuration so that appropriate catabolic inhibitors could be added to the culture medium to reduce sGAG matrix depletion.

Adaptation of joint-scale culture techniques to other tissues may require consideration of several factors that are likely to affect the response seen here, including the maturity of the tissue, tissue configuration, and the presence of serum in the medium. Chondrocyte metabolism decreases with age, making the use of adult tissue necessary to represent most cadaveric allograft storage tissue. The anabolic stimulus in this study was the addition of 10% serum to the incubation medium. Assuming that the tissue had achieved a balanced synthesis and release rate by the end

of the 28d culture duration, the turnover rate or half-life of sGAG with 37°C incubation, on the order of 20d, was comparable to reports in the literature for cartilage explants [5, 7], indicating that after the initial bolus sGAG loss, the tissue achieved a similar synthesis and degradation rate as in explant culture. Preservation of sGAG content during incubation in a joint-scale configuration might be achieved by including anabolic stimuli in the culture medium, such as serum, IGF-1 [45, 47] or TGF-β1 [32], or by providing mechanical stimuli, such as those that stimulate chondrocyte sGAG biosynthesis [14, 46].

The lack of change in tissue stiffness despite the release of sGAG was somewhat surprising, as matrix sGAG content is generally correlated to tissue stiffness [34, 55]. The content of sGAG in cartilage tissue provides the resistance to compression due to its high negative charge density, which creates a swelling pressure that resists compression [29]. One likely explanation for this lack of stiffness change with sGAG release is that the rapid indentation test is most sensitive to the region of tissue immediately adjacent to the indenter, rather than the deep zone where sGAG appears to be predominantly lost (**Fig. B.4B**). Also, since the deep zone is relatively stiff compared to the overlying zones of cartilage [50], changes in deep zone sGAG and stiffness properties may not be reflected by a surface indentation stiffness measurement. More detailed characterization of the cartilage portion of the osteochondral cores, including the deep zone, could be attempted using compression testing, although determination of material properties is complicated by depth-associated variations and would be difficult for such thin cartilage. The thin cartilage

also would have made it difficult to remove the tissue from the underlying bone for traditional isolated tests.

The results of this study may have practical implications for storage of osteochondral grafts and also provide directions for future investigations. Incubation of joints at 37°C may provide an alternative to the standard cartilage tissue culture configurations especially to maintain chondrocyte viability in osteochondral grafts. Delineation of the turnover of cartilage PG in terms of the temperature- and metabolism-dependence of matrix release and retention in a joint-scale configuration provides a foundation for future investigations of cartilage at the joint-scale. The techniques for joint-scale culture developed here could also be useful in the scale-up of tissue engineering for the creation of joint surfaces, as well as for the storage of joints before use. The storage conditions examined in this study identify the importance of temperature and cell-mediated metabolism for the maintenance of extracellular matrix at the joint scale. The same principles may apply to tissue engineered cartilage in various shapes and sizes.

B.6 Acknowledgments

Appendix B, in full, is reproduced from *Tissue Engineering, Part A*, volume 16, number 5, p. 1717-27, 2010 with permission from Mary Ann Liebert, Inc. The dissertation author was the primary author and thanks co-authors Andrea L. Pallante, Rebecca J. Rone, William D. Bugbee, and Robert L. Sah. This work was supported by grants from the National Institutes of Health and an award to UCSD from the Howard Hughes Medical Institute through the HHMI Professors Program (for RLS). The authors would like to thank Harold M. Aberman, DVM, MSE for his donation of goat tissue, Won C. Bae, Ph.D for his work on the image processing script, and EunHee Han, MS for her donation of link protein.

B.7 References

1. Alford JW, Cole BJ: Cartilage restoration, part 2: techniques, outcomes, and future directions. *Am J Sports Med* 33:443-60, 2005.

2. Bae WC, Temple MM, Amiel D, Coutts RD, Niederauer GG, Sah RL: Indentation testing of human cartilage: sensitivity to articular surface degeneration. *Arthritis Rheum* 48:3382-94, 2003.

3. Ball ST, Amiel D, Williams SK, Tontz W, Chen AC, Sah RL, Bugbee WD: The effects of storage media on fresh human osteochondral allografts. *Clin Orthop Relat Res* 418:246-52, 2004.

4. Benya PD, Jaffe S, Raffo A: The capacity of chondrocytes to respond to serum is enhanced by organ culture in the absence of serum, stimulated by serum, and modified by ascorbate. *Arch Biochem Biophys* 232:323-36, 1984.

5. Bolis S, Handley CJ, Comper WD: Passive loss of proteoglycan from articular cartilage explants. *Biochim Biophys Acta* 993:157-67, 1989.

6. Buckwalter JA, Mankin HJ: Articular cartilage. Part I: tissue design and chondrocyte-matrix interactions. *J Bone Joint Surg Am* 79-A:600-11, 1997.

7. Campbell MA, Handley CJ, Hascall VC, Campbell RA, Lowther DA: Turnover of proteoglycans in cultures of bovine articular cartilage. *Arch Biochem Biophys* 234:275-89, 1984.

8. Dumont J, Ionescu M, Reiner A, Poole AR, Tran-Khanh N, Hoemann CD, McKee MD, Buschmann MD: Mature full-thickness articular cartilage explants attached to bone are physiologically stable over long-term culture in serum-free media. *Connect Tissue Res* 40:259-72, 1999.

9. Enneking WF, Campanacci DA: Retrieved human allografts: a clinicopathological study. *J Bone Joint Surg Am* 83-A:971-86, 2001.

10. Enneking WF, Mindell ER: Observations on massive retrieved human allografts. *J Bone Joint Surg Am* 73-A:1123-42, 1991.

11. Farndale RW, Sayers CA, Barrett AJ: A direct spectrophotometric microassay for sulfated glycosaminoglycans in cartilage cultures. *Connect Tissue Res* 9:247-8, 1982.

12. Getty R. Sisson and Grossman's the Anatomy of the Domestic Animals. 5 ed. Philadelphia, London, Toronto: W.B. Saunders Co.; 1975.

13. Görtz S, Bugbee WD: Fresh osteochondral allografts: graft processing and clinical applications. *J Knee Surg* 19:231-40, 2006.

14. Grodzinsky AJ, Levenston ME, Jin M, Frank EH: Cartilage tissue remodeling in response to mechanical forces. *Annu Rev Biomed Eng* 2:691-713, 2000.

15. Han EH, Bae WC, Hsieh-Bonassera ND, Wong VW, Schumacher BL, Gortz S, Masuda K, Bugbee WD, Sah RL: Shaped, stratified, scaffold-free grafts for articular cartilage defects. *Clin Orthop Relat Res* 466:1912-20, 2008

16. Hascall VC, Handley CJ, McQuillan DJ, Hascall GK, Robinson HC, Lowther DA: The effect of serum on biosynthesis of proteoglycans by bovine articular cartilage in culture. *Arch Biochem Biophys* 224:206-23, 1983.

17. Hascall VC, Morales TI, Hascall GK, Handley CJ, McQuillan DJ: Biosynthesis and turnover of proteoglycans in organ culture of bovine articular cartilage. *J Rheumatol* 10S:45-52, 1983.

18. Hascall VC, Sajdera SW: Proteinpolysaccharide complex from bovine nasal cartilage. The function of glycoprotein in the formation of aggregates. *J Biol Chem* 244:2384-96, 1969.

19. Herbage D, Bouillet J, Bernengo J-C: Biochemical and physicochemical characterization of pepsin-solubilized type-II collagen from bovine articular cartilage. *Biochem J* 161:303-12, 1977.

20. Hung CT, Lima EG, Mauck RL, Taki E, LeRoux MA, Lu HH, Stark RG, Guo XE, Ateshian GA: Anatomically shaped osteochondral constructs for articular cartilage repair. *J Biomech* 36:1853-64, 2003.

21. Isogai N, Landis W, Kim TH, Gerstenfeld LC, Upton J, Vacanti JP: Formation of phalanges and small joints by tissue-engineering. *J Bone Joint Surg Am* 81-A:306-16, 1999.

22. Jamali AA, Hatcher SL, You Z: Donor cell survival in a fresh osteochondral allograft at twenty-nine years. A case report. *J Bone Joint Surg Am* 89:166-9, 2007.

23. Kimura JH, Caputo CB, Hascall VC: The effect of cycloheximide on synthesis of proteoglycans by cultured chondrocytes from the Swarm rat chondrosarcoma. *J Biol Chem* 256:4368-76, 1981.

24. Korver GHV, van de Stadt RJ, van Kampen GPJ, Kiljan E, van der Korst JK: Bovine sesamoid bones: a culture system for anatomically intact articular cartilage. *In Vitro Cell Dev Biol* 25:1099-106, 1989.

25. Korver GHV, van de Stadt RJ, van Kampen GPJ, van der Korst JK: Composition of proteoglycans synthesized in different layers of cultured anatomically intact articular cartilage. *Matrix* 10:394-401, 1990.

26. Korver GHV, van de Stadt RJ, van Kampen GPJ, van der Korst JK. Effects of culture and loading on the turnover of proteoglycans in anatomically intact articular cartilage [PhD]. Amsterdam, The Netherlands; 1991.

27. Korver GHV, van de Stadt RJ, van Kampen GPJ, van der Korst JK: The effects of loading on the synthesis of proteoglycans in different layers of anatomically intact articular cartilage in vitro. *J Rheumatol* 19:905-12, 1992.

28. Malinin T, Temple HT, Buck BE: Transplantation of osteochondral allografts after cold storage. *J Bone Joint Surg Am* 88:762-70, 2006.

29. Maroudas AI: Balance between swelling pressure and collagen tension in normal and degenerate cartilage. *Nature* 260:808-9, 1976.

30. McGowan KB, Kurtis MS, Lottman LM, Watson D, Sah RL: Biochemical quantification of DNA in human articular and septal cartilage using PicoGreen and Hoechst 33258. *Osteoarthritis Cartilage* 10:580-7, 2002.

31. McNickle AG, Provencher MT, Cole BJ: Overview of existing cartilage repair technology. *Sports Med Arthrosc* 16:196-201, 2008.

32. Morales TI, Roberts AB: Transforming growth factor-β regulates the metabolism of proteoglycans in bovine cartilage organ cultures. *J Biol Chem* 263:12828-31, 1988.

33. Nugent-Derfus GE, Takara T, O'Neill JK, Cahill SB, Gortz S, Pong T, Inoue H, Aneloski NM, Wang WW, Vega KI, Klein TJ, Hsieh-Bonassera ND, Bae WC, Burke JD, Bugbee WD, Sah RL: Continuous passive motion applied to whole joints stimulates chondrocyte biosynthesis of PRG4. *Osteoarthritis Cartilage* 15:566-74, 2007.

34. Nugent GE, Law AW, Wong EG, Temple MM, Bae WC, Chen AC, Kawcak CE, Sah RL: Site- and exercise-related variation in structure and function of cartilage from equine distal metacarpal condyle. *Osteoarthritis Cartilage* 12:826-33, 2004.

35. Pal S, Tang LH, Choi H, Habermann E, Rosenberg L, Roughley P, Poole AR: Structural changes during development in bovine fetal epiphyseal cartilage. *Coll Relat Res* 1:151-76, 1981.

36. Pallante AL, Bae WC, Chen AC, Gortz S, Bugbee WD, Sah RL: Chondrocyte Viability Is Higher After Prolonged Storage at 37C Than At 4C For Osteochondral Grafts. *Am J Sports Med* Accepted, 2009.

37. Patel KP, Sandy JD, Akeda K, Miyamoto K, Chujo T, An HS, Masuda K: Aggrecanases and aggrecanase-generated fragments in the human intervertebral disc at early and advanced stages of disc degeneration. *Spine* 32:2596-603, 2007.

38. Pearsall AW, Tucker JA, Hester RB, Heitman RJ: Chondrocyte viability in refrigerated osteochondral allografts used for transplantation within the knee. *Am J Sports Med* 32:125-31, 2004.

39. Pennock AT, R CM, Emmerson BC, Wagner F, Bugbee WD, Harwood FL, Amiel D: The effects of varying storage conditions on fresh human

osteochondral allografts during prolonged storage. *Int Cart Repair Soc* 6:12, 2006.

40. Pennock AT, Robertson CM, Wagner F, Harwood FL, Bugbee WD, Amiel D: Does subchondral bone affect the fate of osteochondral allografts during storage? *Am J Sports Med* 34:586-91, 2006.

41. Pylawka TK, Virdi AS, Cole BJ, Williams JM: Reversal of suppressed metabolism in prolonged cold preserved cartilage. *J Orthop Res* 26:247-54, 2008.

42. Roberts CR, Mort JS, Roughley PJ: Treatment of cartilage proteoglycan aggregate with hydrogen peroxide. Relationship between observed degradation products and those that occur naturally during aging. *Biochem J* 247:349-57, 1987.

43. Roberts CR, Roughley PJ, Mort JS: Degradation of human proteoglycan aggregate induced by hydrogen peroxide. Protein fragmentation, amino acid modification and hyaluronic acid cleavage. *Biochem J* 259:805-11, 1989.

44. Rohde RS, Studer RK, Chu CR: Mini-pig fresh osteochondral allografts deteriorate after 1 week of cold storage. *Clin Orthop Relat Res*:226-33, 2004.

45. Sah RL, Chen AC, Grodzinsky AJ, Trippel SB: Differential effects of bFGF and IGF-I on matrix metabolism in calf and adult bovine cartilage explants. *Arch Biochem Biophys* 308:137-47, 1994.

46. Sah RL, Kim YJ, Doong JH, Grodzinsky AJ, Plaas AHK, Sandy JD: Biosynthetic response of cartilage explants to dynamic compression. *J Orthop Res* 7:619-36, 1989.

47. Sah RL, Trippel SB, Grodzinsky AJ: Differential effects of serum, insulin-like growth factor-I, and fibroblast growth factor-2 on the maintenance of cartilage physical properties during long-term culture. *J Orthop Res* 14:44-52, 1996.

48. Sandy JD: A contentious issue finds some clarity: on the independent and complementary roles of aggrecanase activity and MMP activity in human joint aggrecanolysis. *Osteoarthritis Cartilage* 14:95-100, 2006.

49. Sandy JD, Verscharen C: Analysis of aggrecan in human knee cartilage and synovial fluid indicates that aggrecanase (ADAMTS) activity is responsible for the catabolic turnover and loss of whole aggrecan whereas other protease activity is required for C-terminal processing in vivo. *Biochem J* 358:615-26, 2001.

50. Schinagl RM, Gurskis D, Chen AC, Sah RL: Depth-dependent confined compression modulus of full-thickness bovine articular cartilage. *J Orthop Res* 15:499-506, 1997.

51. Sokal RR, Rohlf FJ. Biometry. 3rd ed. New York: WH Freeman and Co.; 1995.

52. Tang L-H, Rosenberg L, Reeiner A, Poole AR: Proteoglycans from bovine nasal and articular cartilage: properties of a soluble form of link protein. *J Biol Chem* 254:10523-31, 1979.

53. Teng MS, Yuen AS, Kim HT: Enhancing osteochondral allograft viability: effects of storage media composition. *Clin Orthop Relat Res* 466:1804-9, 2008.

54. Tiku ML, Gupta S, Deshmukh DR: Aggrecan degradation in chondrocytes is mediated by reactive oxygen species and protected by antioxidants. *Free Radic Res* 30:395-405, 1999.

55. Treppo S, Koepp H, Quan EC, Cole AA, Kuettner KE, Grodzinsky AJ: Comparison of biomechanical and biochemical properties of cartilage from human knee and ankle pairs. *J Orthop Res* 18:739-48, 2000.

56. Wall RS, Gyi TJ: Alcian blue staining of proteoglycans in polyacrylamide gels using the "critical electrolyte concentration" approach. *Anal Biochem* 175:298-9, 1988.

57. Williams GM, Chan EF, Temple-Wong MM, Bae WC, Masuda K, Bugbee WD, Sah RL: Shape, Loading, and Motion in the Bioengineering Design, Fabrication, and Testing of Personalized Synovial Joints. *J Biomech* In Press 08/21/2009, 2009.

58. Williams GM, Lin JW, Sah RL: Cartilage reshaping via in vitro mechanical loading. *Tissue Eng* 13:2903-11, 2007.

59. Williams JM, Virdi AS, Pylawka TK, Edwards RB, 3rd, Markel MD, Cole BJ: Prolonged-fresh preservation of intact whole canine femoral condyles for the potential use as osteochondral allografts. *J Orthop Res* 23:831-7, 2005.

60. Williams RJ, 3rd, Dreese JC, Chen CT: Chondrocyte survival and material properties of hypothermically stored cartilage: an evaluation of tissue used for osteochondral allograft transplantation. *Am J Sports Med* 32:132-9, 2004.

61. Woessner JF: The determination of hydroxyproline in tissue and protein samples containing small proportions of this imino acid. *Arch Biochem Biophys* 93:440-7, 1961.